



**A University of Sussex DPhil thesis**

Available online via Sussex Research Online:

<http://sro.sussex.ac.uk/>

This thesis is protected by copyright which belongs to the author.

This thesis cannot be reproduced or quoted extensively from without first obtaining permission in writing from the Author

The content must not be changed in any way or sold commercially in any format or medium without the formal permission of the Author

When referring to this work, full bibliographic details including the author, title, awarding institution and date of the thesis must be given

Please visit Sussex Research Online for more information and further details

UNIVERSITY OF SUSSEX

Majid Shannon Khalaf

Coordination Chemistry of Bicyclic  
Guanidines and Guanidines

Submitted for the degree of  
Doctor of Philosophy

April 2011

كفى بالعلم شرفاً أن يدعيه من لا يحسنه ، ويفرح به إذا نسب إليه، وكفى بالجهل ذماً أن

يتبرأ منه من هو فيه

الامام علي عليه السلام

*Knowledge is such a dignified thing that he who is not proficient at it claims to be so, and one is pleased for it to be attributed to him, and ignorance is such a rebuked thing that even the one who possesses it claims to be free of it.*

*Imam Ali*

## **Declaration**

I hereby declare that this thesis has not been and will not be submitted in whole or in part to another University for the award of any other degree.

Signature:.....

# Acknowledgements

Thank you to all the people who, through their skill and expertise and patience, helped me to get all this work done. The group in the Lab. 14. I am also grateful to the group of Physical Chemists, Steve Lee and Elizabeth Atkinson. My thanks also goes to Dr. Ian Crossley and Iain and Peter for their experience and knowledge of NMR and X-ray crystallography, Ali, for the mass spectrometry.

To my supervisor Dr. Martyn P. Coles, who is a good person and a great supervisor, for his guidance, direction allowing me free reign at appropriate stages of the research programme. Taking on a mature student with family commitments was a brave thing to do and the hope I will not let him down.

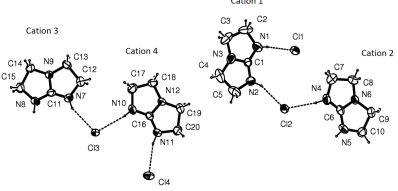
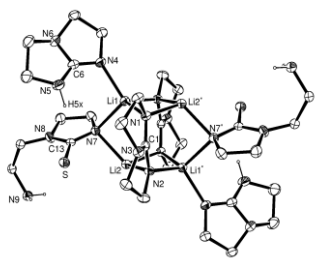
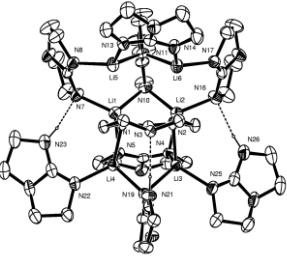
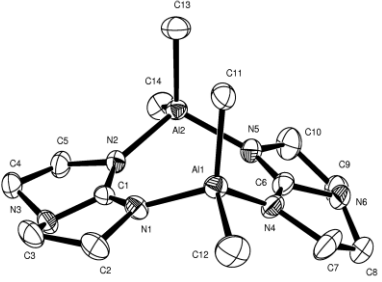
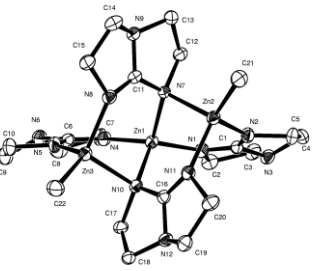
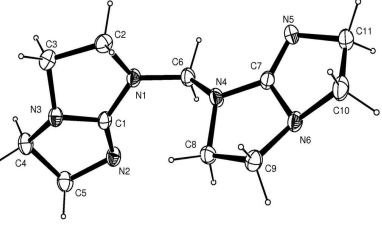
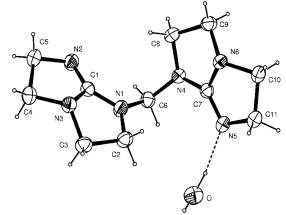
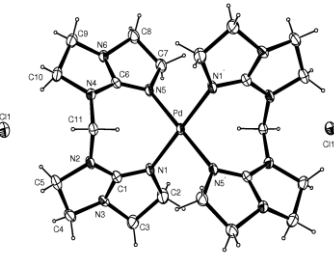
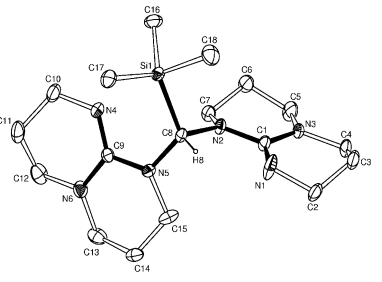
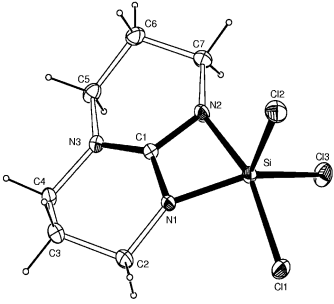
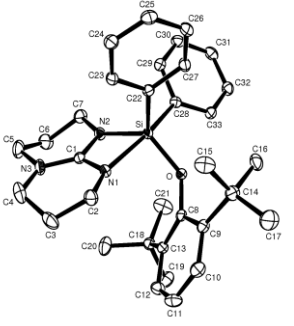
## Summary

A [5:5] ligand based on the bicyclic guanidine 1,4,6-triazabicyclo[3.3.0]oct-4-ene [Htbo] has been synthesised. Two of these tbo units have been linked *via* a carbon bridgehead to form a novel bidentate ligand. Based on the knowledge that the electronic properties and specific steric interactions at a metal can lead to new insights into the relationship between crystal structure and ligand activity, the synthesised compounds have been investigated as polydentate ligands on the assumption that that they could be used to precisely control coordination environment. The corresponding [6:6] system which is based on the bicyclic guanidine 1,3,4,6,7,8-hexahydro-2*H*-pyrimido[1,2-*a*]pyrimidine) [hppH] has also been synthesised and its coordination to silyl groups investigated.

1,4,6-triazabicyclo[3.3.0]oct-4-ene (Htbo) has been deprotonated to form the [tbo]<sup>−</sup> anion, which has been assessed as a ligand at Li, Al and Zn centres, allowing direct structural comparison to be made with the [hpp]<sup>−</sup> analogues. The coordination chemistry of Htbo and its derivatives has been explored through formation of a variety of transition metal complexes. Additionally, crystal structures showed that Htbo coordinates to the metal through the N-imine atom as a monodentate ligand to form trigonal planar, tetrahedral, square planar and octahedral complexes.

The *bis* (tbo) methane H<sub>2</sub>C{tbo}<sub>2</sub> ligand was found to support a range of coordination geometries and upon coordination, ionic structures such as [Pd(H<sub>2</sub>C{tbo}<sub>2</sub>)<sub>2</sub>][Cl]<sub>2</sub> were formed. The synthesis of the monosubstituted compound hppSiCl<sub>3</sub> afforded a series of (hpp) silanes which were isolated and reacted with LiOAr (Ar= 2,6-<sup>t</sup>Bu<sub>2</sub>C<sub>6</sub>H<sub>3</sub>), providing a proof of N-Si bond stabilisation using a metal. Five examples of pentacoordinated silicon species have been synthesised *via* the reaction of [hpp]<sup>−</sup> and R<sub>2</sub>SiCl<sub>2</sub> (R= Ph, Me).

# Compound numbering

 <p>(1)</p>	 <p>(2)</p>	 <p>(3)</p>
 <p>(4)</p>	 <p>(5)</p>	 <p>(6)</p>
 <p>(6')</p>	 <p>(7)</p>	 <p>(8)</p>
 <p>(9)</p>	 <p>(12)</p>	<p>(hpp)SiPh<sub>3</sub> (10)</p> <p>&amp;</p> <p>(hpp)SiMeCl<sub>2</sub> (11)</p>

# Table of Contents

<b>Declaration</b>	i
<b>Summary</b>	ii
<b>Acknowledgements</b>	iii
<b>Compounds</b>	iv
<b>Chapter 1: Overview of guanidines and bicyclic-guanidine</b>	
1.1: Introduction	1-4
1.1.1: Basicity.	4-5
1.1.2: Localized and delocalized form of guanidines.	5-6
1.1.3: Protonation and deprotonation of guanidines: resonance stabilization.	6-8
1.2: Features of bicyclic guanidines.	8
1.2.1: Synthesis of different type of non-substituted bicyclic guanidines.	9-11
1.2.2: Structure of non-substituted bicyclic guanidines.	11-12
1.3: Neutral bicyclic guanidines.	13
1.3.1: Guanidines with no additional donor atoms.	13-14
1.3.2: Guanidines with additional donor atoms	14
1.3.3: Coordination chemistry of hppH.	15
1.3.4: Coordination chemistry of Htbo.	15



1.4: Anionic guanidines (guanidinate salts).	16
1.4.1: Coordination chemistry of [hpp] <sup>−</sup> .	16-17
1.4.2: Coordination chemistry of [tbo] <sup>−</sup> .	18
1.5: Cationic guanidinium ions.	18
1.6: Summary.	19
1.7: References.	20-21
<b>Chapter 2: Hydrogen bonding in a cationic [H<sub>2</sub>tbo]<sup>+</sup> salt</b>	
2.1: Previous work with [hppH <sub>2</sub> ] <sup>+</sup> .	22-23
2.2: Cationic [H <sub>2</sub> tbo] <sup>+</sup> salts.	24
2.2.1: Synthesis of [H <sub>2</sub> tbo][Cl] ( <b>1</b> ).	24-25
2.3: Spectroscopic Properties of [H <sub>2</sub> tbo][Cl] ( <b>1</b> ).	25
2.3.1: Crystallographic details and crystal structure of [H <sub>2</sub> tbo][Cl] ( <b>1</b> ).	26-30
2.4: Discussion- Solution-State structure.	30-31
2.4.1: Discussion-Solid-State structure.	31-32
2.5: Summary.	33
2.6: References.	34

## **Chapter 3: Evaluation of the coordination chemistry of the bicyclic guanidinate derived from 1,4,6 triazabicyclo[3.3.0]oct-4-ene**

3.1: Introduction.	35-36
3.2: Reaction of Htbo with <sup>n</sup> BuLi.	36
3.2.1: General procedure.	37
3.2.2: Isolation of [Li <sub>2</sub> (tbo)( <b>A</b> )(Htbo)] ( <b>2</b> ).	37-41
3.2.3: Synthesis of Li <sub>6</sub> (tbo) <sub>6</sub> (Htbo) <sub>3</sub> ( <b>3</b> ).	41-46
3.3: Synthesis of [Al(tbo)Me <sub>2</sub> ] ( <b>4</b> ).	47
3.3.1: Crystallographic details and crystal structure of [Al(tbo)Me <sub>2</sub> ] <sub>2</sub> [ <b>4</b> ] <sub>2</sub> .	57-52
3.4: Synthesis of Zn <sub>3</sub> (tbo) <sub>4</sub> Me <sub>2</sub> ( <b>5</b> ).	52-53
3.4.1: Crystallographic details and crystal structure of Zn <sub>3</sub> (tbo) <sub>4</sub> Me <sub>2</sub> ( <b>5</b> ).	53-57
3.5: Conclusions.	58
3.6: References.	59-60

## **Chapter 4: Linked bis(guanidine) compounds and their application as bidentate ligands**

4.1: Synthesis of H <sub>2</sub> C{tbo} <sub>2</sub> ( <b>6</b> ).	61-62
4.1.1: Crystallographic details and crystal structure of H <sub>2</sub> C{tbo} <sub>2</sub> ( <b>6</b> ).	62-64
4.2: Generation of H <sub>2</sub> C{tbo} <sub>2</sub> ·H <sub>2</sub> O ( <b>6'</b> ).	64-67
4.3: Synthesis of [Pd (H <sub>2</sub> C{tbo} <sub>2</sub> ) <sub>2</sub> ] [Cl] <sub>2</sub> ( <b>7</b> ).	67-68

4.3.1: Crystallographic details and crystal structure of [Pd (H <sub>2</sub> C{tbo} <sub>2</sub> ) <sub>2</sub> ][Cl] <sub>2</sub> ( <b>7</b> ).	68-71
4.4: Synthesis of (Me <sub>3</sub> Si)HC{hpp} <sub>2</sub> ( <b>8</b> ).	72
4.4.1: Crystallographic details and crystal structure of (Me <sub>3</sub> Si)HC{hpp} <sub>2</sub> ( <b>8</b> ).	73-75
4.5: Summary.	75
4.6: References.	76
 <b>Chapter 5: Synthesis of pentacoordinate hpp-silicon compounds</b>	
5.1: Introduction of hpp-Si Chemistry.	77-79
5.2: Synthesis of (hpp)SiPh <sub>n</sub> Cl <sub>3-n</sub> (n=0, 2, 3).	79-80
5.2.1: Synthesis of (hpp)SiCl <sub>3</sub> (n=0) ( <b>9</b> ).	80-80
5.2.2: Crystallographic details and crystal structure of (hpp)SiCl <sub>3</sub> ( <b>9</b> ).	80-83
5.3: Synthesis of (hpp)SiPh <sub>3</sub> ( <b>10</b> ) and (hpp)SiMeCl <sub>2</sub> ( <b>11</b> ).	83-84
5.4: Synthesis of (hpp)Si(OAr)Ph <sub>2</sub> (Ar=2,6 <sup>t</sup> Bu <sub>2</sub> C <sub>6</sub> H <sub>3</sub> ) ( <b>12</b> ).	84-85
5.4.1: Crystallographic details and crystal structure of (hpp)Si(OAr)Ph <sub>2</sub> ( <b>12</b> ).	85-87
5.5: NMR Spectroscopic analysis of compounds <b>9-12</b> .	88-90
5.6: Summary.	90
5.7: References.	91
 <b>Chapter 6: Experimental section</b>	
6.1: General experimental procedures.	92

6.2: General reagents and starting materials.	93
6.2.1: [a] Htbo [C <sub>5</sub> H <sub>9</sub> N <sub>3</sub> ]	95
6.2.2: [b] hppH [C <sub>7</sub> H <sub>13</sub> N <sub>3</sub> ] .	95
6.2.3: [c] PdCl <sub>2</sub> (COD).	96
6.3: Experimental data for Chapter 2.	96
6.3.1: Synthesis of [HtboH][Cl].(1)	96
6.4 Experimental data for Chapter 3.	97
6.4.1 Isolation of Lithium Guanidinate Complex [Li <sub>2</sub> (tbo)(A)(Htbo)](2)	97
6.4.2: Synthesis of Li <sub>6</sub> (tbo) <sub>6</sub> (Htbo) <sub>3</sub> (3).	97
6.4.3: Synthesis of [Al(tbo)Me <sub>2</sub> ] (4).	98
6.4.4: Synthesis of Zn <sub>3</sub> (tbo) <sub>4</sub> Me <sub>2</sub> (5).	98-99
6.5: Experimental data for Chapter 4.	99
6.5.1: Synthesis of H <sub>2</sub> C{tbo} <sub>2</sub> (6).	99
6.5.2: Generation of H <sub>2</sub> C{tbo} <sub>2</sub> ·H <sub>2</sub> O (6').	100
6.5.3: Synthesis of [Pd (H <sub>2</sub> C{tbo} <sub>2</sub> ) <sub>2</sub> ] [Cl] <sub>2</sub> (7).	100-101
6.5.4: Synthesis of (Me <sub>3</sub> Si)HC{hpp} <sub>2</sub> (8).	101
6.6. Experimental data for Chapter 5.	101
6.6.1: Synthesis of (hpp)SiCl <sub>3</sub> (9).	101-102

6.6.2: Synthesis of (hpp)SiPh <sub>3</sub> ( <b>10</b> ).	102
6.6.3: Synthesis of (hpp)SiMeCl <sub>2</sub> ( <b>11</b> ).	102-100
6.6.4: Synthesis of (hpp)SiPh <sub>2</sub> Cl ( <b>A</b> ).	101
6.6.5: Synthesis of (hpp)Si(OAr)Ph <sub>2</sub> (Ar=2,6 <sup>t</sup> Bu <sub>2</sub> C <sub>6</sub> H <sub>3</sub> ) ( <b>12</b> ).	101-102
Appendix : Publications.	103

## Chapter 1: Overview of guanidines and bicyclic- guanidine

### 1.1. Introduction.

The general formula of the unsubstituted amidine, is  $\text{HC}(=\text{NH})(\text{NH}_2)$ , which may be considered as derived from the acid-amide by replacement of oxygen by the divalent imino ( $=\text{NH}$ ) group. They may be prepared by a number of different routes:

- the action of ammonia or amines on imide chlorides, or on thiamides,
- the action of ammonium chloride or hydrochlorides of amines on nitrites,
- by condensing amines and amides in presence of phosphorus trichloride,
- by the action of hydrochloric acid on acid-amides and by the action of ammonia or amines.<sup>1</sup>

Tri-substituted amidines are the most commonly found and will be the focus of this report. Amidine functionalities may exist as neutral species, amidine anions (amidinates) or amidinium cations depending on the number of protons attached to nitrogen as shown in Figure 1.<sup>2,3</sup>

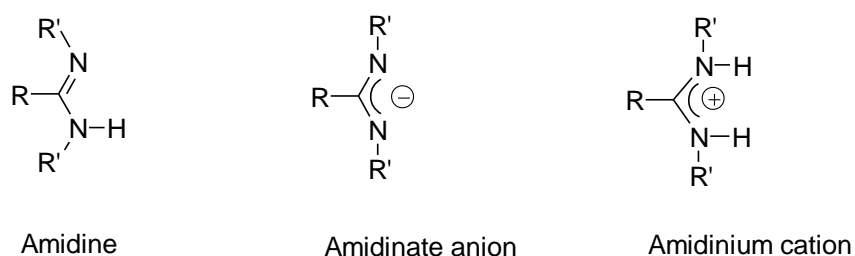
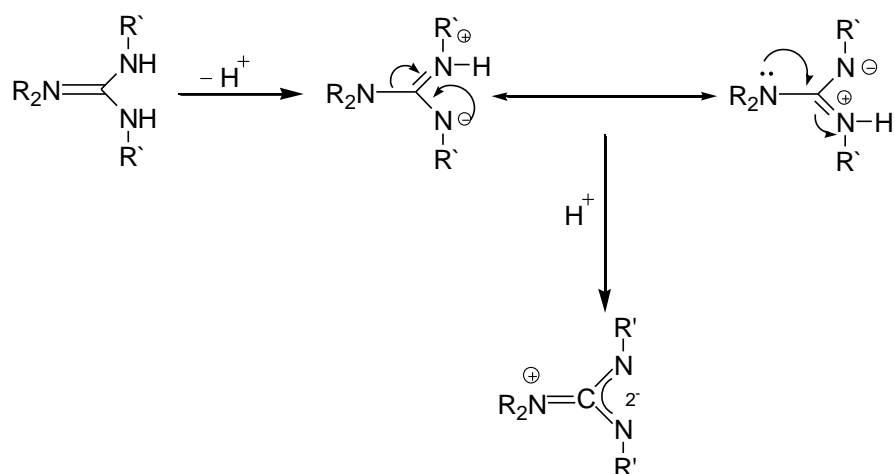


**Figure 1:** The chemical structures of the neutral amidine, the anionic amidinate and cationic amidinium.

The guanidine functionality is closely related to the amidine and consists of a central ( $sp^2$ )-hybridized carbon atom bound to one iminic and two aminic nitrogen atoms.<sup>4</sup> Interest in the guanidine and the amidine comes from their abilities to act as ligands, as well as the formation of anion,<sup>2,3</sup> Guanidines are a class of compounds of great biological and chemical importance. Due to their hydrophilic nature, they also play an important role in the stabilisation of protein conformations through hydrogen bonding and in the mediation of solubility of natural products. In some cases, due to their strong basic character, guanidines can be considered super bases, which readily undergo protonation to generate resonance-stabilised guanidinium cations.<sup>4</sup> Guanidines are encountered in coordination chemistry as guanidinium counter cations, as chelate guanidinate and as neutral guanidine ligands with different metals, partly due to their interesting electronic properties and capacity for simple modification. Zinc complexes, lithium complexes and aluminum complexes containing coordinated guanidates are of recent origin and, to date, are restricted to a relatively small number of examples.<sup>5</sup>



**Scheme 1:** The resonance of guanidinate.

A zwitterion is a chemical compound that is Electrically neutral, but has formal positive and negative charges on different atoms (Scheme 1). Zwitterion are polar and usually have a high solubility in water and a poor solubility in most organic solvent. An example of a natural product containing guanidine moieties is shown in (Figure 2).<sup>6</sup> The guanidine class of compounds has extremely high basicity and many guanidine derivatives have been synthesized with a view to investigating and utilizing this property. These compounds are used routinely in organic chemistry as bases and anion binders in a variety of transformations.<sup>7</sup>

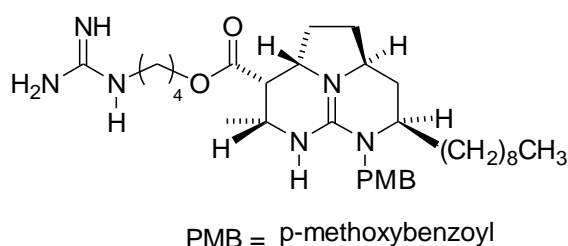


**Figure 2:** The chemical structure of Batzelladine.

Previous work in the Coles group has concentrated on the bicyclic guanidine 1,3,4,6,7,8-hexahydro-2*H*-pyrimido pyrimidine, hppH (C<sub>7</sub>H<sub>13</sub>N<sub>3</sub>), shown in Figure 3a. The compound 1,4,6-triazabicyclo[3.3.0]-oct-4-ene Htbo (C<sub>5</sub>H<sub>9</sub>N<sub>3</sub>) Figure 3b, has been recently reported,<sup>8</sup> and is structurally similar to hppH. The purpose of dealing with Htbo in the current work is to compare reactions with different metal substrates and to see the difference between the two ligands.



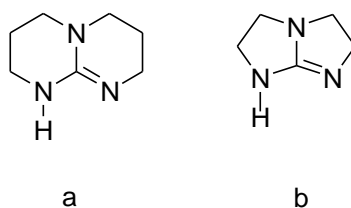


**Figure 3:** The chemical structures of two ligands (a) Hhpp (b) Htbo.

### 1.1.1. Basicity.

There is a shortage of work on the guanidine compounds and their use as strong bases in organic synthesis albeit, they have been known for some time.<sup>9</sup> Recently, it has been noted that chiral bicyclic guanidines have received attention as promoters of enantioselectivity.<sup>10</sup> Results from recent studies showed that tetramethylguanidine (TMG) catalyzed addition of initial nitroalkanes and dialkyl phosphites to a diversity of unsaturated systems constitutes a useful means to achieve the nitroaldol reaction (Henry reaction) and to achieve phosphonate synthons.<sup>11,12</sup>

hppH and its methyl derivative hppMe have been proven to be approximately 100 times more basic than TMG<sup>13</sup> as they were broadly used as potent organic bases for tautomerizing pyrrocorphins.<sup>13,14</sup> Recent work studied their behavior as strong, nonionic, basic catalysts for the purpose of synthesis. In these studies, it has been found that hppH and hppMe catalyze the addition of different nucleophiles to a diversity of unsaturated systems Figure 4.<sup>15</sup>

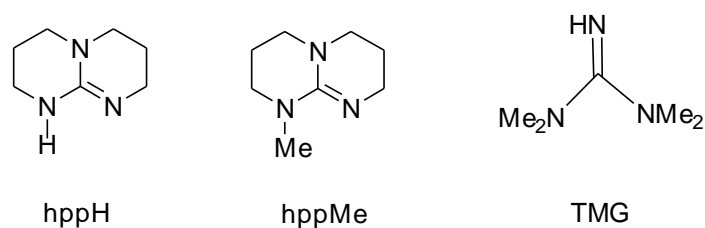
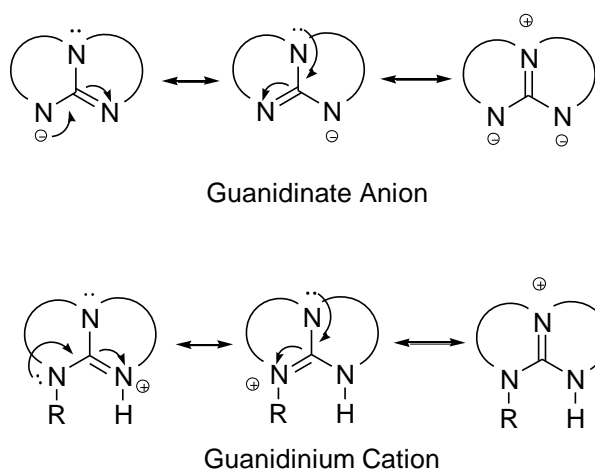


**Figure 4:** Different type of guanidine to measure the basicity.

### 1.1.2. Localized and delocalized form of guanidines.

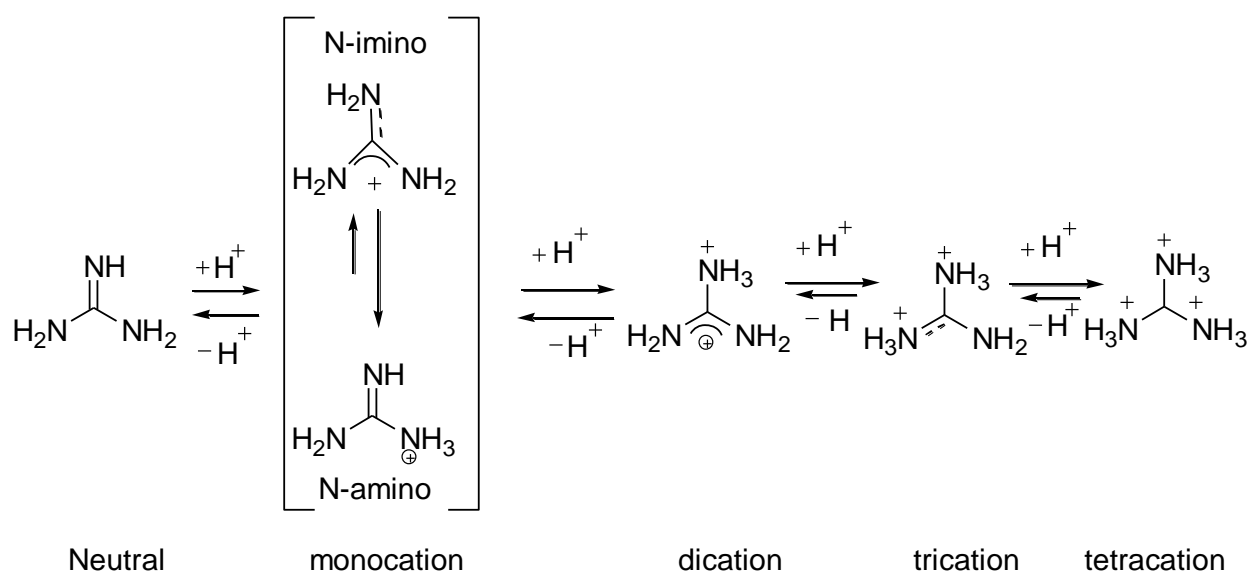
Three main areas can be summarized from the influence that the bicyclic framework applies to the steric and electronic features of the guanidines. The ability to efficiently distribute charge throughout the molecule is one of the important characteristics of guanidines, this distribution is either negative for guanidinate anions or positive for guanidinium cations (Scheme 2). The extent of overlapping between the nitrogen lone-pairs and the p-orbital of the  $sp^2$ -carbon within the  $CN_3$  unit, determines a simple orbital description. A favourable alignment for the lone-pair of the non-amidine nitrogen N(3) atom is generated by constraining the substituents of this atom into the ring system to be included in the delocalization scheme. Acyclic guanidines where steric interactions play a dominant role contrasts this favourable alignment, often favouring an orthogonal displacement of the N(3) substituents with respect to the  $CN_2$  amidine unit.



**Scheme 2:** Localized and delocalized forms of the guanidinate anion and guanidinium cation for bicyclic systems

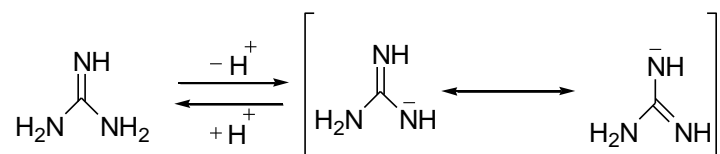
### 1.1.3. Protonation and deprotonation of guanidines: resonance stabilization.

Guanidine possesses three nitrogen atoms, susceptible to protonation. The N- $\pi$  conjugation possible between the amino and imino nitrogens increases the basicity of the N-imino and decreases the basicity of the N-amino atom.<sup>16</sup> As a consequence of this conjugation effect, the N-imino atom is protonated first. The basicity of the N-amino atom is relatively weak. Several quantum chemical calculations showed that in guanidine itself, the N-amino is less basic than the N-imino atom by *ca* 30 Kcal mol<sup>-1</sup>, a similar behaviour was observed in amidines.<sup>17</sup> In the parent amidine molecule, the N-imino atom is much more susceptible to proton attachment than the N-amino atom as shown in Scheme 3.



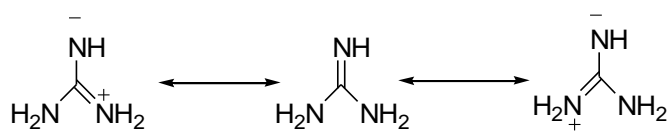
**Scheme 3:** Protonated forms of guanidine.

In neutral guanidine, two types of acidic sites can be distinguished, the amino and imino groups. Bordwell and Ji showed that in dimethyl sulfoxide (DMSO) solution the acidity of guanidine ( $\text{pK}_{\text{HA}} = 28.5$ ) is close to that of 2-aminopyridine ( $\text{pK}_{\text{HA}} = 27.7$ ).<sup>18</sup> Comparison of  $\text{pK}_{\text{HA}}$  values of various imines and amidines led to the conclusion that the amino ( $\text{NH}_2$ ) is more acidic than the imino ( $\text{NH}$ ) group in the amino-imino conjugated systems, and that the  $\text{NH}_2$  is preferentially deprotonated, as shown in Scheme 4.



**Scheme 4:** The deprotonation reaction in guanidine.

Guanidine anion exhibits unusual thermodynamic stability and energetic barriers to rotation due to delocalization of six  $\pi$ -electrons across the  $\text{CN}_3$  core of the ligand. More than 60 years ago the enhanced stability of the neutral and of the ionic forms was considered in terms of resonance theory.<sup>19</sup> According to this theory, the free base may be written using three non-equivalent resonance structures, in two of which the charges are separated, as shown in the Scheme 5.



**Scheme 5:** The resonance stabilization of guanidine.

## 1.2. Features of bicyclic guanidines.

The class of bicyclic guanidine compounds have several general structural properties. The localized ' $\text{N}(2)\text{--C=N}(1)$ ' fragment is a constituent of neutral guanidines at which most chemistry displayed by these molecules occurs, although  $\text{N}(3)$  the tertiary nitrogen, plays an important role in defining the electronic and physical attributes of the guanidines. Our interpretation is restricted to molecules in which constituent atoms of each ring are  $\text{sp}^3$ -carbon atoms, distinguishing these compounds from related nitrogen ligand systems.<sup>20</sup>

### 1.2.1. Synthesis of different type of non-substituted bicyclic guanidines.

The different bicyclic compounds and their abbreviations are shown in Figure 5.

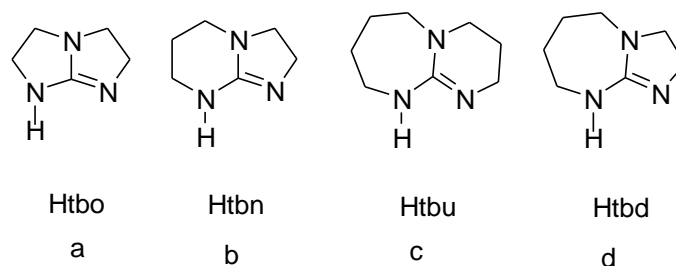
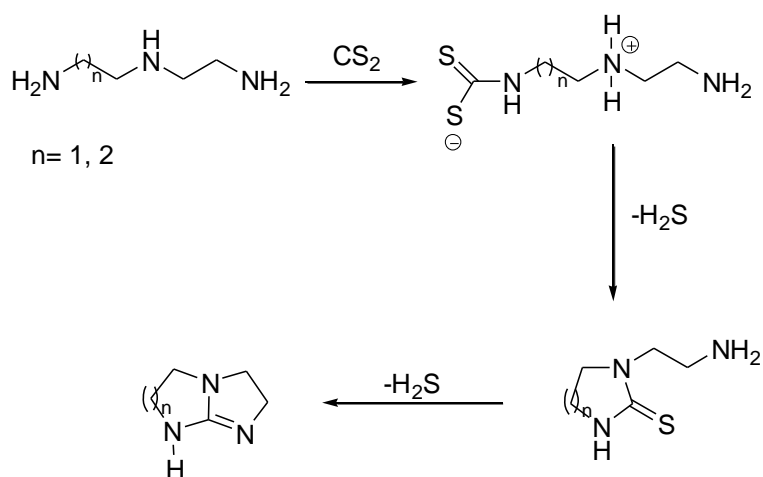


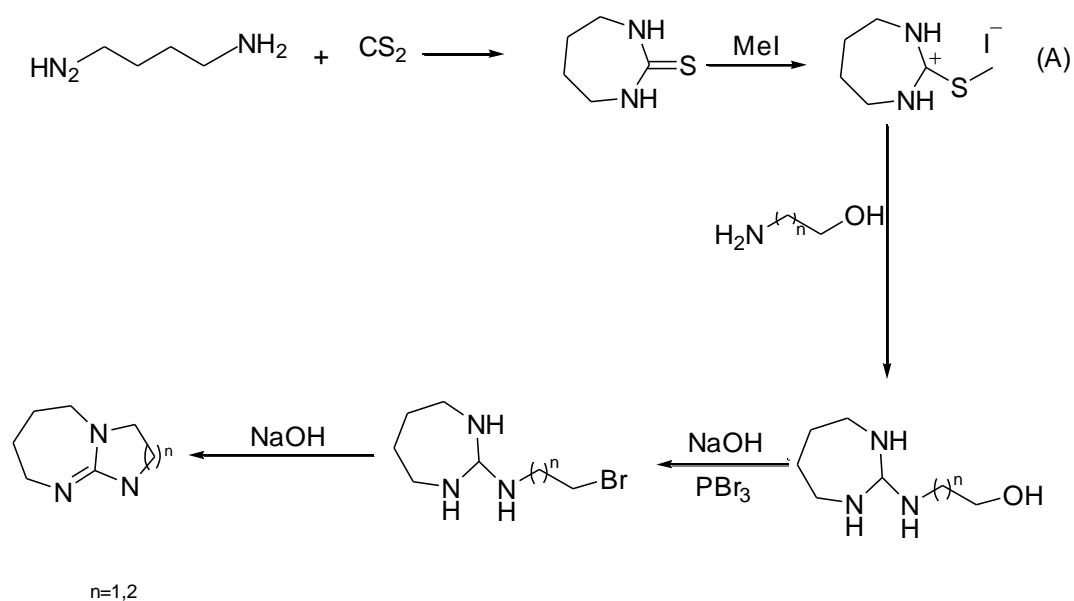
**Figure 5:** Different type of bicyclic guanidine.

The syntheses of non-functionalized bicyclic guanidines was described in the initial studies of guanidines, and involved either multi-step procedures,<sup>21</sup> or the use of expensive starting reagents. In the patent literature a simple one-pot method to the {6,6}- and {5,5}-guanidines, hppH and Htbo in 1990 was published (Scheme 6),<sup>23</sup> this procedure leads to the commercial availability of the former, driven by an interest in the application of these compounds in organocatalysis.<sup>24</sup> The reaction of CS<sub>2</sub> with *N*-(2-aminoethyl)-1,3-propanediamine allowed extension of this synthetic method to the non-symmetric {6,5}-bicyclic model, Htbn, as shown in Scheme 6.<sup>25</sup>



**Scheme 6:** Synthesis of Htbo and Htbn

The {5, 7} Htbd and {7, 6} Htbu compound were prepared using carbon disulfide and 1,4-diaminobutane in ethanol. An intermediate compound (A) was formed and adding ethanolamine to the intermediate leads to Htbd formation while by adding of 3-amino-1-propanol to the intermediate leads to formation of Htbu ligand as shown in Scheme 7.<sup>26</sup>



**Scheme 7:** Syntheses of Htbd and Htbu

Using these different ligands to react with molybdenum led to the formation of new dimolybdenum complexes  $\text{Mo}_2(\text{tbo})_4$ ,  $\text{Mo}_2(\text{tbo})_4\text{Cl}$ ,  $\text{Mo}_2(\text{tbn})_4\text{Cl}_2$ ,  $\text{Mo}_2(\text{tbd})_4\text{Cl}$ ,  $\text{Mo}_2(\text{tbu})_4\text{Cl}$ .<sup>27</sup>

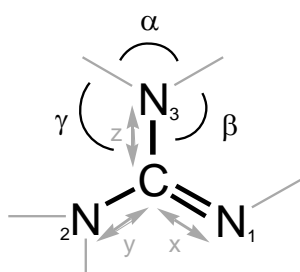
### 1.2.2. Structure of non-substituted bicyclic guanidines.

A comparison of structural features of the complete series of {5,5}, {6,5}, {6,6}, {7,5} and {7,6} bicyclic guanidines can be achieved using X-ray diffraction data. The parameters are defined in Figure 6.<sup>27</sup> In the “ $\text{N}_2\text{-C=N}_1$ ” amidine component, observation of a similar distribution of carbon–nitrogen bond distances for each molecule, with clearly defined  $\text{C=N(1)}$  and  $\text{C-N(2)}$  bonds was observed. However, for  $\text{N(3)}$  a significant range of values for the degree of pyramidalization ( $\text{DP}^\circ$ ) which are ultimately effecting the value of  $\Delta_{\text{CN}}$ .



Nitrogen N(3) is prevented from attaining a planar configuration (higher DP% values) due to the presence of the five-membered ring in H-tbo, H-tbn and H-tbd ( $n = 5$ ) and this is consistent with retention of electron density at this position. This decreases any delocalization of these neutral compounds throughout the  $\text{CN}_3$  core with larger values of  $\Delta_{\text{CN}}$ . The synthetic routes to these derivatives have only recently been published,<sup>28</sup> and the consequences of these differences in delocalization have yet to be explored. It will, however, clearly impact not only the neutral forms of these compounds but also their positive and negative ions which is predicted to result in differences in chemical behaviour.

	Htbo	Htbn	hppH	Htbd	Htbu
C-N1	1.346(2)	1.290(3)	1.328(2)	1.233(2)	1.293(2)
C-N2	1.297(2)	1.347(3)	1.367(2)	1.354(2)	1.356(2)
C-N3	1.391(2)	1.383(3)	1.331(2)	1.355(2)	1.394(2)
DP%	26.58	18.19	0.11	20.74	4.20
$\Delta_{\text{CN}}$	0.048	0.057	0.039	0.062	0.090
$\Delta_{\text{CN}^-}$	0.070	0.065	0.038	0.069	0.034



$$\Delta_{\text{CN}} / \text{\AA} = y - x$$

$$\Delta'_{\text{CN}} / \text{\AA} = z - [(x + y) / 2]$$

$$\text{DP \%} = [360 - (\alpha + \beta + \gamma)] / 0.9$$

**Figure 6:** Definition of parameters used in the comparison of structural data taken from bicyclic guanidines.

### 1.3. Neutral bicyclic guanidines.

Many complexes have been reported which contain a neutral guanidine ligand and these can be classified into two main groups: (1) substituted guanidines with no additional donor atoms and (2) substituted guanidines that contain additional donor atoms. In the coordination chemistry, the major difference of these classifications is the action of the guanidines such that when no additional donor atoms are present, it acts exclusively as a monodentate ligand binding through the lone pair located on the imine nitrogen, whereas in cases where additional donor atoms are present, there is a tendency for the molecules to behave as bidentate ligands. To emphasise the coordination of the guanidine moiety, these two classes will be reviewed separately.

#### 1.3.1 Guanidines with no additional donor atoms

The earlier researches have reported complexes of a guanidine coordinating to a metal focused on the formation of adducts with 1,1,2,tetramethylguanidine [ $\text{HNC}\{\text{N}(\text{CH}_3)_2\}_2$ ] and complexes containing a neutral guanidine contain this ligand. In 1965,<sup>29</sup> Drago and co-workers published for the first time the complexes containing this ligand. Complexes of Co(II), Cu(II), Zn(II), Pd(II), Ni(II) and Cr(III) were prepared with the tetracoordinate cobalt, copper, and zinc perchlorate complexes which are characterised by X-ray powder diffraction, magnetic measurements and spectroscopy. Additionally, elemental analyses verified that these complexes had the composition  $[\text{M}(\text{TMG})_4](\text{ClO}_4)_2$ . Moreover, the IR spectrum displayed a shift towards lower wavenumbers for the  $\nu(\text{C}=\text{N})$  which ultimately confirmed the coordination through the imine nitrogen. Depending on spectral and magnetic measurements,

cobalt complex was suggested to have a tetrahedral geometry although this could not be confirmed from X-ray powder diffraction data. The copper and zinc complexes were also observed to have tetrahedral geometries and their X-ray powder patterns were consistent and suggested that they showed little distortion from true tetrahedral symmetry.

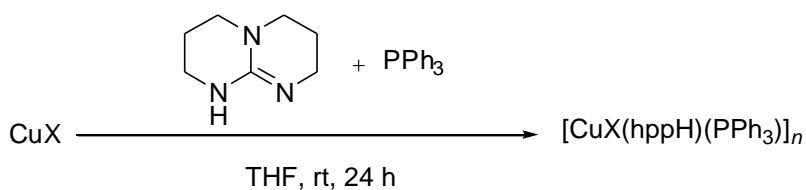
### 1.3.2. Guanidines with additional donor atoms

There is large scope for different substituents (that contains additional donor atoms) onto a guanidine moiety and their stepwise synthesis allows the incorporation and variation of substituent groups. Cyanoguanidine is the most generally encountered example which contains an additional donor atom. However, the cyanoguanidine is invariably found to act as a bidentate, bridging ligand coordinated to two separate metal centres *via* the nitrile nitrogen and the imine nitrogen to which the nitrile is bonded. The main differences between these complexes arise from the interaction of metal–guanidine units with each other to form either dimers or oligomeric structures. This is due to the steric effects imposed on the complexes by the coordination geometry at the metal centre.

From the reaction of ethylenediamine hydrochloride, cyanoguanidine and copper(II) sulphate, the first structurally characterised cyanoguanidine complex was obtained.<sup>30</sup> In the IR spectrum, the isolated crystals analysed as the anticipated product ethylenebisbiguanidecopper(II) sulphate except for the presence of a  $\text{C}\equiv\text{N}$  stretch.

### 1.3.3. Coordination chemistry of hppH.

Coles *et al*, has prepared many complexes containing guanidines in particular hppH as monodenate ligands. For example the complex produced by the reaction of 1:1 mixed PPh<sub>3</sub>/hppH copper (I) in THF, [CuX(hppH)(PPh<sub>3</sub>)]<sub>n</sub>, shown in (Scheme 8).<sup>31</sup>



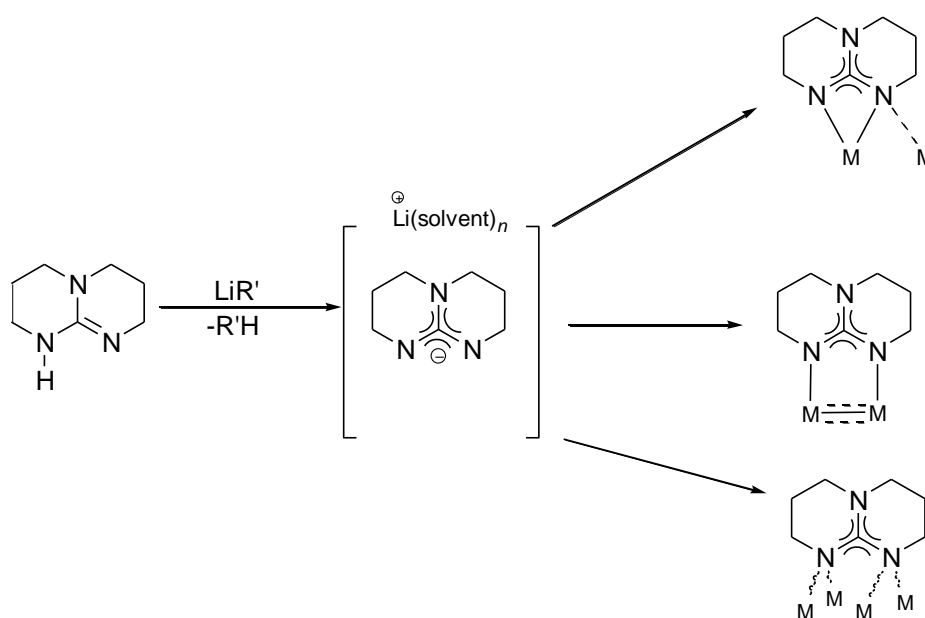
**Scheme 8:** Synthesis of [CuX(hppH)(PPh<sub>3</sub>)]<sub>n</sub> X= Cl, *n*= 1, X=Br, *n*= 2.

### 1.3.4. Coordination chemistry of Htbo.

The coordination chemistry of neutral Htbo has so far not been reported. However, in 2006, Cotton *et al*, reported the preparation of Htbo, which can act as a neutral monodenate or bidentate ligand.<sup>27</sup> Most of this work focused on the application of these ligands in the synthesis of new paddle-wheel complexes, and reflected on the stability of multiply bonded metal complexes bearing [tbo]<sup>-</sup>. Preferential bidentate ligation is determined by the ability of the ligand to bridge two non-bonded metal centres.

## 1.4. Anionic guanidines (guanidinate salts).

Conversion of neutral tetra-substituted guanidines to the corresponding anionic guanidinate can be achieved using organolithium reagents. This conversion occurs *via* loss of the *NH* proton.<sup>32</sup> Although it is possible to isolate examples of lithium guanidinate salts, the anions are normally generated *in situ* for further reactivity, with the most broadly studied reaction being salt metathesis with additional metal-halide substrate. The coordination chemistry of bicyclic guanidinate anions has been classified into three sub-categories Scheme 9.



**Scheme 9:** Different sub-categories of complex

### 1.4.1. Coordination chemistry of [hpp]<sup>-</sup>.

Guanidates have demonstrated a variety of coordination modes to transition and main group metals as both chelating and bridging ligands.<sup>33</sup> The coordination mode adopted by acyclic guanidates may to some extent be influenced by steric interactions of the substituents on nitrogen. Amidates show preference for either chelation or bridge formation depending on the size of the R groups on nitrogen and carbon with a similar effect postulated for

guanidines.<sup>25,26</sup> Bulky R' groups on the backbone nitrogen of the guanidinate increase the C-N-R angle [ $\beta$ ], favouring a chelating bonding mode Figure 7a, while smaller R' substituents allow a more parallel configuration of the  $\sigma$ -donor orbitals favouring a bridging mode Figure 7c

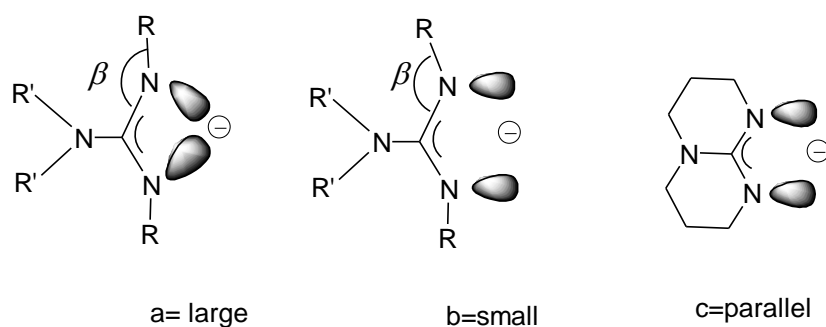


**Figure 7:** The influence of sterics over the projection of the bonding orbitals in guanidines

Their behaviour as bidentate ligand is further demonstrated by their ability to bridge to non-bonded metal centers, further coordination modes have been identified for [hpp]<sup>-</sup> involving different metal centres Figure 8.

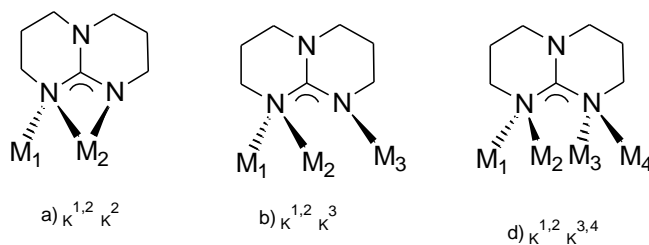


**Figure 8:** Different coordination motifs for the [hpp]<sup>-</sup> anion.

### 1.4.2. Coordination chemistry of [tbo]<sup>-</sup>.

A further geometric constraint on the molecule is imposed by defining the size of the rings. This constraint dictates the projection of the frontier orbitals of the amidine nitrogen atoms. Reducing the ring-size from 6 to 5 (ie. From “hpp” to “tbo”) gives a wide projection band on purely geometric argument. Figure 9 views the differences among the molecular structures of unsubstituted bicyclic guanidines: guanidine, {6,6}- and {5,5}-bicyclic derivatives.

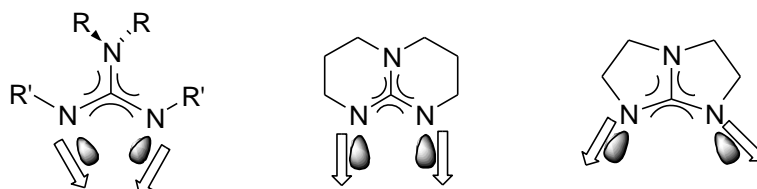


**Figure. 9:** Projection of frontier orbitals for acyclic guanidines compared with the {6,6}- and {5,5}-bicyclic derivatives.

### 1.5. Cationic guanidinium ions.

The basicity of hppH is also evidenced by the formation of the cation  $[H_2hpp]^+$ . The high basicity of the  $[hpp]^-$  anion is one of its attractive features, the hppH molecule itself also has high basicity. This follows from the fact that it is a derivative of the extremely basic prototype guanidine,  $(H_2N)_2C=NH$ . hppH is therefore easily protonated to form the  $[H_2hpp]^+$ , and this happens whenever it is used in an acid medium.<sup>32</sup> For example  $[hppH_2]^+[O_2NCHPh]^-$ ,  $[hppH_2]^+[O_2CCH_3]^{38}$ ,  $[hppH_2]^+[O_2CCF_3]^{38}$  and  $[\{hppH_2\}^+]_3[\{TaCl_6\}^-]_2[Cl]^-$ , are known. Some of these are of interest for the study of reactions involving hppH as a catalyst, such as the Michael addition of nitroalkanes, or as models for hydrogen bonding in nature.

## 1.6. Summary.

Guanidine and amidine units are widely used in chemistry, for their ability to form cationic, anionic and neutral species. Guanidine basicity is due to the high ability of delocalisation of electron density throughout the Y shape  $\text{CN}_3$  and the ability to coordinate to a large number of metal atoms has also been demonstrated. Part of the attractiveness of the use of guanidinate ligands is the ease with which the electron donating ability can be modified in noncyclic anions. The coordination chemistry of the neutral guanidines is known, but until now synthetic chemistry has exclusively used the commercially available bicyclic guanidine hppH, a compound with two-fused six-membered rings. Recently this has been expanded to the derivative with two fused five-membered rings, Htbo. Guanidines are also encountered in coordination chemistry as guanidinium counter cations.

The research outlined in the following pages demonstrates the exploration of the coordination chemistry of new ligand classes. Specifically, the coordination chemistry of hppH as a neutral ligand has been extended to other transition-metal halides, and further studies of the fluxionality that renders the two ring systems within hppH symmetrical at room temperature have been completed. Comparisons between the two guanidine systems have been made by determination of the extent of overlap between the nitrogen lone-pairs and the empty p-orbital on the  $\text{sp}^2$ -carbon within the  $\text{CN}_3$  unit. The effect of the widened angle between the donor orbitals of the {5,5}-bicyclic anion compared with the {6,6}-analogue has been investigated.



## 1.7. References.

1. O. Wallach, *Chem. Ges.*, 1882, **15**, 208.
2. Z. Maksic, B. Kovacevic., *Org Chem.*, 2000, **65** (11), 3303-9.
3. M. Costa, D. Taffurelli, G. Dalmonego, *Chem. Soc.*, 1998, 1541- 1546.
4. P. Baily. S. Pace, *Coordination chem.*, 2001, **214**, 55-141
5. S. Boss, M. Coles, R. Haigh, P. Hitchcock, R. Snaith and A. E. H. Wheatley, M. McPartlin, J. Morey and H. Naka, *Dalton Trans Chem.*, 2003, **42**, 5574 5593..
6. P. Murphy, T. Hohlraum, *Phys. Rev.*, 1998, **45**, 9481-9488.
7. R. Drago and R. Longhi, *Inorg. Chem.*, 1965, **4**, 11.
8. F. Cotton, C. Murillo, X. Wang and C. Wilkinson, *Inorg.Chem.*, 2006, **45**, 5493.
9. R. Drago and R. Longhi, *Inorg. Chem.*, 1965, **4**, 23.
10. M. J. Grogan, E. J. Corey, *Org. Lett.*, 1999, **1**, 157-160.
11. S. Smith, *The Chemistry of Open Chain Nitrogen Compounds*. W.A. Benjamin, New York, 1965, **1**, 233-290.
12. S. Invidiata, S. Ferroni, R. Lampronti, I. Roberti, M. Pollini, *Tetrahedron Letters*, 1997, **38**, 2745-2749.
13. V. Rasetti, A. Pfaltz, C. Kratkyt, and A. Eschenmoser. *Angew. Chem., Int.*, 1981, **20**, 261-265.
14. A. Kratky, C. Eschenmoser., A. Angew, *Chem. Int.*, 1981, **20**, 263-266S.
15. S. Invidiata, S. Ferroni, R. Lampronti, I. Roberti, M. Pollini, *Tetrahedron Letters*, 1998, **39**, 7615-7618
16. P. Müller, J. Mareda, *Chimia*, 1985, **39**, 234-235.
17. J. E. Johansen, V. Piermattie, C. Angst, E. Diener, C. Kratky, A. Eschenmoser, *Ange., Chem., Int. Ed., Engl.*, 1981, **20**, 261-263.
18. G. Olah, T. Burrichter, A. Rasul, G. Prakash, *J. Am. Chem. Soc.*, 1997, **119**, 12923.

19. T. Raczyn, M. Coles., I. Leito, M. Decouzon, T. Drapała, F. Anvia; J. Tortajada, E. Leon, *Physical Organic Chemistry*, 1995, **69**, 12919.
20. G. Frederick, G. Bordwell, *J. Am. Chem. Soc.*, 1991, **113**, 8398-8401.
21. L Brockway, J. Beach, *J. Am. Chem. Soc*, 1935, **57**, 2705.
22. M. Berger, F. Schmidtchen, *Chem. Rev.*, 1997, **97**, 1609-1646.
23. A. McKay and M.-E. Kreling, *J. Chem. Soc.*, 1957, **35**, 1438-1445
24. F. Schmidtchen, *Chem. Ber.*, 1980, **113**, 2175-2182.
25. R. Court, *Eur. Pat.*, 1990, 680.
26. M. Green, *Eur. Pat*, 1983, 629.
27. F. Cotton, X. Wang and C. Wilkinson, *Inorg.Chem.*, 2006, **45**, 5493.
28. F. Cotton, X. Wang and C. Wilkinson, *Dalton Trans.*, 2006, 4623.
29. Z. Maksic and B. Kovacevic, M. P. Coles and P. B. Hitchcock, *J. Chem. Soc., Perkin Trans.*, 2003, **22**, 2623-2629.
30. F. Albert Cotton, Xiaoping Wang, and Chad C. Wilkinson, *Inorg. Chem.*, 2006, **45**, 4623-4631.
31. S. Oakley, PhD thesis 2004, University of Sussex.
32. M. Mitewa, *Coordination Chem Reviews*, 1995, 140.
33. L. Coghi, M. Nardelli, G. Pelizzi, L. Sozzi, *J. Chem. Soc. Chem. Commun.*, 1968, 1475.
34. M. Khalaf, M. Coles and. P. Hitchcock., *Dalton Trans.*, 2008, 4288-4295
35. J. Bailey and S. Pace, *Coordination chem.*, 2001, **214**, 55.
36. O. Ciobanu and H. Himmel, *Eur. J. Inorg. Chem.*, 2007, 3565-3572
37. S. Boguslaw, L. Jarczewski, A. Nowak-Wydra, B. and Brzezinski, *J. Mol. Str.*, 1995, **77**, 344.
38. F. A. Cotton and D. J. Timmons, *J. Am. Chem. Soc.*, 1998, **17**, 179-184.

## Chapter 2: Hydrogen bonding in a cationic [H<sub>2</sub>tbo]<sup>+</sup> salt.

### 2.1 Previous work with [hppH<sub>2</sub>]<sup>+</sup>

From experimental results, the p*K*<sub>a</sub> values of the conjugate acid [hppH<sub>2</sub>]<sup>+</sup> in acetonitrile is 26.03<sup>1</sup> and the neutral guanidines are therefore often referred to as ‘superbases’. The formation of the [hppH<sub>2</sub>]<sup>+</sup> cation, its structure and how it interacts with different anions, have been comprehensively studied using a combination of spectroscopy (NMR, UV-vis and vibrational analysis), calorimetry and conductivity.<sup>2,3</sup> Recently, these studies have been complemented by computational work.<sup>4</sup> Many examples have also been structurally characterized showing extensive variety in both short and long range order in the solid-state. Pertinent examples include metal-oxide<sup>5</sup> and metal–halide<sup>6,7</sup> species, oxoanions based on nitrogen,<sup>8</sup> sulfur,<sup>3,9</sup> functionalities, and several aryloxide derivatives (Figure 1).

A study of the crystal structure of the {5,5}-hydrochloride salt, [H<sub>2</sub>tbo][Cl], will form the main part of this chapter, confirming an increased angle between the projection of the hydrogen bonds, which leads to the formation of extended structures in the solid state.

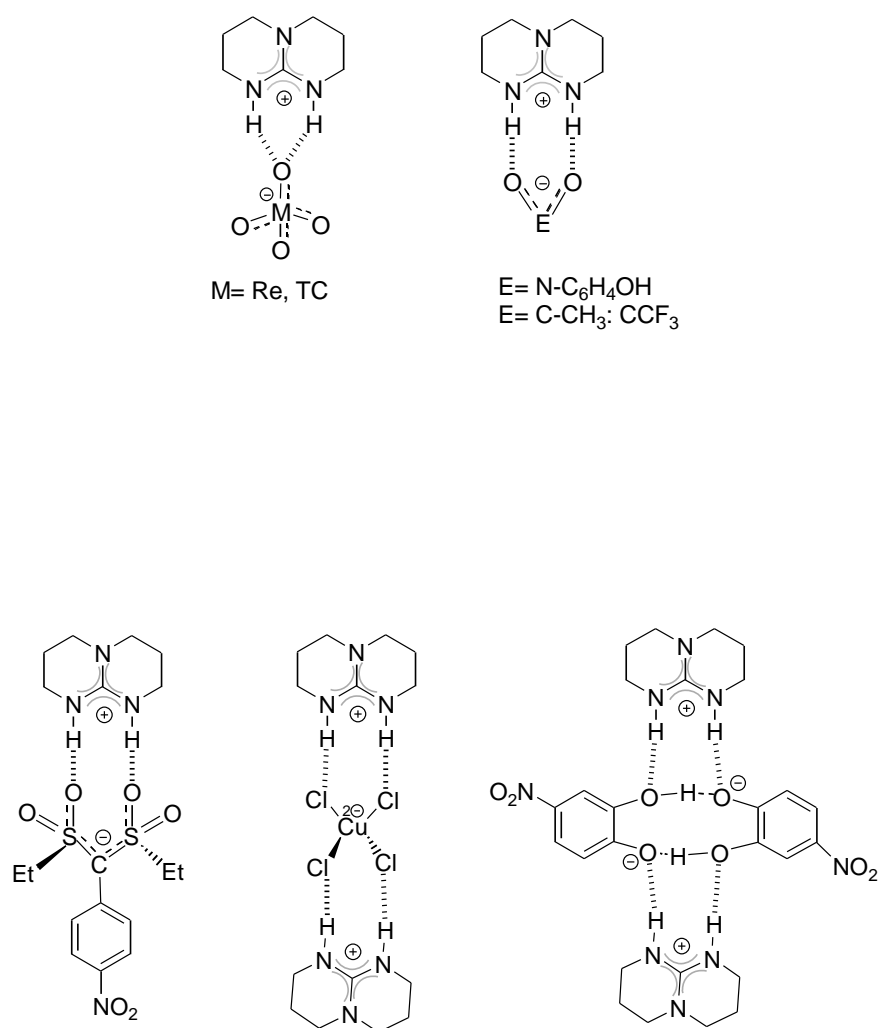


**Figure 1:** Structurally characterized examples of guanidinium salts involving the cation



## 2.2 Cationic $[\text{H}_2\text{tbo}]^+$ salts

Reducing the size of the heterocyclic rings from {6,6}- to {5,5}- in the  $[\text{H}_2\text{tbo}]^+$  salt is predicted to promote the formation of extended structures due to a wider angle between the projected hydrogen-bonds (Figure 2).

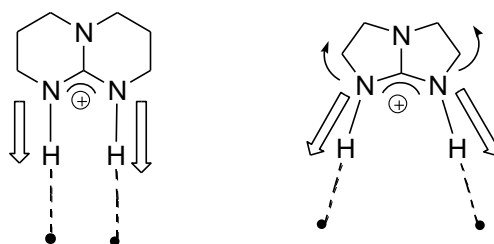
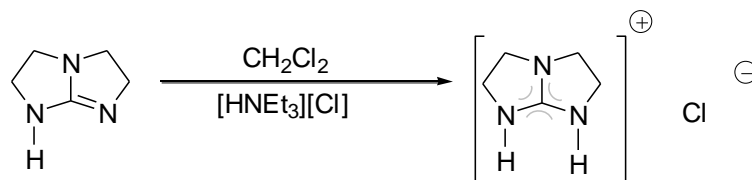


**Figure 2:** Hydrogen-bonds direction for  $[\text{hppH}_2]^+$  and  $[\text{H}_2\text{tbo}]^+$

To establish proof-of-concept, the work has been restricted to hydrochloride salts. Additionally this enables us to make a direct comparisons between the {6,6}- and {5,5}- systems, as the  $[\text{hppH}_2][\text{X}]$  salts ( $\text{X} = \text{Br}, \text{Cl}$ ) are known.<sup>6</sup>

### 2.2.1 Synthesis of $[\text{H}_2\text{tbo}][\text{Cl}]$ (1)

Due to the high basicity the formation of the  $[\text{H}_2\text{tbo}]^+$  cation can occur immediately through the protonation of 1,4,6-triazabicyclo[3.3.0]oct-4-ene  $[\text{Htbo}]$ . The protonation process occurred using  $[\text{HNEt}_3][\text{Cl}]$  and the result was  $[\text{H}_2\text{tbo}][\text{Cl}]$ , analogous to the formation of  $[\text{hppH}_2][\text{Cl}]$  (Scheme 1). A solution of  $\text{Htbo}$  in dichloromethane was added drop wise to a solution of  $[\text{HNEt}_3][\text{Cl}]$  at room temperature and the resulting solid was isolated and washed with hexane, to give  $[\text{H}_2\text{tbo}][\text{Cl}]$  in 91% yield.



**Scheme 1:** The formation of  $[\text{H}_2\text{tbo}][\text{Cl}]$  (**1**)

## 2.3 Spectroscopic Properties of $[\text{H}_2\text{tbo}][\text{Cl}]$ (**1**)

$^1\text{H}$  NMR spectroscopic data showed two resonances for the annular methylene protons, and a single resonance for  $\text{NH}$  at 3.95 ppm. The  $^{13}\text{C}$  NMR spectrum showed a shift of the central  $\text{CN}_3$  carbon from 165.4 in Htbo to 166.8 ppm. In (**1**).

IR spectroscopy is also a useful analytical tool for the investigation of these systems. The spectrum of Htbo (KBr) reported a series of peaks for the  $\text{NH}$  stretch ( $3310\text{--}3048\text{ cm}^{-1}$ ).<sup>10</sup> Upon protonation, the salt  $[\text{H}_2\text{tbo}][\text{Cl}]$  displayed multiple broad absorptions in the  $\nu(\text{NH})$  region and a strong absorption  $1682\text{ cm}^{-1}$  that is likely due to  $\nu(\text{C}=\text{N})$ . This latter absorption is shifted from  $1750\text{ cm}^{-1}$  in Htbo, reflecting delocalization and decrease in the bond order.

### 2.3.1 Crystallographic details and crystal structure of $[\text{H}_2\text{tbo}][\text{Cl}]$ (**1**)

The solid-state structure of (**1**) was solved by X-ray diffraction analysis for crystals grown by slow cooling of a saturated MeCN solution. As seen in Figure 3, the unit cell consists of four

independent cations which bridge *via* hydrogen bonds to chloride anions. A summary of bond lengths (Å) and angles (°) of (**1**) is shown in Table 1.

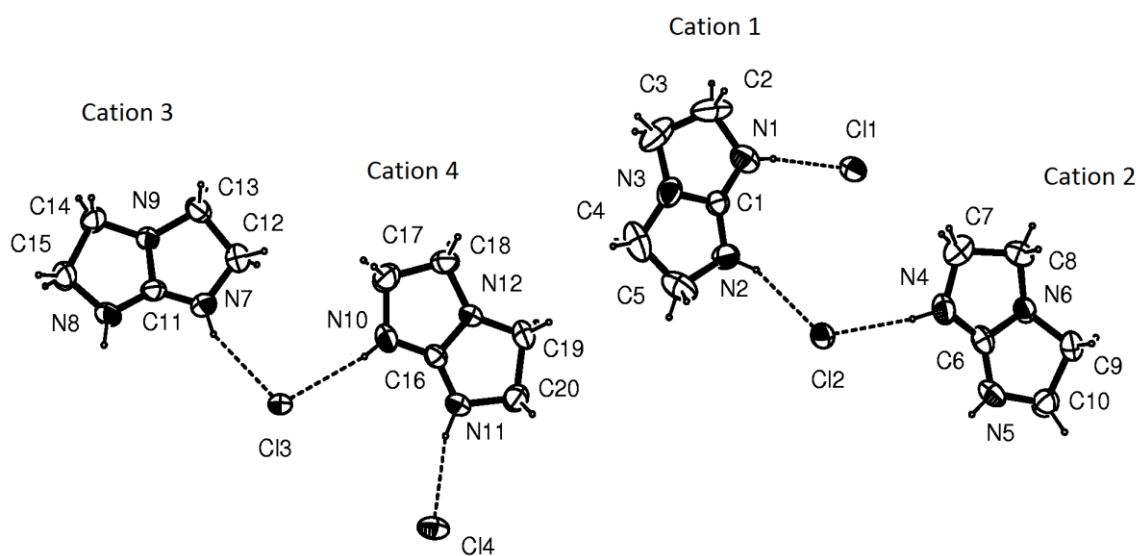


**Figure 3:** Ellipsoids (30%) of [H<sub>2</sub>tbo]Cl (**1**), showing the four independent cations in the unit cell.

Table 1. Bond length (Å) and angles (°) for [H<sub>2</sub>tbo]Cl (**1**)

N(1)-C(1)	1.300(4)	N(7)-C(11)	1.306(4)
N(2)-C(1)	1.318(4)	N(8)-C(11)	1.312(4)
N(3)-C(1)	1.343(3)	N(9)-C(11)	1.329(3)
N(4)-C(6)	1.309(4)	N(10)-C(16)	1.316(4)
N(5)-C(6)	1.314(4)	N(11)-C(16)	1.305(4)
N(6)-C(6)	1.346(3)	N(12)-C(16)	1.323(3)
N(1)-C(1)-N(2)	134.5(3)	N(4)-C(6)-N(5)	134.6(3)
N(1)-C(1)-N(3)	113.6(3)	N(4)-C(6)-N(6)	113.1(3)

N(2)-C(1)-N(3)	111.9(2)	N(5)-C(6)-N(6)	112.1(2)
N(7)-C(11)-N(8)	134.8(3)	N(11)-C(16)-N(10)	135.3(3)
N(7)-C(11)-N(9)	112.5(2)	N(11)-C(16)-N(12)	112.3(2)
N(8)-C(11)-N(9)	112.7(2)	N(10)-C(16)-N(12)	112.3(2)
C(16)-N(11)-C(20)	109.5(2)	C(1)-N(3)-C(4)	108.1(2)
C(16)-N(12)-C(19)	111.7(2)	C(1)-N(3)-C(3)	107.7(3)
C(16)-N(12)-C(18)	111.0(2)	C(4)-N(3)-C(3)	130.5(3)
C(16)-N(10)-C(17)	109.6(2)	C(6)-N(4)-C(7)	108.4(2)

In the solid-state, formation of a salt containing bridging guanidinium cations was confirmed; two hydrogen bonds are formed to different halide anions affording extended structures. It could not have been predicted, however, that polymeric chains from cations 1 and 2 and tetrameric units from cations 3 and 4 would form within the same crystal structure.

In the hydrogen-bonded polymers formed by cations 1 and 2 two-dimensional chains linked by two-chloride bridges are present (Figure 5). The hydrogen-bonding within the chain unit is similar to that in the tetramer, with both planar and non-planar portions.



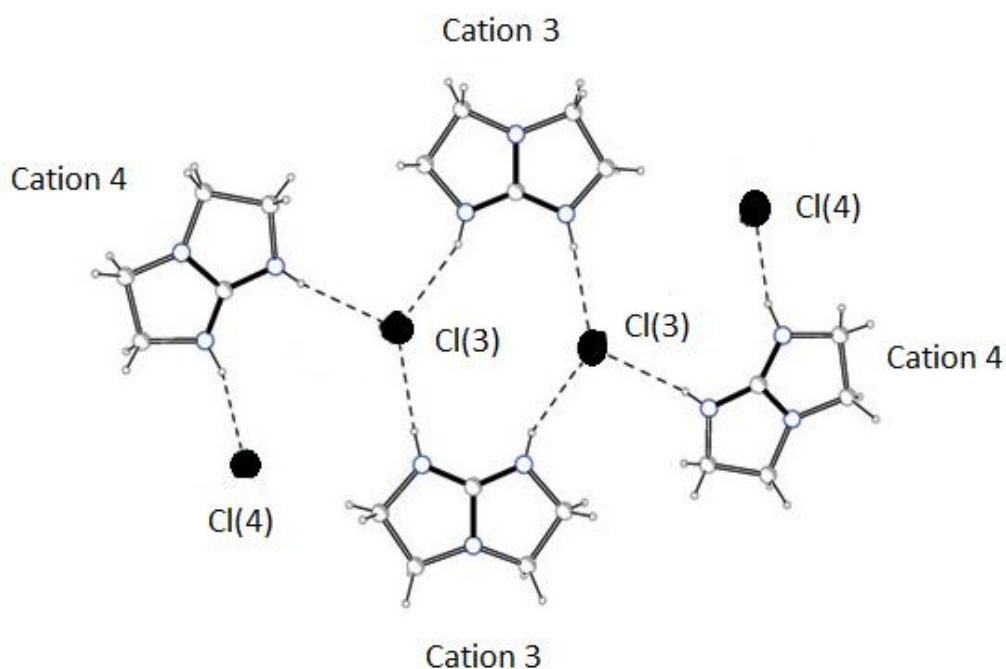


**Figure 4:** The tetrameric unit of cations 3 and 4 in the crystal structure of  $[\text{H}_2\text{tbo}]\text{Cl}$  (**1**).

The tetrameric units are composed of pairs of cations and anions related by a centre of inversion (Figure 4). Chloride Cl3 is involved with hydrogen bonding to three NH atoms in a distorted planar arrangement. Chloride Cl3 is located  $0.14 \text{ \AA}$  out of the plane defined by the  $\text{CN}_3$  atoms of the two cation 3 units, giving a roughly planar central core, whereas cation 4 is twisted such that the Cl4 anions lie  $1.57 \text{ \AA}$  out of this approximate plane.

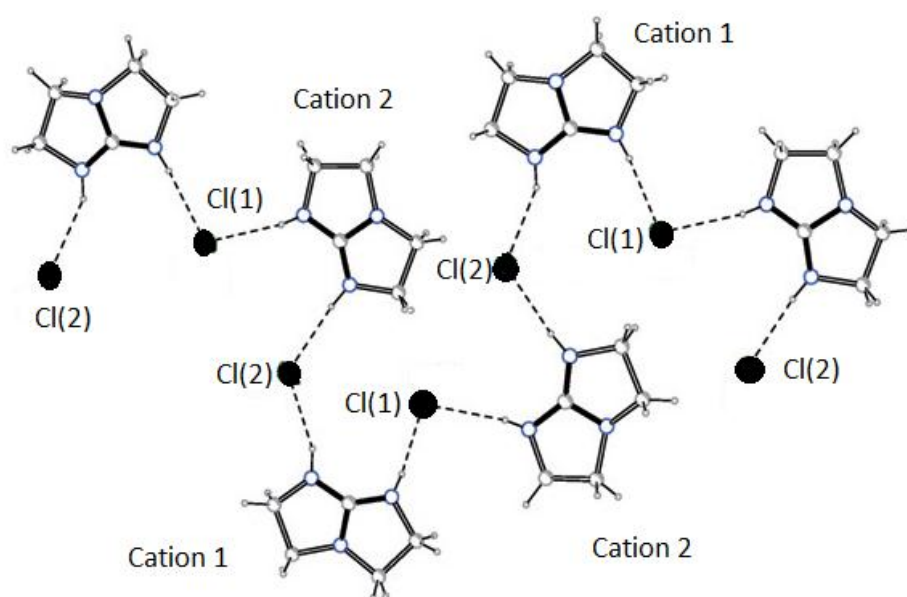


**Figure 5:** The chains unit of cations 1 and 2 in the crystal structure of  $[\text{H}_2\text{tbo}]\text{Cl}$  (**1**).

The polymeric chains of cations and anions in the crystal structure of  $[\text{H}_2\text{tbo}][\text{Cl}]$  show formation of an “upper deck “ and a “lower deck” (Figure 6). The upper deck is formed of  $([\text{H}_2\text{tbo}]\cdots\text{Cl}\cdots[\text{H}_2\text{tbo}])^+$  units and is generated by Cl1 being coplanar with the  $\text{CN}_3$  cores of the two cations to which it is bonded (deviation= 0.03 Å). Chloride Cl2 is located 1.44 Å away from this plane, relating to another similar unit that forms the lower deck (distance of 1.46 Å).

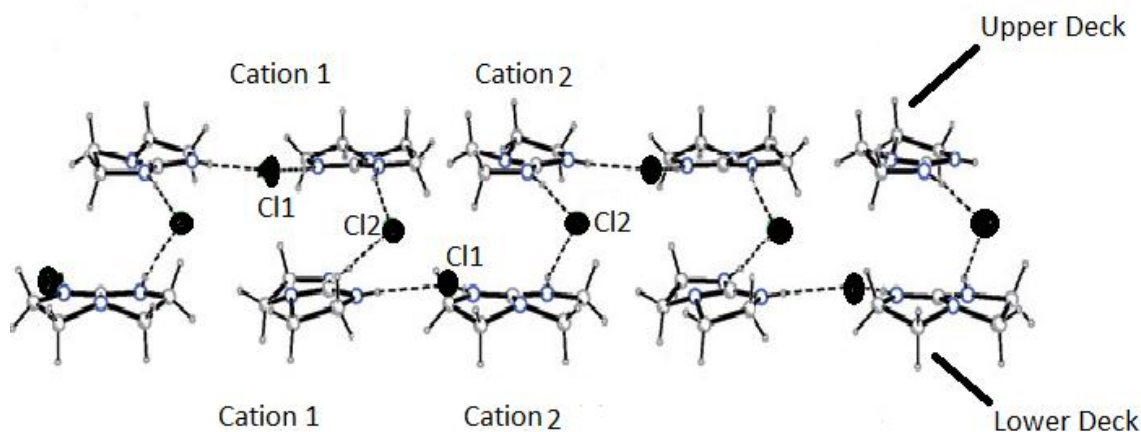


**Figure 6:** The polymeric chains of cations and anions in the crystal structure of  $[\text{H}_2\text{tbo}][\text{Cl}]$  (1).

## 2.4 Discussion: Solution-State structure

In solution, the  $^1\text{H}$  and  $^{13}\text{C}$  NMR spectra of the neutral guanidine Htbo are consistent with  $C_2$ -symmetry; half the number of resonances are displayed as predicted for a structure in which the two rings are inequivalent, which would be the case with isolated single and double bonds to nitrogen. These data suggest a rapid proton exchange between the two nitrogen atoms of the amidine component or an intermolecular process in which hydrogen transfer is occurring between more than one guanidine.

The NMR spectra of the protonated guanidinium salts  $[\text{H}_2\text{tbo}]^+$  also indicate a symmetric structure for the bicyclic ring units of the cation, consistent with a fully delocalized structure (Figure 7a), or a rapid equilibration between the tautomeric structures (Figure 7b, 7c and 7d).

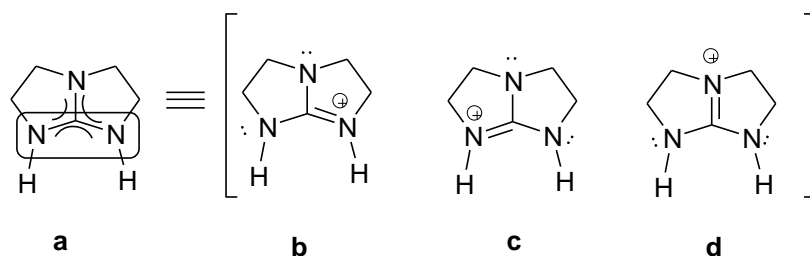


**Figure 7:** Resonance structure contributing to the bonding in the guanidinium cation  $[\text{H}_2\text{tbo}]^+$

### 2.4.1 Discussion: Solid-State structure

The salt  $[\text{hppH}_2][\text{Cl}]$  consists of a monomeric guanidinium cation in which the protonated imine nitrogen and the secondary amino nitrogen form two  $\text{NH}\cdots\text{X}$  hydrogen-bonds to the halide counter-ion. An association of the ion-pairs into dimers is observed in which the halide anions are located above the  $\text{C1-N3}$  portion of the  $[\text{hppH}_2]^+$  cation (Figure 8).

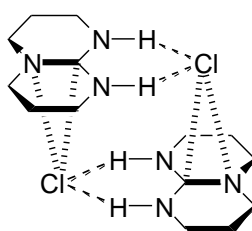


**Figure 8:** Association of ion pairs into dimeric units in which the halide anion are located above C-N

Examination of the solid-state structures of a range of cationic  $[\text{hppH}_2]^+$  salts showed that the distances of all three  $\text{C}(sp^2)\text{-N}$  bonds are in the range 1.323 to 1.344 Å, which are intermediate between those of  $\text{C}(sp^2)\text{-N}$  single [1.38 Å] and double [1.28 Å], bonds.<sup>11</sup> In contrast the hydrochloride salt of  $[\text{H}_2\text{tbo}][\text{Cl}]$  consists of chains of  $[\text{H}_2\text{tbo}]^+$  and  $[\text{Cl}]^-$  ions with longer  $\text{C}_x\text{-N}_3$  bonds and delocalization limited to the amidine component of the cation.(Figure 9).

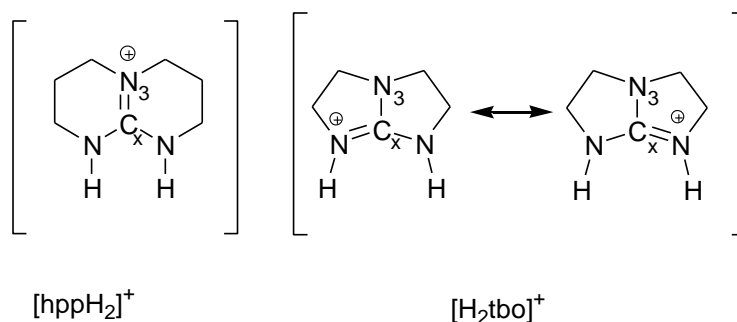


**Figure 9:** The minor variation for  $[\text{hppH}_2]^+$  and  $[\text{H}_2\text{tbo}]^+$

The molecular structure of  $[\text{hppH}_2]^+$  and  $[\text{H}_2\text{tbo}]^+$  (Figure 9) showed that the carbon–nitrogen  $\text{C}_x\text{-N}_3$  bond length in the first compound is shorter<sup>12</sup> than that in  $[\text{H}_2\text{tbo}]^+$  (Table 1) reflecting a large resonance contribution from d (Figure 10) which locates significant positive charge in this region of the cation.

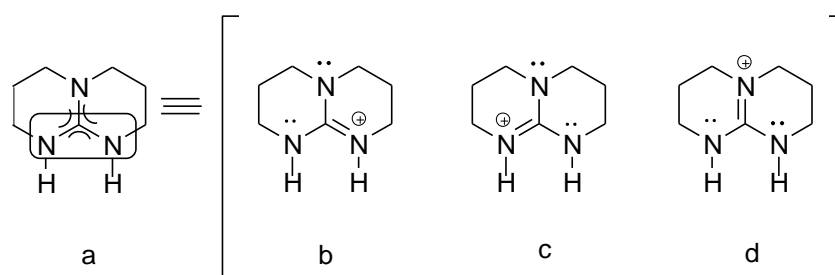


**Figure 10:** The resonance structures for the guanidinium cation,  $[\text{hppH}_2]^+$

## 2.5 Summary

The crystal structure of the cationic {5,5} bicyclic guanidine system was unusual in that it contained both polymeric and tetrameric sequences. Data analysis showed that two components play important roles in determining the long range order. These components are: the angle between the two hydrogen bonds and the deviation of the anion from the planar  $\text{CN}_3^-$  portion of the cation. Reducing of the size of the fused rings in bicyclic guanidines promotes formation of extended hydrogen bonded chains in the solid-state upon conversion to the corresponding hydrochloride salts. During this study, a detailed analysis of the bond parameters within the cations has indicated that  $\pi$ -bonding is more effectively distributed throughout the  $\text{CN}_3$ -core of the  $[\text{hppH}_2]^+$  cation, whilst the retention of electron density is indicated at the tertiary nitrogen atom of the  $[\text{H}_2\text{tbo}]^+$  cation.

## 2.6 References.

1. I. Kaljurand, L. Sooväli, T. Rodima, V. Mäemets, I. Leito, and Ilmar A. Koppel *J. Org. Chem.*, 2005, **70**, 1019-1028.
2. B. Linton and A. Hamilton, I. Majerz, L. Sobczyk, B. Brzezinski, G. Wojciechowski and E. Grech, Kovalenko, *Tetrahedron*, 1999, **55**, 6027-6038.
3. I. Binkowska, A. Katrusiak, G. Wojciechowski, B. Brzezinski, *J. Mol. Struct.*, 2001, **597**, 101-107.
4. A. Jarczewski, J. Koput and A. Jarczewski, *J. Mol. Struct.*, 2006, **788**, 138-144.
5. P. Leibnitz, H. Pietzsch, G. Reck, *Inorganic chemistry*. 2001, **311**, 34-35, 36-38.
6. U. Wild, E. Kaifer, J. Mautz, O. Hubner, H. Wadepohl and H. J. Himmel, *J. Inorg. Chem.*, 2008, 1248.
7. B. Soria, M. Coles and P. Hitchcock, *J. Organomet. Chem.*, 2005, **22**, 2731-2737.
8. A. Meetsma, E. van. F. Bolhuis, H. Wynberg, *J. Chem. Soc.*, 1993, **47**, 1874-1876.
9. K. Wijaya, A. Blaschette and P. G. Jones, *Z. Naturforsch B, Chem. Sci.*, 1999, **54**, 1441-1449.
10. F. Cotton, X. Wang and C. Wilkinson, *Inorg. Chem.*, 2006, **45**, 5493.
11. J. Grogan, M. Grogan, *Org. Lett*, 1999, **1**, 157-160.
12. S. Oakley, M. Coles and P. Hitchcock, *Dalton Trans.*, 2004, 537.

## Chapter 3: Evaluation of the coordination chemistry of the bicyclic guanidinate derived from 1,4,6-triazabicyclo[3.3.0]oct-4-ene.

### 3.1 Introduction

Bicyclic guanidines that contain fused {5:5}-, {5:6}<sup>-1</sup> and {7:5}-, {7:6}<sup>-2</sup> ring systems have recently been reported by Cotton and co-workers, and the family of {6:6}-, bicyclic guanidines has been expanded by the introduction of alkyl substituents to the carbon skeleton.<sup>3</sup> So far, efforts have focused on application of these ligand precursors in the synthesis of new paddle-wheel complexes, although a recent study has been presented in which the anion derived from 1,4,6-triazabicyclo[3.3.0]oct-4-ene (Htbo) was employed as a ligand in gold (I) chemistry.<sup>4</sup> In general our group is interested in the application of these compounds as ligands in coordination chemistry.<sup>5</sup> In this chapter the [tbo]<sup>-</sup> anion (Figure 1) is assessed as a ligand at Li, Al and Zn centres allowing direct structural comparison to be made with their [hpp]<sup>-</sup> analogues.

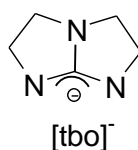
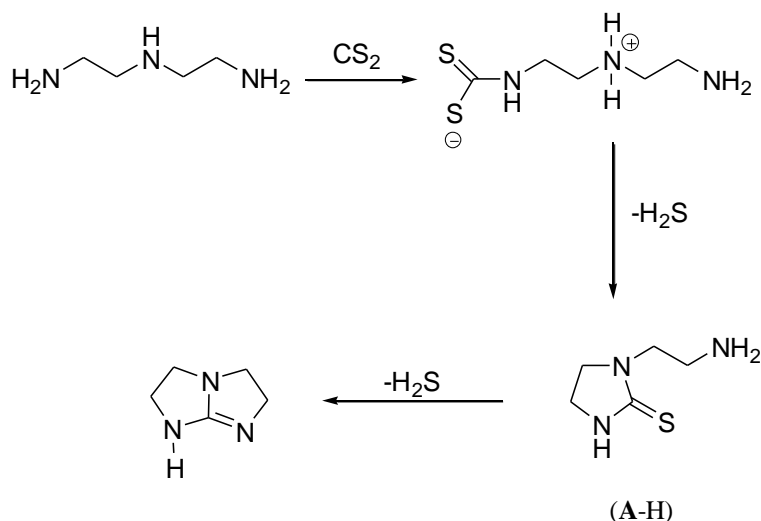


**Figure 1:** Anion derived from 1,4,6-triazabicyclo[3.3.0]oct-4-ene (Htbo)



The Htbo ligand was prepared according to published procedures from the reaction of diethylenetriamine with carbon disulfide, in refluxing *p*-xylene solvent (Scheme 1).<sup>6</sup>



**Scheme 1:** Synthesis of Htbo highlighting the intermediate 1-(2-aminoethyl)-2-imidazolidinethione (**A-H**)

### 3.2 Reaction of Htbo with <sup>n</sup>BuLi

The most common procedure for attaching a guanidinate anion to a metal is *via* salt metathesis between a metal halide and the corresponding lithium (guanidinate). Typically, this method does not involve isolation of the lithium species, which is produced and reacted *in situ* by adding an alkyl lithium reagent to a neutral guanidine in a donor solvent. However, examining the bonding of the [tbo]<sup>−</sup> anion using X-ray crystallography is one of main interests in this chapter, and so attempts were made to isolate Li(tbo) species.

### 3.2.1 General procedure

A general procedure for the reaction of Htbo with  $^n\text{BuLi}$  has been used based on the published procedure of the generation of “Li(hpp)”.<sup>7,8</sup> A sample of the neutral guanidine, Htbo, was dissolved in  $\text{Et}_2\text{O}$  or THF and cooled to  $-78\text{ }^\circ\text{C}$ .  $^n\text{BuLi}$  (1.0 equivalent) was added *via* syringe and the reaction warmed up to room temperature. The solution was filtered to remove any particulate material and crystal growth was attempted under various conditions.

### 3.2.2 Isolation of $[\text{Li}_2(\text{tbo})(\text{A})(\text{Htbo})]$ (**2**)

The first attempted synthesis of  $\text{Li}(\text{tbo})$  involved the lithiation of Htbo in THF at  $-78\text{ }^\circ\text{C}$ , warming to room temperature and after filtering, a small quantity of crystals (**2**) suitable for X-ray analysis were isolated. Due to the low yield no further analysis was obtained on this product. However, the structure is worth describing as it highlights several key features of the chemistry of Htbo.

The molecular structure of (**2**) (Figure 2) corresponds to the formula  $[\text{Li}_2(\text{tbo})(\text{A})(\text{Htbo})]$ , indicating that the batch of Htbo used in this reaction was contaminated with the intermediate monocyclic compound 1-(2-aminoethyl)-2-imidazolidinethione (**A-H**) Scheme 1, which apparently co-sublimes with the guanidine.

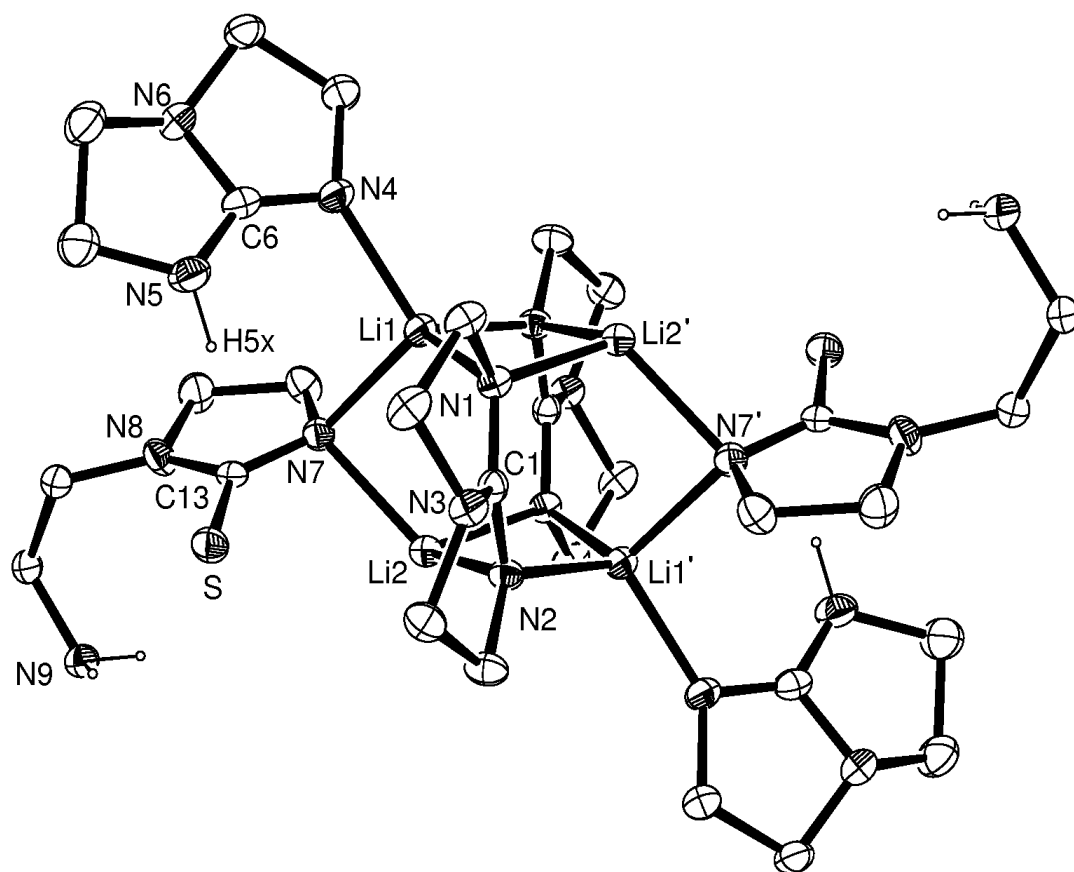


**Figure 2:** Molecular structure of  $[\text{Li}_2(\text{tbo})(\text{A})(\text{Htbo})]_2([\text{2}]_2)$ , with thermal ellipsoids drawn at the 30% level. Hydrogen atoms, except NH of Htbo and  $\text{NH}_2$  of  $[\text{A}]^-$ , are omitted

As expected, 1-(2-aminoethyl)-2-imidazolidinethione) also reacted with  $^n\text{BuLi}$  to produce the corresponding imidazolinethionate anion, and the product was shown to contain a 1:1 ratio of both the  $[\text{tbo}]^-$  and  $[\text{A}]^-$  anions with one equivalent of neutral Htbo.

**Table 1 Selected bond lengths (Å) and bond Angles (°) for Li<sub>2</sub>(tbo)(A)(Htbo)**

Li(1)-N(4)	2.040(3)	Li(2)-N(7)	2.121(3)
Li(1)-N(1)	2.050(3)	S-C(13)	1.7217(18)
Li(1)-N(2)'	2.054(3)	N(1)-C(1)	1.323(2)
Li(1)-N(7)	2.101(3)	N(1)-C(2)	1.483(2)
Li(2)-N(9)''	2.068(4)	N(1)-Li(2)'	2.099(4)
Li(2)-N(1)'	2.099(4)	N(2)-C(1)	1.330(2)
Li(2)-N(2)	2.103(4)	N(2)-C(5)	1.485(2)
N(9)-Li(2)''	2.068(4)	N(2)-Li(1)'	2.054(3)
<b>Bond Angles (°) for Li<sub>2</sub>(tbo)(A)(Htbo)</b>			
C(6)-N(4)-Li(1)	119.81(16)	N(4)-Li(1)-N(1)	113.33(16)
C(7)-N(4)-Li(1)	130.57(16)	N(4)-Li(1)-N(2)'	117.95(15)
C(6)-N(5)-C(10)	108.21(18)	N(1)-Li(1)-N(2)'	102.07(14)
C(6)-N(6)-C(9)	107.99(17)	N(4)-Li(1)-N(7)	103.34(14)
C(6)-N(6)-C(8)	104.90(16)	N(1)-Li(1)-N(7)	116.98(15)
C(9)-N(6)-C(8)	128.51(18)	N(2)''-Li(1)-N(7)	103.39(14)
C(13)-N(7)-C(11)	106.97(15)	N(9)''-Li(2)-N(1)'	106.54(16)
C(13)-N(7)-Li(1)	132.76(15)	N(9)''-Li(2)-N(2)	114.31(16)
C(11)-N(7)-Li(1)	102.66(14)	N(1)''-Li(2)-N(2)	98.83(14)
C(13)-N(7)-Li(2)	105.25(14)	N(9)''-Li(2)-N(7)	105.91(15)
C(11)-N(7)-Li(2)	125.82(15)	N(1)''-Li(2)-N(7)	103.50(14)
Li(1)-N(7)-Li(2)	85.19(13)	N(2)-Li(2)-N(7)	125.43(16)
' -x+1, -y+1, -z+1		" -x+1, -y, -z+1	

The molecular structure of **2** is composed of  $[\text{Li}_2(\text{tbo})(\text{A})(\text{Htbo})]_2$  dimers that are formed through the generation of two  $\text{Li}_2\text{N}_2$  units that form a pseudo-cubic central core (Figure 2). The  $[\text{tbo}]^-$  anion bonds to four lithium atoms in a similar facz-capping coordination ( $\kappa^{1,2}\text{N}-\kappa^{3,4}\text{N}'$ ) to that observed in  $[\text{hpp}]^-$  supported cubic-based frameworks of lithium atoms.<sup>7,8</sup> Anion (**A**) bonds to two lithium atoms through the deprotonated N-atom of the imidazolidinethione ring (N7), and the neutral Htbo bonds to a single lithium through the imine group (N4). Additional interactions in the dimeric structure of **2** include  $[\text{NH}5\text{x}\cdots\text{S}]$  hydrogen bonds to sulphur that distort the tetrahedral geometry of (Li1) (e.g.  $\text{N4-Li-N7}=103.34(14)^\circ$ ). Finally  $[\textbf{2}]_2$  units are bonded into a one dimensional chain *via* macrocyclic  $[(\text{C}_3\text{N}_2\text{S})\text{CH}_2\text{CH}_2\text{NH}_2\text{Li}]_2$  structures, with the  $\text{Li2-N9''}$  bonds of 2.068(4) Å suggesting strong links (Figure 3).

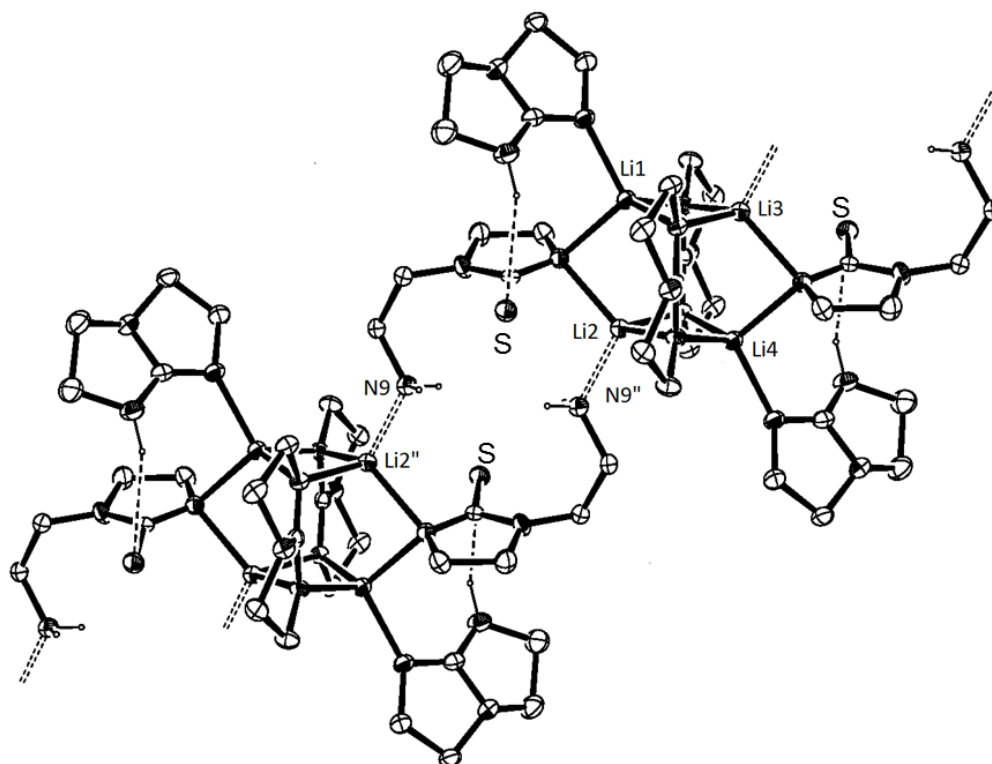


**Figure 3:** Chain structure of the  $[\text{Li}_2(\text{tbo})(\text{A})(\text{Htbo})]_4$ . ( $[\textbf{2}]_4$ ) with thermal ellipsoids drawn at the 30% level.

The carbon–nitrogen bonds within the amidine component of the neutral Htbo are more localized than in the anion, that is clearly shown by the greater value for  $\Delta_{\text{CN}}$  (Htbo, 0.058 Å;  $[\text{tbo}]^-$ , 0.007 Å). In contrast to the  $\pi$ -delocalization typically observed throughout the  $\text{CN}_3$  core of the  $[\text{hpp}]^-$  anion (Figure 6 Chapter 1), examination of carbon–nitrogen distances shows that the distance from the central carbon to the non-bonding nitrogen in  $[\text{tbo}]^-$  is relatively long [ $\text{C1-N3} = 1.407(2)$  Å], resulting in a large  $\Delta'_{\text{CN}}$  value of 0.081 Å. This is consistent with preservation of electron-density at N3, and is supported by the high degree of pyramidalization (DP= 29.1%) at this atom. To put these values into context, the corresponding results for fourteen independent examples of the  $[\text{hpp}]^-$  anion with the same  $\text{K}^{1,2}\text{N-K}^{3,4}\text{N}'$ -bonding mode in lithium clusters gave a range of  $\Delta'_{\text{CN}}$  from 0.008 Å to 0.065 Å, and a maximum DP value of 1.7%.<sup>7,8</sup>

### 3.2.3 Synthesis of $\text{Li}_6(\text{tbo})_6(\text{Htbo})_3$ (**3**)

In order to remove the A-H contaminant from the Htbo, a new batch of ligand was made and the sublimation was performed twice on the product. Using the pure sample of Htbo with (1.0 equivalent)  $^n\text{BuLi}$  and allowing the reaction to stir for 15 h at room temperature, colourless crystals (**3**) appropriate for analysis by X-ray diffraction were isolated. Elemental analysis of the crystalline solid indicated a Li: tbo: tboH ratio of 2:2:1. Spectroscopic analysis of **3** was not possible due to the low solubility of the product. The structure was shown by X-ray diffraction to be  $\text{Li}_6(\text{tbo})_6(\text{Htbo})_3$  which shows that the deprotonation is incomplete, affording mixed guanidinate-guanidine salt (Figure 4).



These neutral ligands are further secured by hydrogen bonds between the NH and either a nitrogen from the amidinate component of a bridging [tbo]<sup>−</sup> anion (N7 and N16) or to the non-bonding nitrogen of a capping ligand (N3).

**Table 2 Selected bond lengths (Å) and Bond Angles (°) for Li<sub>6</sub>(tbo)<sub>6</sub>(Htbo)<sub>3</sub>.**

Li(1)-N(7)	2.010(3)	N(4)-C(7)	1.486(2)
Li(1)-N(10)	2.063(4)	N(5)-C(6)	1.327(2)
Li(1)-N(1)	2.100(3)	N(5)-C(10)	1.479(2)
Li(1)-N(5)	2.122(3)	N(6)-C(6)	1.405(2)
Li(1)-C(16)	2.717(4)	N(6)-C(9)	1.453(3)
Li(2)-N(10)	2.035(3)	N(6)-C(8)	1.455(3)
Li(2)-N(16)	2.036(3)	N(7)-C(11)	1.330(2)
Li(2)-N(2)	2.108(3)	N(7)-C(12)	1.481(3)
Li(2)-N(4)	2.114(3)	N(8)-C(11)	1.312(2)
Li(3)-N(25)	2.020(3)	N(8)-C(15)	1.474(3)
Li(3)-N(4)	2.043(3)	N(9)-C(11)	1.409(2)
Li(3)-N(19)	2.118(3)	N(9)-C(14)	1.445(3)
Li(3)-N(2)	2.183(3)	N(9)-C(13)	1.449(3)
Li(3)-C(1)	2.778(3)	N(10)-C(16)	1.321(2)
Li(4)-N(22)	2.023(3)	N(10)-C(17)	1.479(2)
Li(4)-N(5)	2.042(3)	N(11)-C(16)	1.316(2)
Li(4)-N(19)	2.056(3)	N(11)-C(20)	1.482(2)
Li(4)-N(1)	2.179(3)	N(12)-C(19)	1.379(3)



Li(5)-N(13)	1.994(4)	N(12)-C(18)	1.383(3)
Li(5)-N(8)	2.002(4)	N(12)-C(16)	1.400(2)
Li(5)-N(11)	2.049(4)	N(13)-C(21)	1.321(2)
Li(5)-C(20)	2.768(4)	N(13)-C(22)	1.467(2)
Li(6)-N(14)	1.971(4)	C(39)-N(24)	1.467(5)
Li(6)-N(17)	1.987(4)	C(39)-C(40)	1.513(4)
Li(6)-N(11)	2.032(4)	N(1)-C(2)	1.489(2)
Li(6)-N(2)	2.624(4)	N(2)-C(1)	1.329(2)
N(1)-C(1)	1.324(2)	N(2)-C(5)	1.492(2)
N(3)-C(1)	1.410(2)	N(3)-C(4)	1.465(2)
N(3)-C(3)	1.467(2)	N(4)-C(6)	1.325(2)
<b>Bond Angles (°) for Li<sub>6</sub>(tbo)<sub>6</sub>(Htbo)<sub>3</sub>.</b>			
N(22)-Li(4)-N(19)	111.17(15)	N(7)-Li(1)-N(10)	111.21(15)
N(5)-Li(4)-N(19)	108.87(14)	N(7)-Li(1)-N(1)	111.47(15)
N(22)-Li(4)-N(1)	121.42(15)	N(10)-Li(1)-N(1)	115.11(15)
N(5)-Li(4)-N(1)	101.77(14)	N(7)-Li(1)-N(5)	112.55(16)
N(19)-Li(4)-N(1)	106.52(14)	N(10)-Li(1)-N(5)	104.17(14)
N(13)-Li(5)-N(8)	119.16(18)	N(1)-Li(1)-N(5)	101.77(14)
N(13)-Li(5)-N(11)	106.48(16)	N(7)-Li(1)-C(16)	94.09(13)
N(8)-Li(5)-N(11)	115.44(17)	N(10)-Li(1)-C(16)	28.07(7)
N(13)-Li(5)-C(20)	89.71(13)	N(1)-Li(1)-C(16)	104.21(13)
N(8)-Li(5)-C(20)	103.69(15)	N(5)-Li(1)-C(16)	132.19(14)

N(11)-Li(5)-C(20)	31.57(8)	Li(4)-Li(1)-C(16)	149.54(15)
N(14)-Li(6)-N(17)	114.40(18)	N(10)-Li(2)-N(16)	113.58(16)

The overall arrangement of lithium atoms in  $\text{Li}_6(\text{tbo})_6(\text{Htbo})_3$  is therefore best described as two intersecting  $\text{Li}_4$ -planes with a fold angle of  $68.81^\circ$  at Li1 and Li2 (Figure 5). This is somewhat unusual given the propensity for lithium guanidinate species to aggregate into three dimensional structures,<sup>7-8</sup> although in the majority of these cases an interstitial ion is present, the structural importance of which is unknown. The guanidinate centred at C1 effectively blocks the lithium atoms wrapping around to form a more compact cluster and, although long to be considered a ‘true bond’ (N1-Li5 and N2-Li6 distances = 2.76 Å and 2.62 Å, respectively) there is likely to be an electrostatic interaction between these atoms.

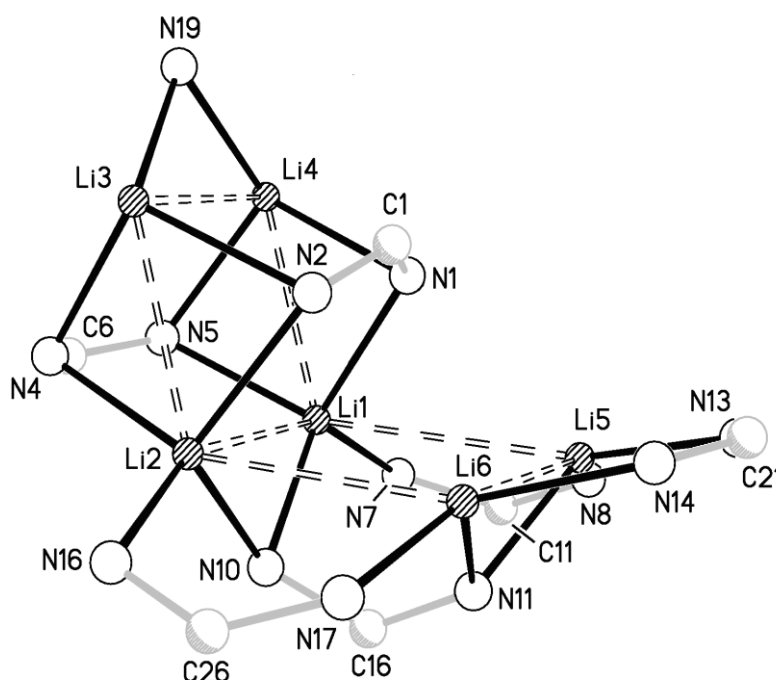


**Figure 5:**  $\text{Li}_6$ -core arrangement in  $\text{Li}_6(\text{tbo})_6(\text{Htbo})_3$

Result of examining the bonding parameters for the guanidinate component of (**3**) as shown in [Table 3] once again note relatively large  $\Delta_{\text{CN}}$  values (range 0.079–0.096 Å) with predominantly pyramidal non-bonding nitrogen atoms. The relatively low DP value of 8.3% for N12 is due to the ligand being effectively sandwiched between two additional guanidates, forcing the substituents into the plane of the nitrogen atom. This sterically induced configuration does not, however, appear to promote delocalization of the lone-pair into the  $\text{CN}_3$  core to any great extent, as the  $\Delta_{\text{CN}}$  value is unexceptional for this class of anion.

**Table 3** Summary of bonding parameters within the  $[\text{tbo}]^-$  and Htbo ligands of  $\text{Li}_6(\text{tbo})_6(\text{Htbo})_3$

Atoms	Bonding type	$\Delta_{\text{CN}}/\text{\AA}$	$\Delta'_{\text{CN}}/\text{\AA}$	DP
C1 N1–3	$\text{K}^{1,2}\text{N}-\text{K}^{3,4}\text{N}'-$	0.005	0.084	N3: 26.8% $[\text{tbo}]^-$
C6 N4–6	$\text{K}^{1,2}\text{N}-\text{K}^{3,4}\text{N}'-$	0.002	0.079	N6: 25.7% $[\text{tbo}]^-$
C11 N7–9	$\text{K}^1\text{N}-\text{K}^2\text{N}'-$	0.018	0.088	N9: 29.6% $[\text{tbo}]^-$
C16 N10–12	$\text{K}^{1,2}\text{N}-\text{K}^{3,4}\text{N}'-$	0.005	0.082	N12: 8.3% $[\text{tbo}]^-$
C21 N13–15	$\text{K}^1\text{N}-\text{K}^2\text{N}'-$	0	0.094	N15: 29.3% $[\text{tbo}]^-$
C26 N16–18	$\text{K}^1\text{N}-\text{K}^2\text{N}'-$	0.017	0.096	N18: 30.8% $[\text{tbo}]^-$
C31 N19–21	$\text{K}^{1,2}\text{N}-$	0.062	—	N20: 20.6% Htbo
C36 N22–24	$\text{K}^1\text{N}-$	0.066	—	— Htbo
C41 N25–27	$\text{K}^1\text{N}-$	0.049	—	N27: 24.9% Htbo

### 3.3 Synthesis of [Al(tbo)Me<sub>2</sub>] (4)

The reaction between Htbo and AlMe<sub>3</sub> was carried out using a similar procedure to that outlined in section 3.2.3 for the reaction with <sup>n</sup>BuLi. AlMe<sub>3</sub> was added dropwise to Htbo in Et<sub>2</sub>O at -78 °C. After warming to room temperature, the solution was stirred for 15 h, filtered and maintained at room temperature yielding colourless crystals (4) suitable for X-ray analysis. The crystals analyzed by elemental analysis as the mono-guanidinate complex, Al(tbo)Me<sub>2</sub> (4). <sup>1</sup>H and <sup>13</sup>C NMR spectroscopy showed two resonances for the annular methylene groups of the guanidinate ligand and a single high field singlet for the AlMe<sub>2</sub> groups, [δ -0.26 ppm] consistent with a symmetric species in solution. The highest mass peak in the EI-mass spectrum (319 amu), however, corresponded to [Al<sub>2</sub>(tbo)<sub>2</sub>Me]<sup>+</sup>, formed by loss of a methyl group from the dimer, [4]<sub>2</sub>.

#### 3.3.2 Crystallographic details and crystal structure of [Al(tbo)Me<sub>2</sub>]<sub>2</sub> [4]<sub>2</sub>

X-ray crystallographic analysis confirms that [Al(tbo)Me<sub>2</sub>]<sub>2</sub> is dimeric in the solid-state (Figure 6).

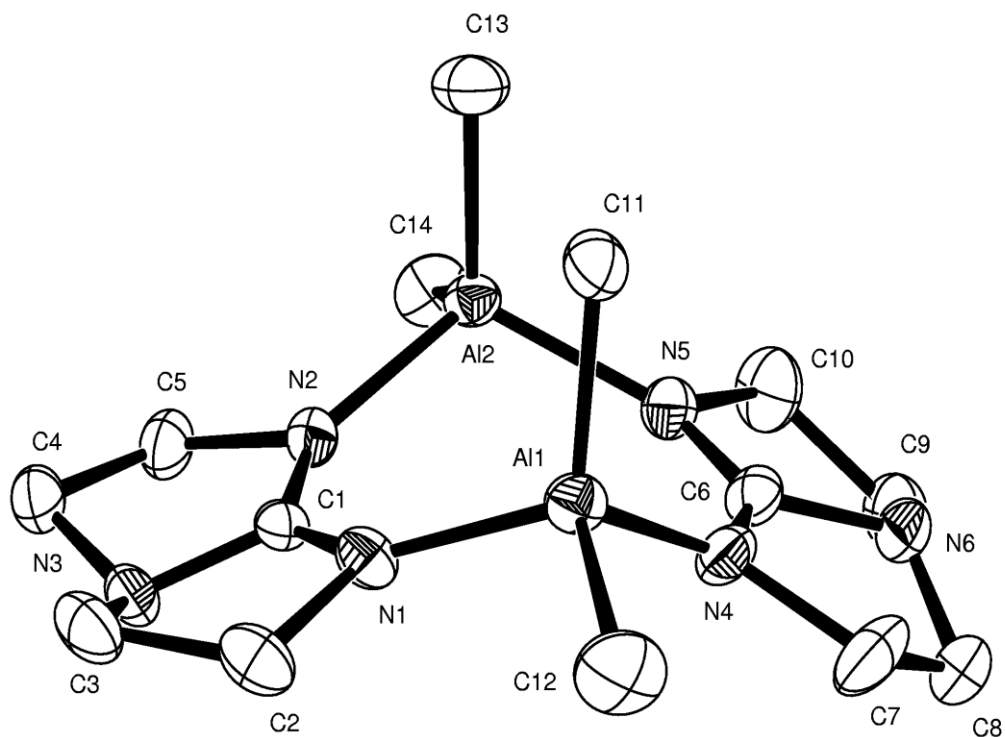


**Figure 6:** Molecular structure of  $[\text{Al}(\text{tbo})\text{Me}_2]_2 [\mathbf{4}]_2$  with thermal ellipsoids drawn at the 30% level.

**Table 4** Selected bond lengths (Å) and angles (°) for  $[\text{Al}(\text{tbo})\text{Me}_2]_2 [\mathbf{4}]_2$

Al(1)-N(1)	1.9026(14)	Al(1)-N(4)	1.9143(15)
Al(1)-C(11)	1.9605(17)	Al(2)-C(13)	1.9644(17)
Al(1)-C(12)	1.9790(18)	Al(2)-C(14)	1.9747(17)
N(1)-C(1)	1.329(2)	N(4)-C(6)	1.326(2)
N(2)-C(1)	1.3244(19)	N(5)-C(6)	1.326(2)
N(3)-C(1)	1.3837(19)	C(6)-N(6)	1.403(2)
Al(2)-N(2)	1.9084(13)	Al(2)-N(5)	1.9166(13)

N(1)-Al(1)-N(4)	108.04(6)	N(2)-Al(2)-N(5)	109.86(6)
N(1)-Al(1)-C(11)	112.88(7)	N(2)-Al(2)-C(13)	110.83(7)
N(4)-Al(1)-C(11)	110.85(7)	N(5)-Al(2)-C(13)	113.62(7)
N(1)-Al(1)-C(12)	104.76(8)	N(2)-Al(2)-C(14)	105.10(7)
N(4)-Al(1)-C(12)	104.92(8)	N(5)-Al(2)-C(14)	103.40(7)
C(11)-Al(1)-C(12)	114.82(9)	C(13)-Al(2)-C(14)	113.48(8)
C(1)-N(1)-C(2)	105.45(13)	C(6)-N(4)-C(7)	105.44(14)
C(1)-N(1)-Al(1)	137.08(10)	C(6)-N(4)-Al(1)	134.98(11)
C(2)-N(1)-Al(1)	117.40(10)	C(7)-N(4)-Al(1)	117.77(12)
C(1)-N(2)-C(5)	105.47(12)	C(6)-N(5)-C(10)	105.27(13)
C(1)-N(2)-Al(2)	138.42(10)	C(6)-N(5)-Al(2)	138.61(11)
C(5)-N(2)-Al(2)	115.80(10)	C(10)-N(5)-Al(2)	116.03(11)
C(1)-N(3)-C(4)	106.64(12)	C(6)-N(6)-C(9)	108.09(15)
C(1)-N(3)-C(3)	106.34(13)	C(6)-N(6)-C(8)	104.9(2)
C(4)-N(3)-C(3)	124.81(13)	C(9)-N(6)-C(8)	128.65(19)
N(2)-C(1)-N(1)	132.68(13)	N(5)-C(6)-N(4)	132.83(14)
N(2)-C(1)-N(3)	113.70(13)	N(5)-C(6)-N(6)	112.26(15)
N(1)-C(1)-N(3)	113.61(13)	N(4)-C(6)-N(6)	114.91(15)

The guanidinate ligand in  $[4]_2$  bridges two aluminium centers in an analogous  ${}_K^1N-{}_K^2N'$ -mode to that of the guanidinate in the  $[hpp]^-$  compound,<sup>9</sup> to generate an eight-membered metallacycle. In contrast, however, a ‘boat-like’ form is adopted in  $[4]_2$  rather than the less sterically congested ‘chair’ in  $[Al(hpp)Me_2]_2$  (Figure 7).

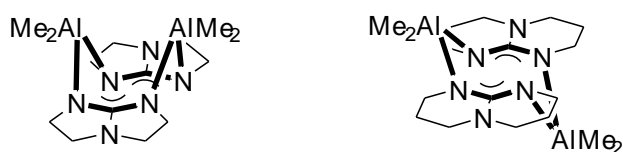
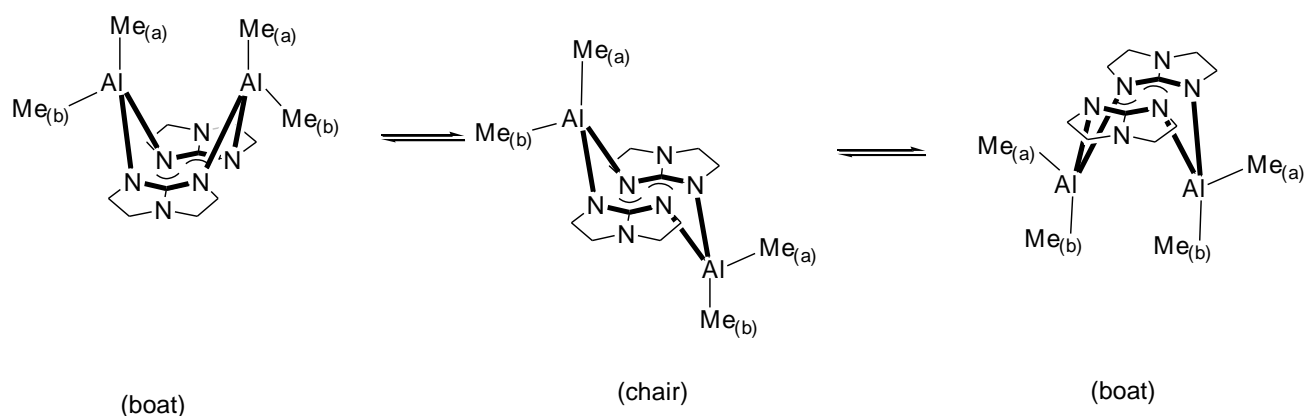


**Figure 7:** Boat and chair conformation for  $[Al(tbo)Me_2]_2$   $[4]_2$  and  $[Al(hpp)Me_2]_2$

The boat conformation can not be present as a rigid structure in solution, as only a single environment is noted for the  $AlMe_2$  group in  $^1H$  and  $^{13}C$  NMR spectra. The different methyl environments in the solid-state do not resolve in the  $^1H$  NMR spectrum upon cooling a sample (toluene) to  $-40\text{ }^\circ\text{C}$ . Although rupture and reformation of the metallacycle cannot be ruled out, this fluxional behavior is most likely explained by a rapid chair-to-boat conformational change (Scheme 2).



**Scheme 2:** A rapid chair and boat conformation exchanging Me(a) and Me(b) positions.

The boat conformation of  $[4]_2$  is similar to that in  $[Al(N\{2-C_5H_4N\}Ph)Me_2]_2$ <sup>13</sup> while  $[Al(hpp)Me_2]_2$ ,<sup>10</sup> and  $[Al(MeC\{NMe\}_2)Me_2]_2$ ,<sup>11</sup> have a chair conformation. The geometry of the aluminium atoms is close to tetrahedral with interligand angles in the range 103.40(7) Å.-114.82(9) Å. In particular, the C(11)–Al(1)–C(12) angle [114.82(9)°] is significantly larger than the corresponding angles in  $[Al(hpp)Me_2]_2$ , [111.01(1)°] and  $[Al(MeC\{NMe\}_2)Me_2]_2$ , [112.5(1)°]. The Al–N distances in  $[4]_2$  (1.9055 Å average) are very similar to those in  $[Al(hpp)Me_2]_2$ , [1.916(2) Å],  $[Al(MeC\{NMe\}_2)Me_2]_2$ , [1.925(2) Å] and  $[Al(N\{2-C_5H_4N\}Ph)Me_2]_2$  [1.94745(18) Å].

As expected, the  $\Delta_{CN}$  values for the  $[tbo]^-$  anions are negligible, consistent with delocalization across the amidinate part. A much greater pyramidalization (DP = 24.7 % for both N3 and N6) is noted than for the corresponding non-bonding nitrogen in the  $[hpp]^-$  analogue (DP = 0 %). The increased electron density at the bonding nitrogen atoms in  $[hpp]^-$  would be expected to give shorter Al–N distances.<sup>13</sup> However this electronic effect is



compensated for by a reduced steric bulk of the  $[\text{tbo}]^-$  ligand, resulting trivial differences in the average Al–N distances.

### 3.4 Synthesis of $\text{Zn}_3(\text{tbo})_4\text{Me}_2$ (**5**)

The syntheses of  $\text{Zn}_3(\text{tbo})_4\text{Me}_2$  (**5**) was accomplished *via* the addition of a solution of  $\text{ZnMe}_2$  dropwise to  $\text{Htbo}$  in toluene at  $-78\text{ }^\circ\text{C}$  (1:1) equivalent. After warming to room temperature, the mixture was stirred at ambient conditions for 18 h, affording a cloudy solution. Heating to  $80\text{ }^\circ\text{C}$  and filtering gave a clear solution that was allowed to cool slowly to room temperature, affording colourless crystals (**5**) appropriate for analysis by X-ray diffraction. Elemental analysis revealed a ratio of Zn, tbo and Me, 3:4:2, consistent with  $\text{Zn}_3(\text{tbo})_4\text{Me}_2$  (**5**). The NMR spectra showed two distinct environments for the guanidinate ligand most evident from the  $^{13}\text{C}$  NMR spectrum. Two resonances at  $\delta$  182.2 and 178.5 were observed for the  $\text{CN}_3$  atom, with  $\text{CH}_2$  groups resonating at  $\delta$  55.8, 55.7, 50.8 and 48.8. These data are consistent with two types of symmetrically bound  $[\text{tbo}]^-$  ligand (a & b, Figure 8) rather than a single non-symmetrically bound  $[\text{tbo}]^-$  (c, Figure 8).

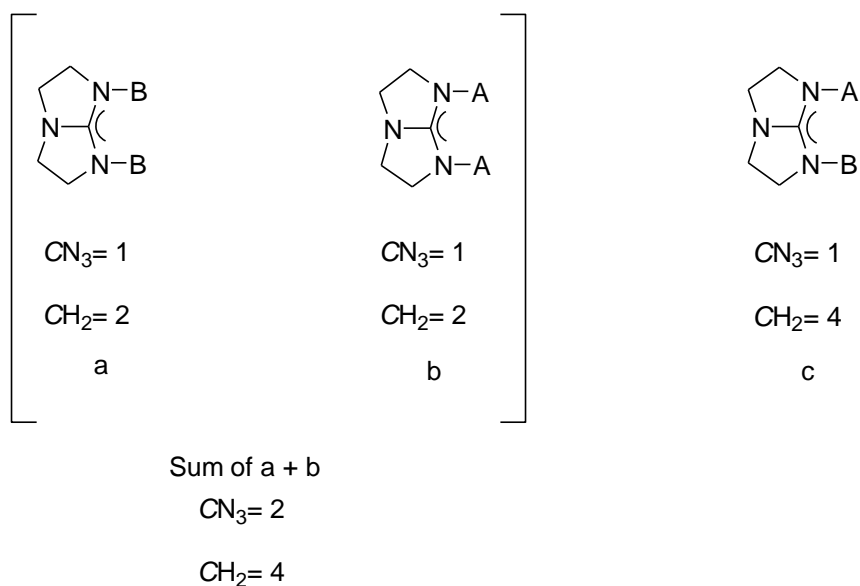


**Figure 8:** Type and number of carbon environments for bridging [tbo]<sup>−</sup> ligands

### 3.4.1 Crystallographic details and crystal structure of Zn<sub>3</sub>(tbo)<sub>4</sub>Me<sub>2</sub> (**5**)

Formation of trimetallic complex, Zn<sub>3</sub>(tbo)<sub>4</sub>Me<sub>2</sub> (**5**) was confirmed by X-ray diffraction analysis, and shows that the molecular structure of Zn<sub>3</sub>(tbo)<sub>4</sub>Me<sub>2</sub> is analogous to that formed from the reaction between hppH and ZnMe<sub>2</sub>.<sup>14</sup> The molecular structure contains a distorted trigonal planar group of three zinc atoms with two types of symmetrically bridging [tbo]<sup>−</sup> ligand in agreement with spectroscopic data (Figure 9).

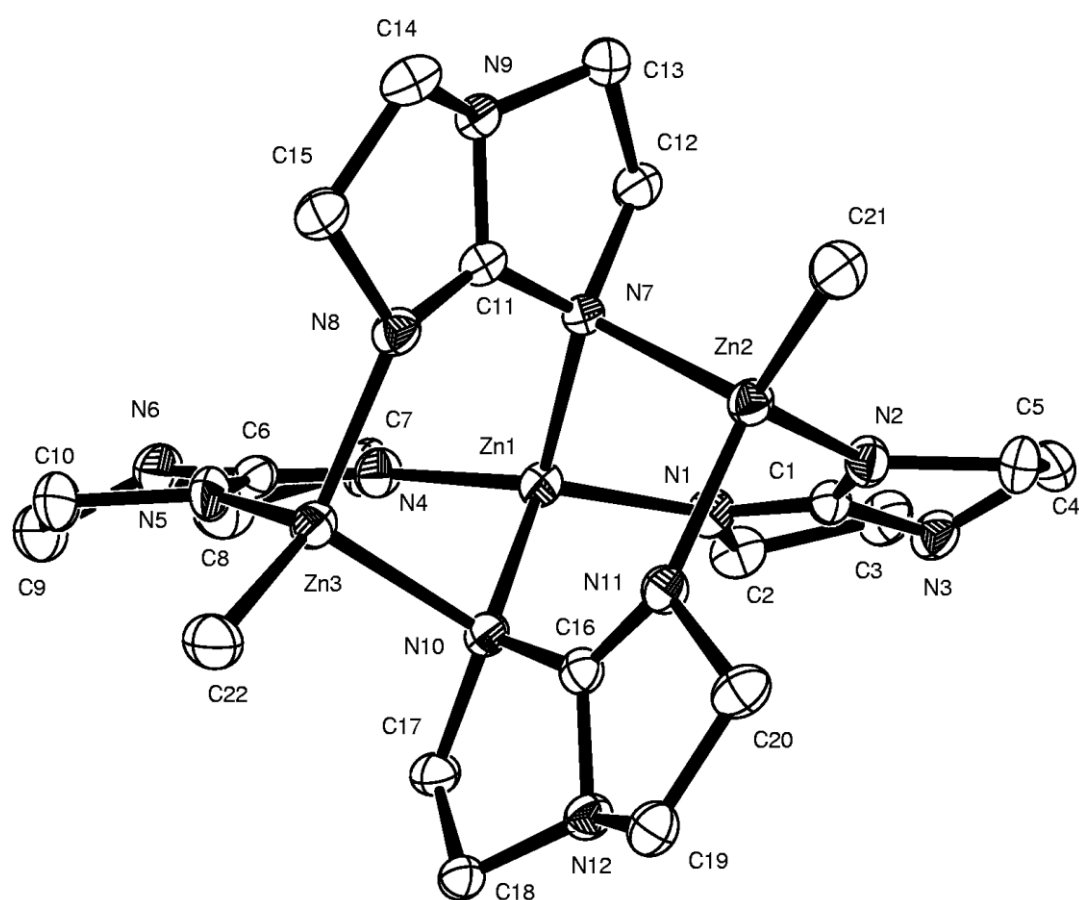


**Figure 9:** Molecular structure of  $\text{Zn}_3(\text{tbo})_4\text{Me}_2$  (**5**) with thermal ellipsoids drawn at the 30% level. Hydrogen atoms and toluene solvate molecules are omitted

**Table 5** Selected bond lengths (Å) and angles (°) for  $\text{Zn}_3(\text{tbo})_3\text{Me}_2$  (**5**)

Zn(1)-N(4)	1.956(6)	N(1)-C(1)	1.336(10)
Zn(1)-N(1)	1.963(6)	N(2)-C(1)	1.314(10)
Zn(1)-N(7)	2.027(6)	N(3)-C(1)	1.406(10)
Zn(1)-N(10)	2.056(7)	N(4)-C(6)	1.324(11)
Zn(2)-C(21)	1.972(8)	N(5)-C(6)	1.310(12)
Zn(2)-N(2)	2.006(6)	N(6)-C(6)	1.390(11)

Zn(2)-N(11)	2.019(6)	N(7)-C(11)	1.381(9)
Zn(2)-N(7)	2.204(6)	N(8)-C(11)	1.297(10)
Zn(3)-C(22)	1.969(10)	N(9)-C(11)	1.373(9)
Zn(3)-N(8)	2.009(7)		
Zn(3)-N(5)	2.025(8)		
Zn(3)-N(10)	2.193(6)		
N(4)-Zn(1)-N(1)	117.6(3)	C(1)-N(1)-Zn(1)	121.9(5)
N(4)-Zn(1)-N(7)	116.5(3)	C(2)-N(1)-Zn(1)	131.7(5)
N(1)-Zn(1)-N(7)	102.2(3)	C(1)-N(2)-Zn(2)	129.7(5)
N(4)-Zn(1)-N(10)	101.6(3)	C(5)-N(2)-Zn(2)	125.6(5)
N(1)-Zn(1)-N(10)	117.0(3)	C(6)-N(4)-Zn(1)	123.2(6)
N(7)-Zn(1)-N(10)	101.3(2)	C(7)-N(4)-Zn(1)	129.3(6)
C(21)-Zn(2)-N(2)	116.4(4)	C(6)-N(5)-Zn(3)	130.3(5)
C(21)-Zn(2)-N(11)	120.0(4)	C(10)-N(5)-Zn(3)	124.4(7)
N(2)-Zn(2)-N(11)	103.4(3)	C(11)-N(7)-C(12)	104.4(6)
C(21)-Zn(2)-N(7)	116.9(3)	C(11)-N(7)-Zn(1)	118.7(5)
N(2)-Zn(2)-N(7)	95.7(2)	C(12)-N(7)-Zn(1)	118.0(5)
N(11)-Zn(2)-N(7)	100.7(2)	C(11)-N(7)-Zn(2)	107.3(5)
C(22)-Zn(3)-N(8)	122.2(4)	C(12)-N(7)-Zn(2)	107.1(4)
C(22)-Zn(3)-N(5)	114.4(4)	Zn(1)-N(7)-Zn(2)	100.5(2)
N(8)-Zn(3)-N(5)	104.6(3)	C(11)-N(8)-Zn(3)	125.8(5)
C(22)-Zn(3)-N(10)	114.7(4)	C(15)-N(8)-Zn(3)	123.8(5)
N(8)-Zn(3)-N(10)	101.7(2)	C(16)-N(10)-Zn(1)	117.3(5)
N(5)-Zn(3)-N(10)	95.2(3)	C(17)-N(10)-Zn(1)	118.5(5)

N(2)-C(1)-N(1)	132.4(7)	C(16)-N(10)-Zn(3)	109.6(5)
N(5)-C(6)-N(4)	131.4(7)	C(16)-N(11)-Zn(2)	127.2(5)
N(11)-C(16)-N(10)	129.6(7)	C(20)-N(11)-Zn(2)	121.0(5)
Zn(1)-N(10)-Zn(3)	100.3(3)		

Each of the zinc centres has a tetrahedral geometry; two of the centres (Zn2 and Zn3) retain a methyl substituent with the third (Zn1) bound only by nitrogen. The guanidates centred about C1 and C6 bridge zinc atom in a  $\kappa^1\text{N}, \kappa^2\text{N}'$ -coordination, the remaining two anions centered at C11 and C16 are present in a  $\kappa^{1,2}\text{N}, \kappa^3\text{N}'$ -coordination to all three metal atoms.

From (Figure 10) we can see the inter-metal distance of  $[\text{hpp}]^-$  anion is smaller than the  $[\text{tbo}]^-$  analogue. We can explain this difference in simple geometric terms by the fact that the angle between the outward projecting orbitals is greater for two fused pentagons versus two hexagons. This is analogous to the wide projection of  $\text{NH}\cdots\text{Cl}$  hydrogen bonds for  $[\text{H}_2\text{tbo}]^+$  noted in the previous chapter.

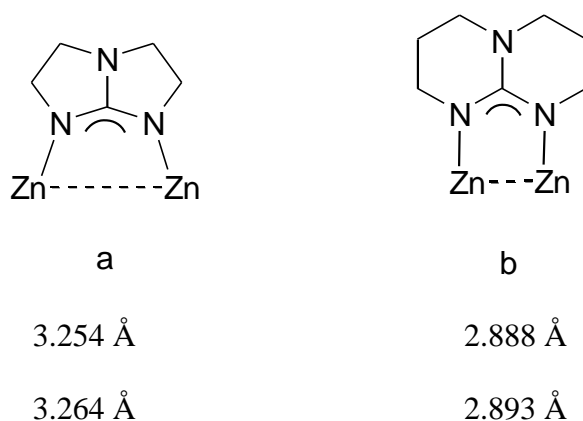
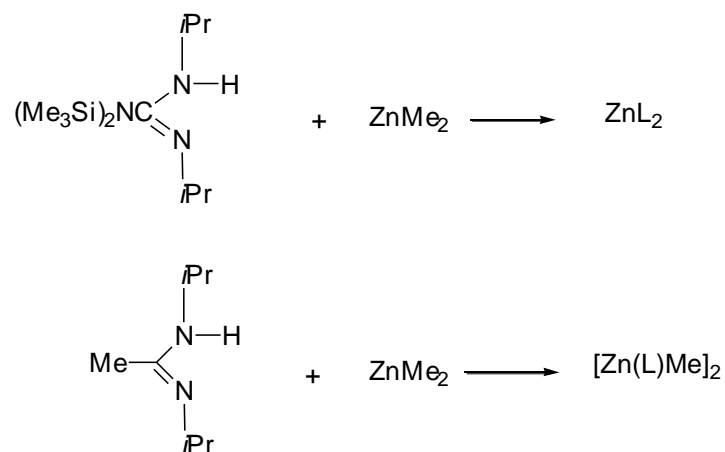


**Figure 10:** Crystallographically determined zinc $\cdots$ zinc distances for  $\text{Zn}_3(\text{L})_4\text{Me}_2$  (a)  $\text{L} = [\text{tbo}]^-$ , (b)  $\text{L} = [\text{hpp}]^-$

Significant differences are noted in the structural patterns between (**5**) and the products obtained with acyclic guanidines (Scheme 3).<sup>15</sup>



**Scheme 3:** Synthesis of zinc guanidinate complexes

According to these previous observations the 1:1 reaction between Htbo and  $\text{ZnMe}_2$  should yield  $[\text{Zn}(\text{tbo})_2]$  or  $[\text{Zn}(\text{tbo})\text{Me}]_2$ . Compound **5** may be considered as combination of their two predicted structures consisting of  $\text{Zn}(\text{L})_2 + 2 \text{Zn}(\text{L})\text{Me}$  ( $= \text{Zn}_3(\text{L})_4\text{Me}_2$ ).

Although the mechanism of the formation of **5** has not been studied in detail, it represent a stable core structure, and has also observed for the product of the reaction between  $\text{ZnMe}_2$  and  $(p\text{-tol})\text{NH}(2\text{-C}_6\text{H}_4\text{N})$ .<sup>14</sup>

### 3.6 Conclusions

Deprotonation of Htbo with  $n\text{BuLi}$  generated the guanidinate anion,  $[\text{tbo}]^-$  which is an effective ligand at lithium, aluminium and zinc centres, with bridging between metals a preferred coordination mode in each case. Using the same conditions used for hppH, which affords  $[\text{Li}(\text{hpp})]$  the corresponding reaction with Htbo does not appear to go to completion under mild reaction conditions, and formation of the mixed guanidinate:guanidine complex (**3**)  $\text{Li}_6(\text{tbo})_6(\text{Htbo})_3$  resulted. Examination of the structural parameters of the  $[\text{tbo}]^-$  guanidinate in the metal complexes reported in this study clearly demonstrates retention of electron density at the non-bonding nitrogen atom, as shown by the large degree of pyramidalization at the non-bonded nitrogen. Other structural differences are also noted between the compounds formed with  $[\text{tbo}]^-$  and their  $[\text{hpp}]^-$  analogues. The metallacycle in the dimeric aluminium compound  $[\text{Al}(\text{tbo})\text{Me}_2]_2$  (**4**), forms a ‘boat’ in the solid-state meaning there are differences in energy arising from crystal packing forces, as spectroscopic measurements indicate that this spatial arrangement is not maintained in solution. With the trimetallic zinc complex  $\text{Zn}_3(\text{tbo})_4\text{Me}_2$ , (**5**) the significant increase in the inter-metallic  $\text{Zn}\cdots\text{Zn}$  distance compared with  $\text{Zn}_3(\text{hpp})_3\text{Me}_2$  is attributed to a wider projection of donor orbitals. This will be very important in the further development of coordination compounds incorporating to  $[\text{tbo}]^-$  anion.

### 3.7 References

1. F. Cotton, X. Wang and C. Wilkinson, *Inorg.Chem.* 2006, **45**, 5493.
2. F. Cotton, A. Murillo, X. Wang and C. Wilkinson *Dalton Trans.*, 2006, 4623.

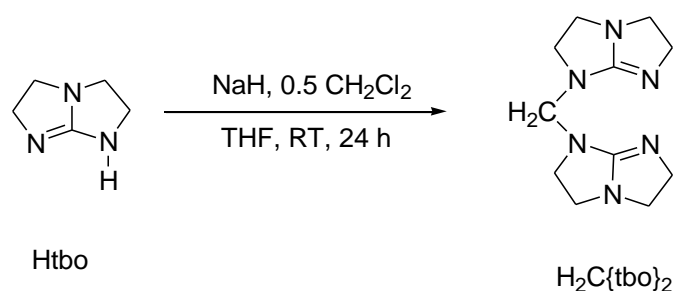
3. F. Cotton, A. Murillo, X. Wang and C. Wilkinson, *Dalton Trans.*, 2007, 3943.
4. A. Mohamed, A. Mayer, H. Abdou, M. Irwin, L. Pérez and J. Fackler, *Inorg. Chem.*, 2007, **46**, 11165.
5. M. Coles, *Dalton Trans.*, 2006, 985.
6. F. Cotton, C. Murillo and R. Walton, *Multiple Bonds between Metal Atoms*, Science and Business Media Inc., New York, 2005.
7. S. Boss, M. Coles, R. Haigh, P. Hitchcock, R. Snaith and A. Wheatley, *Angew. Chem., Int. Ed.*, 2003, **42**, 5593.
8. M. Coles and P. Hitchcock, *Chem. Commun.*, 2005, 3165.
9. S. Aeilts, M. Coles, D. Swenson, R. Jordan, *Organometallics*, 1998, **17**, 3265.
10. P. Longhi, R. Drago, *Inorg. Chem.* 1965, **4**, 11.
11. M. Coles, D. Swenson and R. Jordan, *Organometallics*, 1998, **17**, 4042.
12. H. Hausen, F. Gerstner and W. Schwarz, *Organometallics*, 1997, **16**, 5183.
13. D. Armstrong, R. Davies, J. Linton, R. Snaith, P. Schooler and A. Wheatley. *Dalton Trans.*, 2001, **39**, 2843.
14. S. Birch, S. Boss, S. Cole, M. Coles, R. Haigh, P. Hitchcock and A. Wheatley, *Dalton Trans.*, 2004, 3568.
15. M. Coles and P. Hitchcock, *Eur. J. Inorg. Chem.*, 2004, 2662.



## **Chapter 4: Linked bis(guanidine) compounds and their application as bidentate ligands**

## 4.1 Synthesis of $\text{H}_2\text{C}\{\text{tbo}\}_2$ (**6**)

In an analogous procedure to that used for the synthesis of  $\text{H}_2\text{C}\{\text{hpp}\}_2$ ,<sup>1</sup> deprotonation of Htbo with one equivalent of NaH in the presence of 0.5 equivalent of  $\text{CH}_2\text{Cl}_2$  gives the methylene linked bis compound  $\text{H}_2\text{C}\{\text{tbo}\}_2$  **6** (Scheme 1).



**Scheme 1:** Synthesis of methylene linked bis guanidine  $\text{H}_2\text{C}\{\text{tbo}\}_2$  (**6**)

$^1\text{H}$  NMR spectroscopy data showed four resonances for the annular methylene protons, and a single resonance for  $\text{H}_2\text{C}\{\text{tbo}\}_2$  at 4.76 ppm (Figure 1). These data indicate that the methylene groups within “tbo” are inequivalent, consistent with a static structure in solution. Furthermore mass spectrometry  $[\text{EI}]^+$  analysis showed a fragment at 234  $[\text{m/z}]$  for  $\text{H}_2\text{C}\{\text{tbo}\}_2$ . Elemental analysis revealed a ratio of N, H and C consistent with  $\text{H}_2\text{C}\{\text{tbo}\}_2$ . Crystals suitable for an X-ray study were isolated by crystallization from  $\text{Et}_2\text{O}$  at  $-30\text{ }^\circ\text{C}$ . (Figure 2).

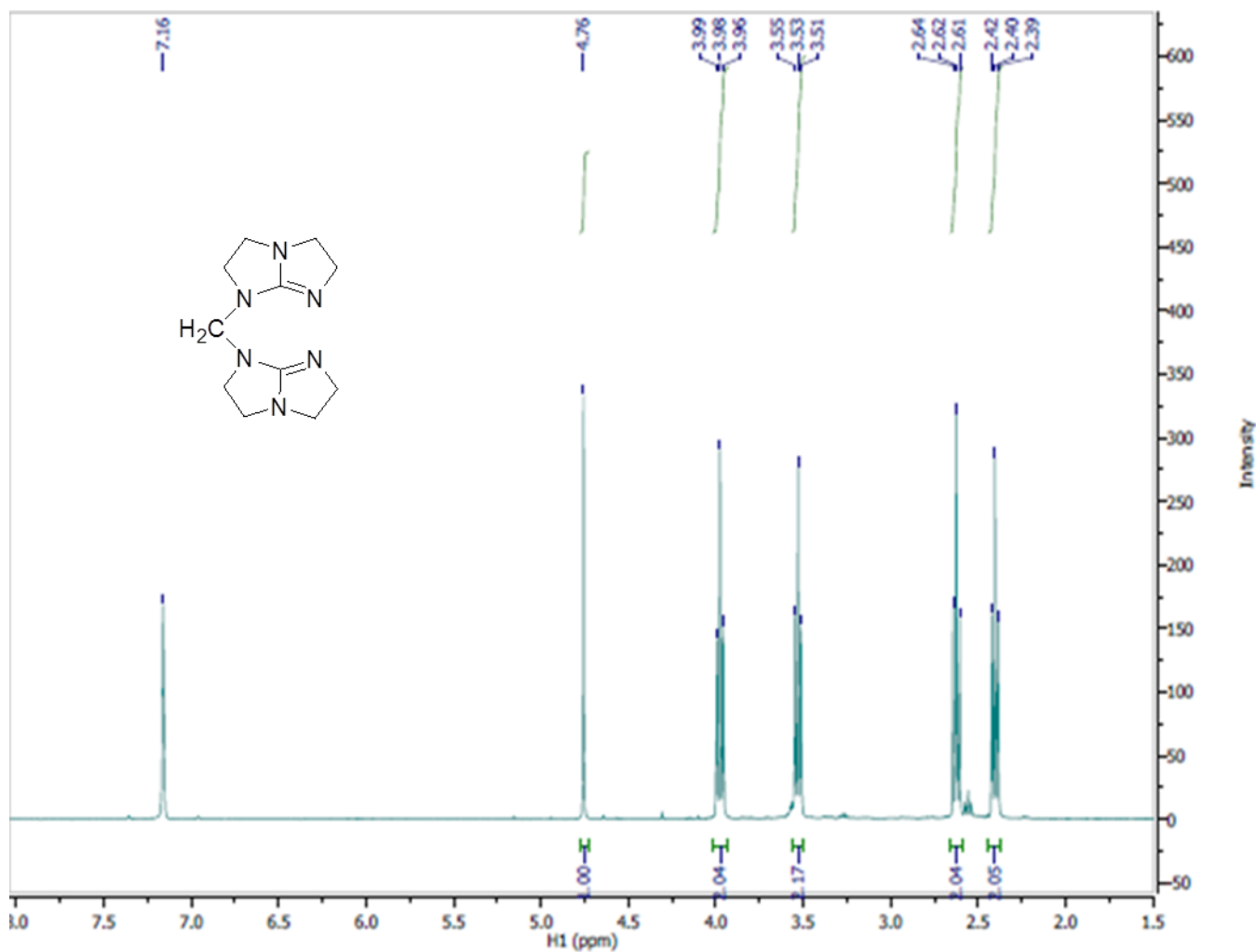


**Figure 1:**  $^1\text{H}$  NMR spectrum of  $\text{H}_2\text{C}\{\text{tbo}\}_2$  (**6**) (400 MHz,  $\text{d}_6$ -benzene, 303K)

#### 4.1.1 Crystallographic details and crystal structure of $\text{H}_2\text{C}\{\text{tbo}\}_2$ (**6**)

Single crystal X-ray diffraction has been used to determine the molecular structure of  $\text{H}_2\text{C}\{\text{tbo}\}_2$  allowing comparison with the  $\text{H}_2\text{C}\{\text{hpp}\}_2$  analogue.<sup>1</sup> The  $\text{H}_2\text{C}\{\text{hpp}\}_2$  molecule lies on a crystallographic 2-fold rotation axis through the bridging methylene. Crystallographically, the two guanidyl fragments in **6** are however distinct, with carbon-

nitrogen bond lengths consistent with isolated C–N single and C=N double bonds ( $\Delta_{\text{CN}}$  range: 0.07 Å–0.10 Å).<sup>1</sup> The distance from the central carbon to the non-bonding nitrogen is relatively long [1.3881(19) Å] and [1.387(2) Å], resulting in large  $\Delta'_{\text{CN}}$  values of 0.0815 Å and 0.022 Å. This observation is consistent with retention of electron-density at the non-bonding nitrogen atoms.

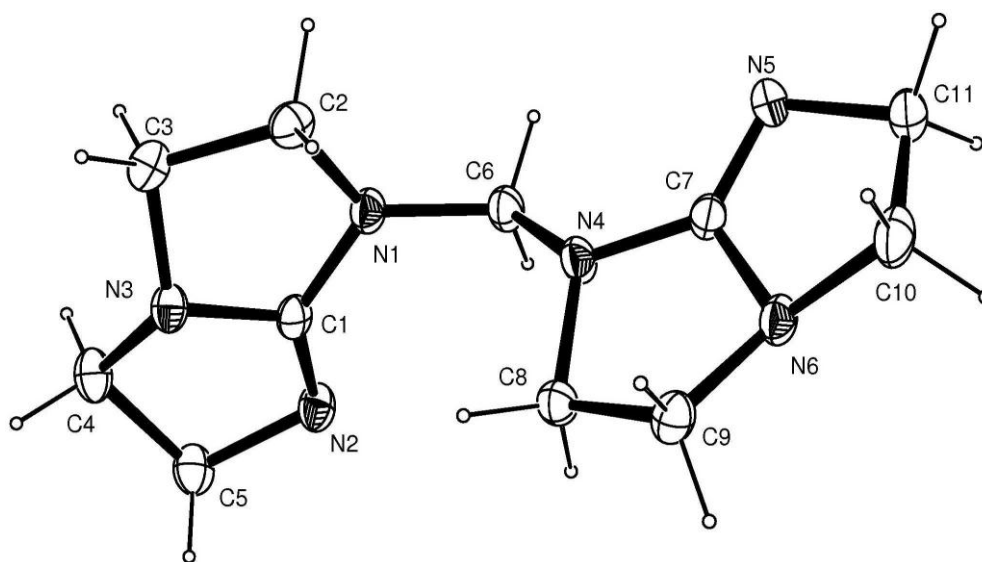


**Figure 2:** ORTEP representation of the structure of  $\text{H}_2\text{C}\{\text{tbo}\}_2$  with thermal ellipsoids drawn at the 30% level.

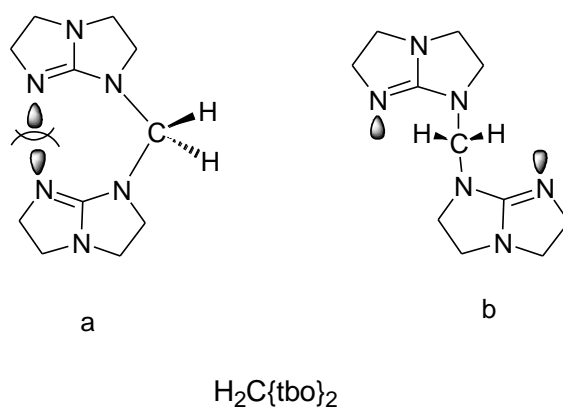


**Figure 3:** Conformation of  $\text{H}_2\text{C}\{\text{tbo}\}_2$  to prevent steric interference of the  $\text{N}_{\text{imine}}$  lone pairs

In order to act as a chelating ligand both nitrogen lone pairs must point in the same direction (Figure 3a). In the absence of the metal, however, the guanidine groups point in opposing directions about the  $\text{CH}_2$  bridgehead (Figure 3b). This is also noted in  $\text{H}_2\text{C}\{\text{hpp}\}_2$  to minimize the interaction between the lone-pairs in the  $\text{N}_{\text{imine}}$  atoms.

## 4.2 Generation of $\text{H}_2\text{C}\{\text{tbo}\}_2 \cdot \text{H}_2\text{O}$ (**6'**)

On one occasion, crystallization of **6** gave needle-like crystals in contrast to the usual prisms. X-ray molecular structure of the needles showed that the linked guanidine was bonded to one molecule of  $\text{H}_2\text{O}$  from N5 giving  $\text{H}_2\text{C}\{\text{tbo}\}_2 \cdot \text{H}_2\text{O}$  (**6'**) (Figure 4). Analysis of the bond lengths and angles show that these have been not affected compared with **6** (Table 1). In **6'**, the  $\text{H}_2\text{C}\{\text{tbo}\}_2$  molecules are linked into chains by the hydrogen-bonded water molecules with typical  $\text{N} \cdots \text{H}$  distances 2.94 Å and 2.91 Å. (Figure 5).

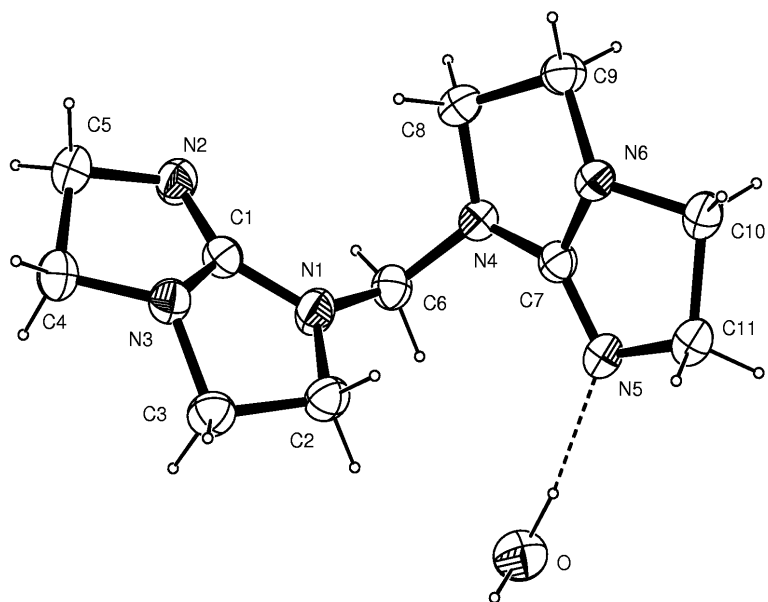


**Figure 4:** ORTEP representation of the structure of  $\text{H}_2\text{C}\{\text{tbo}\}_2 \cdot \text{H}_2\text{O}$  (6') with thermal ellipsoids drawn at the 30% level.

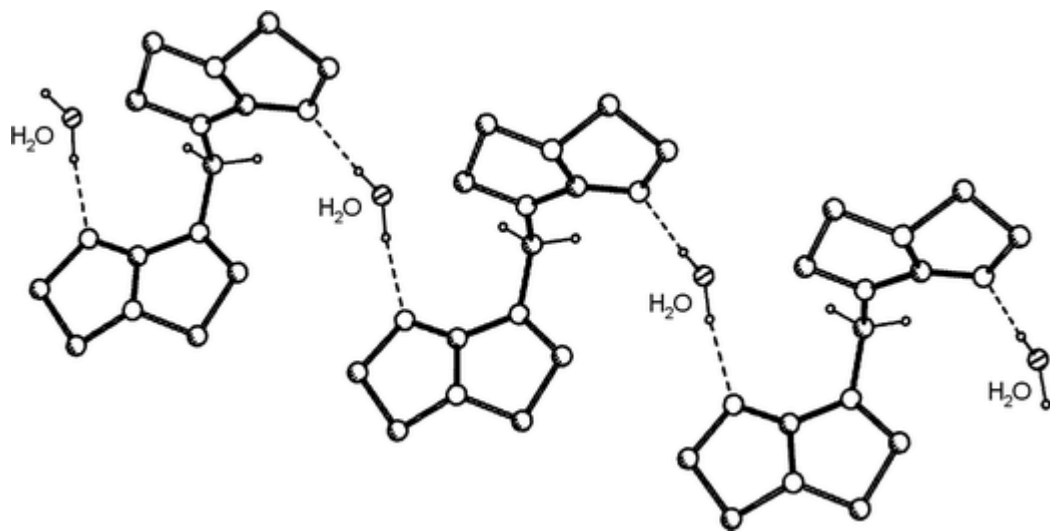


**Figure 5:** Hydrogen bonded chains of  $\text{H}_2\text{C}\{\text{tbo}\}_2 \cdot \text{H}_2\text{O}$  (6')

In contrast to the hpp derivative,  $\text{H}_2\text{C}\{\text{tbo}\}_2$  was stable towards water demonstrated by the structural characterization of the mono-hydrate  $\text{H}_2\text{C}\{\text{tbo}\}_2\cdot\text{H}_2\text{O}$  containing the intact  $\text{H}_2\text{C}\{\text{tbo}\}_2$  unit.

**Table 1 Selected bond lengths (Å) and angles (°) for  $\text{H}_2\text{C}\{\text{tbo}\}_2$  (**6**)**

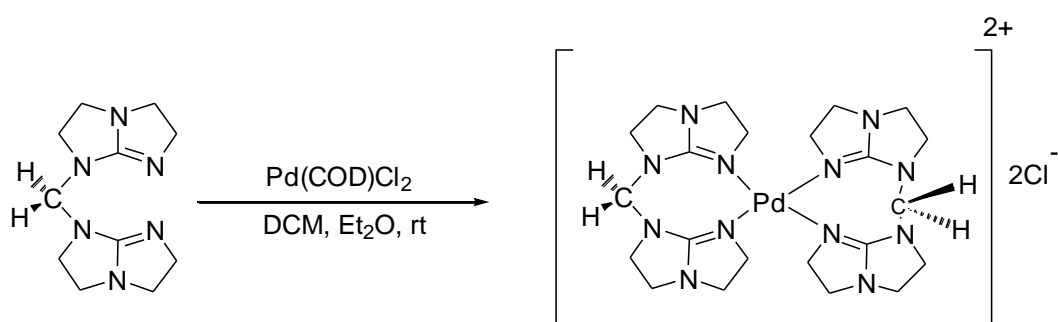
**Table 1** Selected bond lengths (Å) and angles (°) for  $\text{H}_2\text{C}\{\text{tbo}\}_2$  (**6**) and  $\text{H}_2\text{C}\{\text{tbo}\}_2\cdot\text{H}_2\text{O}$  (**6'**)

	$\text{H}_2\text{C}\{\text{tbo}\}_2$ ( <b>6</b> )	$\text{H}_2\text{C}\{\text{tbo}\}_2\cdot\text{H}_2\text{O}$ ( <b>6'</b> )
C1-N1	1.3676(19)	1.362(3)
C1-N2	1.2861(19)	1.287(2)
C1-N3	1.3881(19)	1.389(3)
C7-N4	1.3604(18)	1.380(3)
C7-N5	1.290(2)	1.284(2)
C7-N6	1.387(2)	1.378(3)
C6-N1	1.4343(19)	1.448(3)
C6-N4	1.4499(19)	1.446(3)
N1-C1-N2	131.79(14)	132.45(19)
N1-C1-N3	109.39(13)	109.13(16)
N2-C1-N3	118.62(13)	118.30(18)
C1-N3-C3	107.42(12)	107.09(15)
C1-N3-C4	103.32(11)	103.53(15)
C3-N3-C4	125.03(13)	124.38(17)
N4-C7-N5	131.72(14)	131.62(19)

N4-C7-N6	109.35(13)	109.94(16)
N5-C7-N6	118.83(13)	118.33(18)
C7-N6-C9	107.92(12)	108.13(15)
C7-N6-C10	103.67(13)	105.08(16)
C9-N6-C10	127.28(13)	127.01(17)

### 4.3 Synthesis of [Pd (H<sub>2</sub>C{tbo}<sub>2</sub>)<sub>2</sub>] [Cl]<sub>2</sub> (7)

Palladium metal and the H<sub>2</sub>C{tbo}<sub>2</sub> ligand were chosen because the structure of the corresponding H<sub>2</sub>C{hpp}<sub>2</sub> complex is known, allowing comparisons of the chemistry to be drawn.<sup>2</sup> The reaction of H<sub>2</sub>C{tbo}<sub>2</sub> with PdCl<sub>2</sub>(COD) in DCM was therefore performed (Scheme 2).



**Scheme 2:** Synthesis of [Pd (H<sub>2</sub>C{tbo}<sub>2</sub>)<sub>2</sub>] [Cl]<sub>2</sub> **7**



An orange powder formed on mixing the two reagents that was purified through layering a saturated dichloromethane solution with Et<sub>2</sub>O at room temperature. The result was formation of red prismatic crystals. In contrast to the analogous H<sub>2</sub>C{hpp}<sub>2</sub> reaction, which afforded the mono-ligand compound PdCl<sub>2</sub>(H<sub>2</sub>C{hpp}<sub>2</sub>),<sup>2</sup> elemental analysis of these crystals was consistent with the *bis*-ligand complex. The reaction was therefore repeated with 2 equivalents of H<sub>2</sub>C{tbo}<sub>2</sub>, forming the same product in greater yield. The low solubility of the isolated product, initially hampered acquisition of NMR data. Finally, NMR data were obtained in D<sub>2</sub>O, showing the protons of the bridging CH<sub>2</sub> split as an AB pattern at [ $\delta$  7.06 and 4.73 ppm; <sup>2</sup>J<sub>HH</sub> = 16.0 Hz], indicative of ligand coordination.

#### 4.3.1 Crystallographic details and crystal structure of [Pd(H<sub>2</sub>C{tbo}<sub>2</sub>)<sub>2</sub>][Cl]<sub>2</sub> (7)

X-ray diffraction studies showed that the molecular structure of **7** consists of the ionized product [Pd(H<sub>2</sub>C{tbo}<sub>2</sub>)<sub>2</sub>][Cl]<sub>2</sub> (Figure 6) with 6 molecules of dichloromethane solvent included in the lattice.

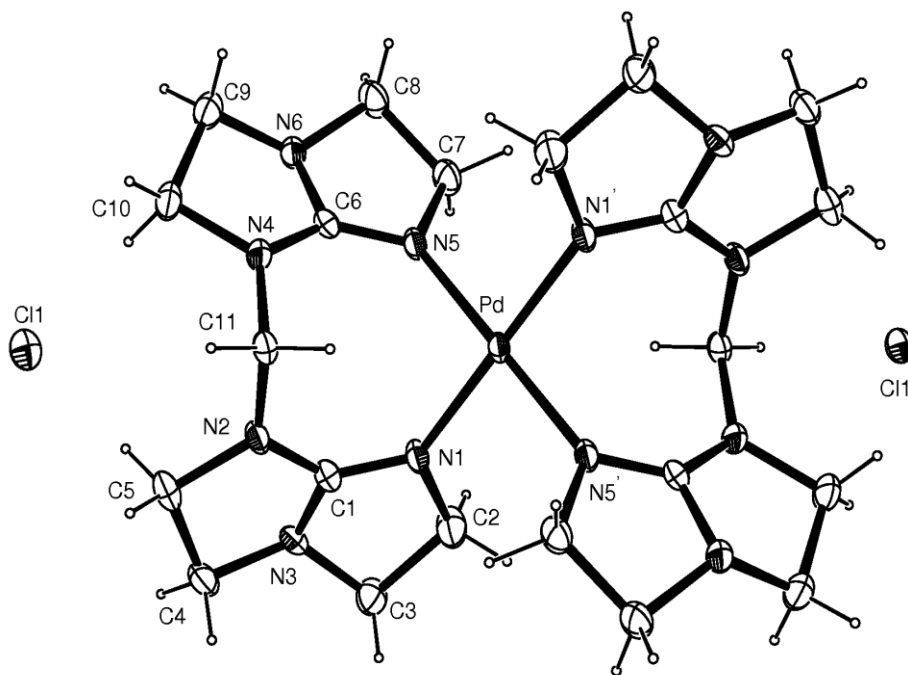


**Figure 6 :** ORTEP representation of the structure of  $[\text{Pd} (\text{H}_2\text{C}\{\text{tbo}\}_2)_2][\text{Cl}]_2$  **7** with thermal ellipsoids drawn at the 30% level. (' -x+1/2,-y+1/2,-z+1 " -x+1,y,-z+3/2)

In the structure of **7**, the doubly charged palladium centre is chelated to each of the *bis*-guanidyl ligands, with the chloride counter ions hydrogen bonded to dichloromethane solvate molecules (Figure 7a & b). The resulting metal geometry is square planar, in which palladium sits at an inversion centre with a range of bond angles  $87.55(14)^\circ$  -  $92.45(14)^\circ$ , and the two metallacycles project above and below the plane of  $\text{PdN}_4$  (Figure 7a). The Pd–N distances in either neutral or cationic palladium complexes of  $\text{H}_2\text{C}\{\text{hpp}\}_2$  are shorter than those in **7** [ $2.011(3)$  Å and  $2.014(3)$  Å] (Table 2)<sup>1</sup>, despite the formally doubly charged metal centre. Within the guanidyl groups, bond lengths and angles are consistent with retention of electron density at the tertiary amino nitrogens. This is supported by the DP% values [ $\text{N3} = 23.9\%$ ;

N6 = 23.4%], which are much greater than those of the remaining nitrogen atoms [less than 2.5%].

**Table 2** Selected bond lengths (Å) and angles (°) for [Pd (H<sub>2</sub>C{tbo}<sub>2</sub>)<sub>2</sub>][Cl]<sub>2</sub> (**7**)

Pd(1)-N(1)	2.011(3)	C(1)-N(3)	1.363(10)
Pd(1)-N(5)	2.014(3)	N(5)-C(6)	1.294(5)
N(1)-C(1)	1.302(5)	N(6)-C(6)	1.371(5)
N(2)-C(1)	1.336(6)	N(4)-C(6)	1.340(5)
N(1)-Pd(1)-N(1)'	180.000(1)	N(1)-Pd(1)-N(5)	92.45(14)
N(1)-Pd(1)-N(5)'	87.55(14)	N(1)'-Pd(1)-N(5)	87.55(14)
N(1)'-Pd(1)-N(5)'	92.45(14)	N(5)'-Pd(1)-N(5)	180.00(9)
C(1)-N(1)-Pd(1)	130.3(3)	N(5)-C(6)-N(4)	133.1(4)
C(2)-N(1)-Pd(1)	123.6(3)	N(5)-C(6)-N(6)	115.5(4)
C(6)-N(5)-Pd(1)	130.3(3)	N(2)-C(11)-N(4)	114.8(4)
C(7)-N(5)-Pd(1)	123.9(3)	N(1)-C(1)-N(2)	133.5(4)

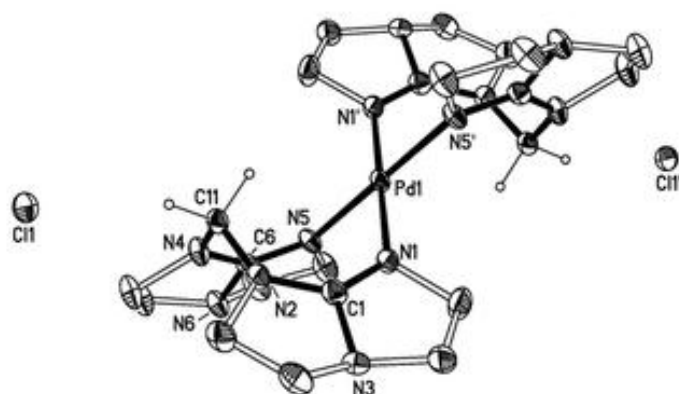


**Figure 7a:** Thermal ellipsoid plot (30%) of  $[\text{Pd}(\text{H}_2\text{C}\{\text{tbo}\}_2)_2][\text{Cl}]_2$  **7** Hydrogens except those of the bridging methylene group and dichloromethane solvates omitted.

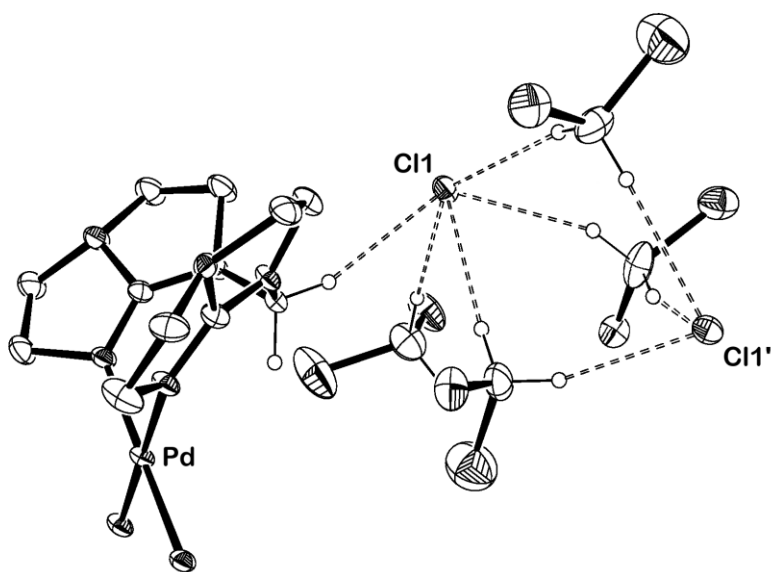
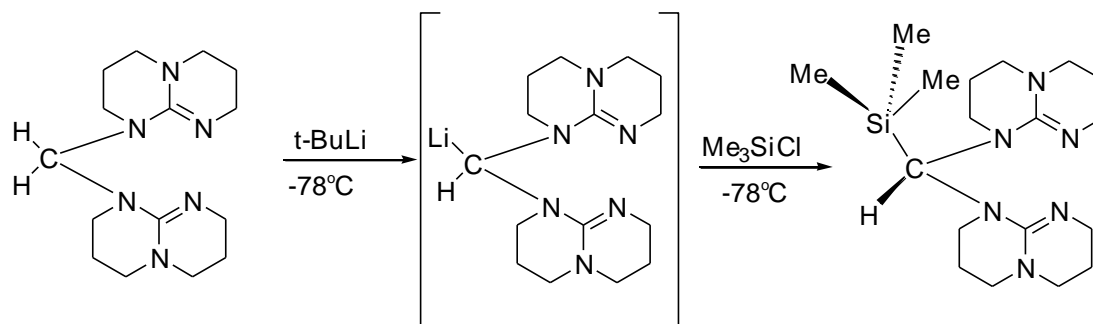


**Figure 7b:** Thermal ellipsoid plot (30%) of a portion of the crystal structure of **7**, showing hydrogen bonding of dichloromethane solvate molecules.

#### 4.4 Synthesis of (Me<sub>3</sub>Si)HC{hpp}<sub>2</sub> (**8**)

The modification of H<sub>2</sub>C{hpp}<sub>2</sub> by substitution on the central carbon atom was investigated. The H<sub>2</sub>C{hpp}<sub>2</sub> was reacted with <sup>t</sup>BuLi, at -78 °C, with a colour change from yellow to dark red observed immediately on addition of the <sup>t</sup>BuLi. All attempts to isolate the presumed carbanionic intermediate failed, so the reaction was quenched at -78°C using Me<sub>3</sub>SiCl (Scheme 3).



**Scheme 3:** Proposed synthesis of (Me<sub>3</sub>Si)HC{hpp}<sub>2</sub>

Clear, colourless crystals of **8** were obtained in a good yield from toluene at -30 °C. <sup>1</sup>H NMR spectroscopy showed six resonances for the annular methylene groups of the guanidine component and a single high field singlet for the SiMe<sub>3</sub> groups, [δ 0.25 ppm] consistent with a symmetric species in solution. The highest mass peak in the EI-mass spectrum is 362 amu.

#### 4.5.2 Crystallographic details and crystal structure of (Me<sub>3</sub>Si)HC{hpp}<sub>2</sub> (**8**)

The solid-state structure was solved by X-ray diffraction analysis for (**8**) of crystals grown from toluene -30 °C. A summary of bond lengths (Å) and angles (°) is shown in Table 4. The gross structural features of the compound consist of distorted tetrahedral Si atom bound by three methyl groups and the bridgehead carbon atom, with angles in the range of 98.39(6)°-120.39(6)° (Figure 8).

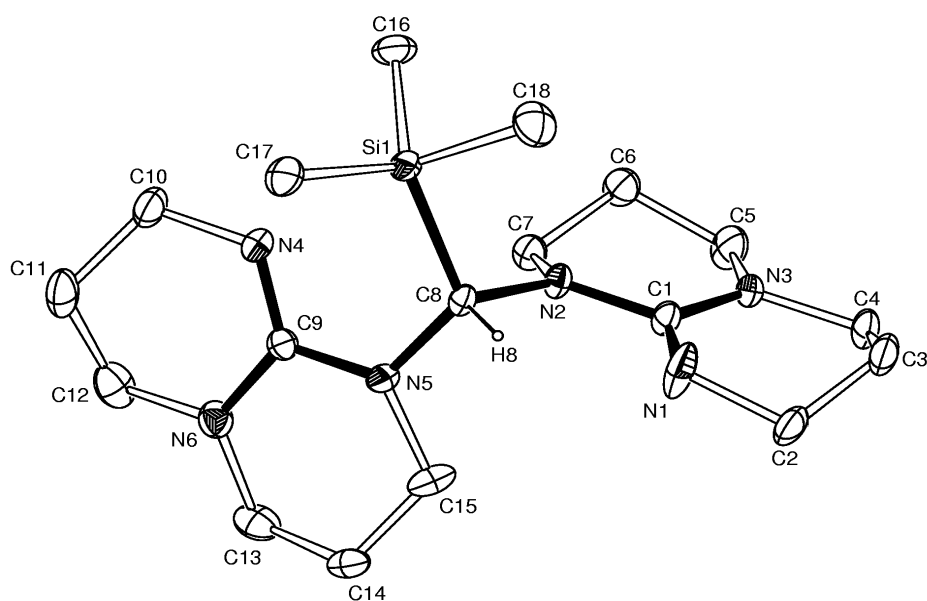


**Figure 8:** ORTEP representation of the structure of (Me<sub>3</sub>Si)HC{hpp}<sub>2</sub> (**8**) with thermal ellipsoids drawn at the 30% level

**Table 3:-** Bond length (Å) and angles (°) for (Me<sub>3</sub>Si)HC{hpp}<sub>2</sub> (**8**)

Si-C(17)	1.8695(13)	N(5)-C(15)	1.474(5)
Si-C(16)	1.8744(14)	N(6)-C(9)	1.3762(16)
Si-C(18)	1.9021(15)	C(1)-N(1)	1.305(7)
Si-C(8)	1.9076(11)	N(1)-C(2)	1.472(6)
N(2)-C(1)	1.3922(14)	N(2)-C(7)	1.4553(15)
N(3)-C(1)	1.3814(15)	N(2)-C(8)	1.4745(13)
N(3)-C(4)	1.435(12)	N(4)-C(9)	1.2892(16)
N(3)-C(5)	1.4491(19)	N(4)-C(10)	1.4608(16)
N(5)-C(9)	1.3797(15)	N(5)-C(8)	1.4603(14)
C(17)-Si-C(16)	114.75(7)	N(1)-C(1)-N(2)	117.3(3)
C(17)-Si-C(18)	102.89(7)	N(3)-C(1)-N(2)	115.56(11)
C(16)-Si-C(18)	101.56(8)	N(3)-C(5)-C(6)	111.98(11)
C(17)-Si-C(8)	114.39(6)	N(5)-C(8)-N(2)	112.23(9)
C(16)-Si-C(8)	120.39(6)	N(5)-C(8)-Si	119.23(7)
C(18)-Si-C(8)	98.32(6)	N(2)-C(8)-Si	109.56(7)
C(1)-N(2)-C(7)	121.05(9)	N(4)-C(9)-N(6)	125.82(11)
C(1)-N(2)-C(8)	119.31(9)	N(4)-C(9)-N(5)	116.96(11)
C(7)-N(2)-C(8)	117.24(9)	N(6)-C(9)-N(5)	117.09(10)
C(1)-N(3)-C(4)	117.8(4)	C(1)-N(1)-C(2)	116.8(5)

C(1)-N(3)-C(5)	124.58(11)	C(8)-N(5)-C(15)	113.04(17)
C(4)-N(3)-C(5)	115.5(4)	C(9)-N(6)-C(12)	118.41(11)
C(9)-N(4)-C(10)	119.09(12)	C(9)-N(6)-C(13)	121.1(2)
C(9)-N(5)-C(8)	119.57(9)	C(12)-N(6)-C(13)	117.3(2)
C(9)-N(5)-C(15)	122.90(19)	N(1)-C(1)-N(3)	126.7(3)

The hpp-groups of (Me<sub>3</sub>Si)HC{hpp}<sub>2</sub> are oriented as noted previously in H<sub>2</sub>C{hpp}<sub>2</sub><sup>1</sup> (Figure 3a), to minimize the interaction between the lone-pairs in the N<sub>imine</sub> atoms. The bridging carbon is approximately tetrahedral with N5-C8-N2 angle of 112.23(9). The N1-C1 [1.305(7) Å] and N2-C1 [1.3922(14) Å] bond lengths within the guanidine core are consistent with localised C-N and C=N.

## 4.6 Summary

To allow comparison with the chemistry of H<sub>2</sub>C{hpp}<sub>2</sub>, the {5,5}-derivative H<sub>2</sub>C{tbo}<sub>2</sub> was synthesized. H<sub>2</sub>C{hpp}<sub>2</sub> decomposes in moist air in contrast to H<sub>2</sub>C{tbo}<sub>2</sub> that crystallized as mono-hydrate (**6**). H<sub>2</sub>C{hpp}<sub>2</sub>, *bis*-guanidine compound acts as an *N,N'*-chelating ligand at square planar Pd(II) centers, and forms the simple adduct PdCl<sub>2</sub>(H<sub>2</sub>C{hpp}<sub>2</sub>); the dication [Pd(H<sub>2</sub>C{tbo}<sub>2</sub>)<sub>2</sub>][Cl]<sub>2</sub>, was formed from the coordination of H<sub>2</sub>C{tbo}<sub>2</sub>. It is not clear why H<sub>2</sub>C{hpp}<sub>2</sub> generates the simple adduct with PdCl<sub>2</sub> whereas H<sub>2</sub>C{tbo}<sub>2</sub> forms the dication. The differences in the reactivity of the two bicyclic guanidyl systems, however, encourage us to continue exploring this area, in an attempt to gain better understanding of the factors controlling the chemistry.



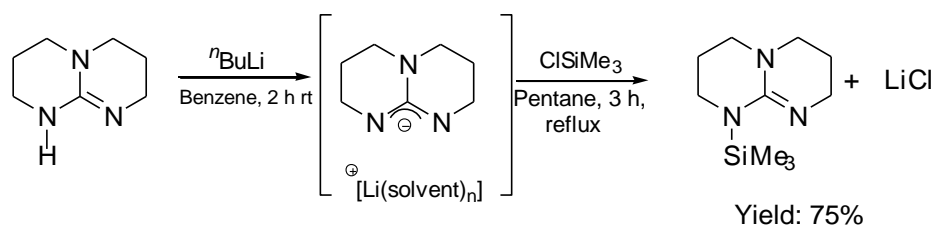
## 4.7 References

1. M. Coles, S. Lee, S. Oakley, G. Estiu and P. Hitchcock, *Org. Biomol. Chem.*, 2007, **5**, 3909–3911.
2. S. Oakley, M. Coles and P. Hitchcock, *Inorg. Chem.*, 2004, **43**, 7564–7566.
3. S. Oakley, M. Coles and P. Hitchcock, *Dalton Trans.*, 2004, 1113–1114.

## Chapter 5: Synthesis of pentacoordinate hpp-silicon compounds.

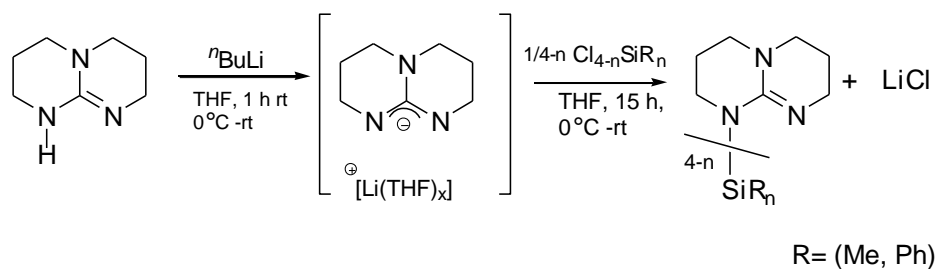
## 5.1. Introduction of hpp-Si Chemistry.

In 1993, Kummer *et al.* reported the formation of hppSiMe<sub>3</sub> via the reaction of <sup>n</sup>BuLi with hppH, followed by the addition of ClSiMe<sub>3</sub> (Scheme 1).<sup>1</sup> The yield of the reaction was 75%. Previous work in the Coles group produced the same product with higher yield (90%) using alternative conditions (THF solvent, 15h reflux).<sup>2</sup>



**Scheme 1:** Synthesis of hppSiMe<sub>3</sub> via the route reported by Kummer *et al.*

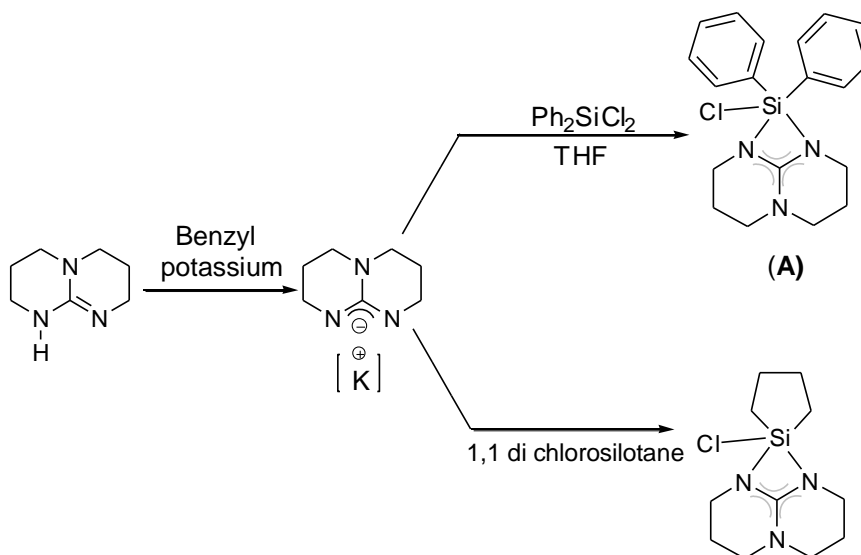
In 2004 the synthesis of poly(hpp) alkyl or aryl-silanes was reported using a common protocol to that reported for the synthesis of the monosubstituted compound hppSiMe<sub>3</sub>. A series of bis- and tris-(hpp)silanes were isolated and coordinated to CuCl giving proof that the N-Si bond was stable with a metal coordination (Scheme 2).<sup>3</sup>



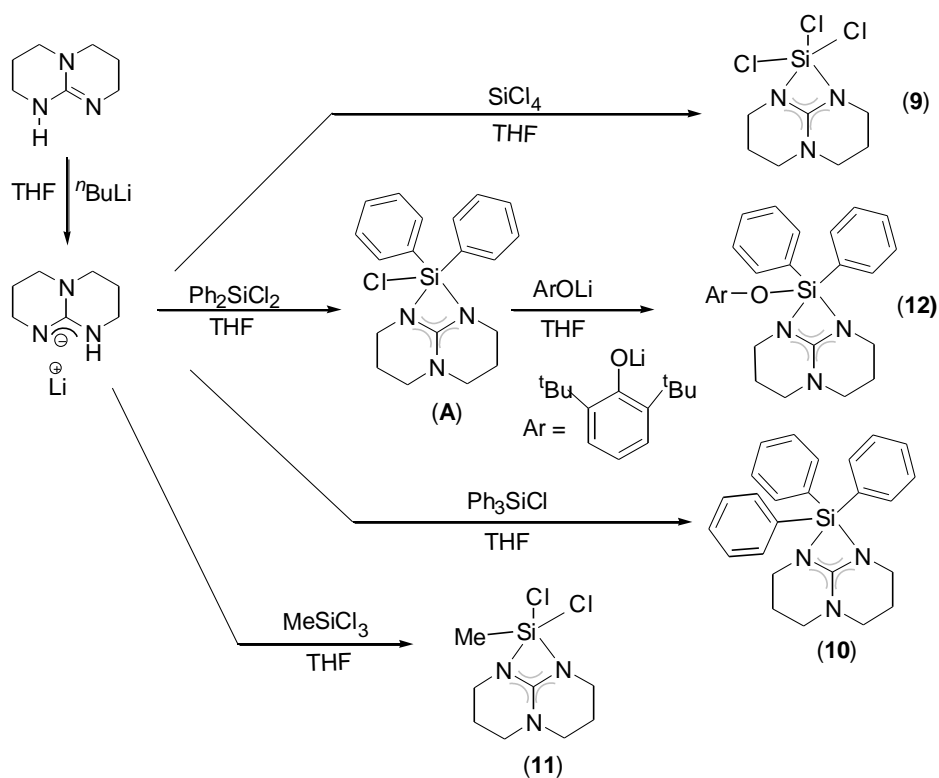
**Scheme 2:** Synthesis of poly(hpp)alkyl-or aryl-silanes

In 2006, Andell *et al.* synthesised and structurally characterized examples of 5-coordinate hpp-silicon species (hpp)SiR<sub>2</sub>Cl (**A**) (R<sub>2</sub>Cl= Ph<sub>2</sub>Cl, [cyclo-(CH<sub>2</sub>)<sub>4</sub>]Cl) (Scheme 3).<sup>4</sup>

In this chapter, we present five examples of pentacoordinated silicon species that have been synthesised *via* the reaction of [hpp]<sup>-</sup> and R<sub>2</sub>SiCl<sub>2</sub> (R= Ph, Me ) (Scheme 4).



**Scheme 3:** Synthesis of (hpp)SiPh<sub>2</sub>Cl, reported by Andell *et al.*



**Scheme 4:** Synthesis of (hpp)SiCl<sub>3</sub> (**9**), (hpp)SiPh<sub>2</sub>Cl (**A**), (hpp)SiPh<sub>3</sub> (**10**), (hpp)SiMeCl<sub>2</sub> (**11**), and (hpp)Si(OAr)Ph<sub>2</sub> (**12**)

## 5.2. Synthesis of (hpp)SiPh<sub>n</sub>Cl<sub>3-n</sub> (n = 2, 3)

### 5.2.1. Synthesis of (hpp)SiCl<sub>3</sub> (**9**)

The compound (hpp)SiCl<sub>3</sub> (**9**) was synthesised according to Scheme 4. The compound was prepared in THF, and recrystallisation from toluene at -30 °C to give colourless crystals in 91% yield. The <sup>1</sup>H NMR spectroscopy showed three resonances for the annular methylene protons which indicate a symmetrically bound guanidinate. <sup>29</sup>Si NMR showed a singlet at (C<sub>6</sub>D<sub>6</sub>, δ) -103.7 ppm, which is at higher field than the compound of Andell (**A** = δ -77.3) reflecting the presence of three chloride ligands. Elemental analysis showed a ratio of C, H

and N consistent with (hpp)SiCl<sub>3</sub>, and mass spectrometry [EI]<sup>+</sup> analysis showed a fragment at 272 [m/z] for [(hpp)SiCl<sub>3</sub>]<sup>+</sup>.

### 5.2.2. Crystallographic details and crystal structure of (hpp)SiCl<sub>3</sub> (**9**)

A summary of bond length (Å) and angles (°) of **9** is shown in Table 1.

**Table 1:-** Bond length (Å) and angles (°) for (hpp)SiCl<sub>3</sub> (**9**)

Cl(1)-Si	2.1656(11)	Si-N(2)	1.858(3)
Cl(2)-Si	2.0753(12)	N(3)-C(1)	1.301(4)
Cl(3)-Si	2.0872(11)	N(1)-C(1)	1.365(4)
Si-N(1)	1.779(3)	N(2)-C(1)	1.331(4)
C(1)-N(2)-Si	90.59(19)	N(1)-Si-N(2)	71.67(12)
C(7)-N(2)-Si	147.1(2)	N(1)-Si-Cl(2)	117.14(10)
N(3)-C(1)-N(2)	128.4(3)	N(2)-Si-Cl(2)	97.81(10)
N(3)-C(1)-N(1)	127.1(3)	N(1)-Si-Cl(3)	133.48(10)
N(2)-C(1)-N(1)	104.4(3)	N(2)-Si-Cl(3)	93.22(10)
Cl(2)-Si-C(1)	113.54(8)	Cl(2)-Si-Cl(3)	108.22(5)
Cl(3)-Si-C(1)	115.13(9)	N(1)-Si-Cl(1)	91.45(9)
Cl(1)-Si-C(1)	127.00(9)	N(2)-Si-Cl(1)	161.62(10)
C(1)-N(1)-Si	92.92(19)	Cl(2)-Si-Cl(1)	96.38(5)
		Cl(3)-Si-Cl(1)	93.39(5)

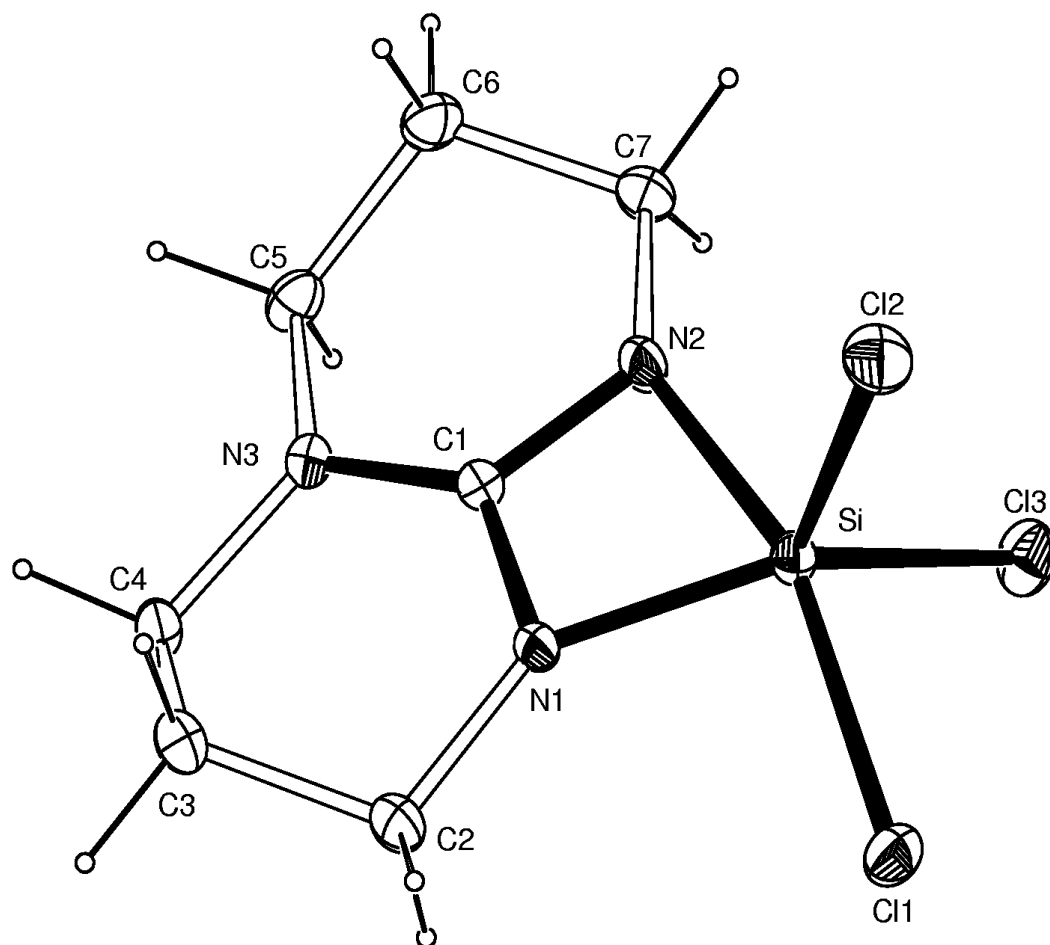


**Figure 1:** ORTEP representation of the structure of (hpp)SiCl<sub>3</sub> (**9**) with thermal ellipsoids drawn at the 30% level.

The geometry about the silicon atom in compound **9** is trigonal bipyramidal (Figure 1). The axial positions are occupied by the nitrogen (N2) and the chloride (Cl1) atoms, with the N2-Si-Cl1 angle 161.62(10)°. The remaining two chlorides Cl2 and Cl3 and N1 form the equatorial plane of the trigonal bipyramid silicon. Distortion from trigonal bipyramidal geometry can be described as the distance of the central atom from the plane of the equatorial substituents. In **9** this distance is 0.12 Å towards the side of N2. The Si-N(2) bond [1.858(3) Å] is significantly larger than Si-N(1) [1.779(3) Å] reflecting the axial vs. equatorial

positions about the central silicon. Within the guanidine this is seen as a shorter C(1)-N(2) and C(1)-N(1) 1.331(4) Å and 1.365(4) Å respectively, previously assigned in amidinate chemistry to larger contributions from resonance **B** (Figure 2). In the case of [hpp]<sup>−</sup> however, the remaining C-N bond is also short (C1-N3= 1.301(4) Å) indicating resonance form **C** also plays an important part in hpp-Si bonding in (**9**).

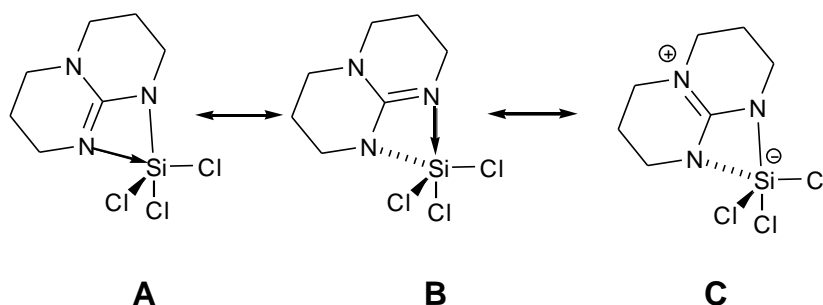


**Figure 2:** The bonding resonance structure for (hpp)SiCl<sub>3</sub>

The axial Si–Cl and the Si–N bonds (2.1656(11) Å and 1.858(3) Å) in the crystal structure of (hpp)SiCl<sub>3</sub> (**9**) are shorter than the corresponding axial Si–Cl (2.240(2) Å and Si–N bonds 1.978(4) Å) in (hpp)SiPh<sub>2</sub>Cl (**A**) as well as C1-N3 bonds for (**A**) and (**9**) in the short range (1.312 and 1.301(4) Å) respectively which corresponds approximately to the result of the difference among the substituted groups (Figure 3).<sup>4</sup>

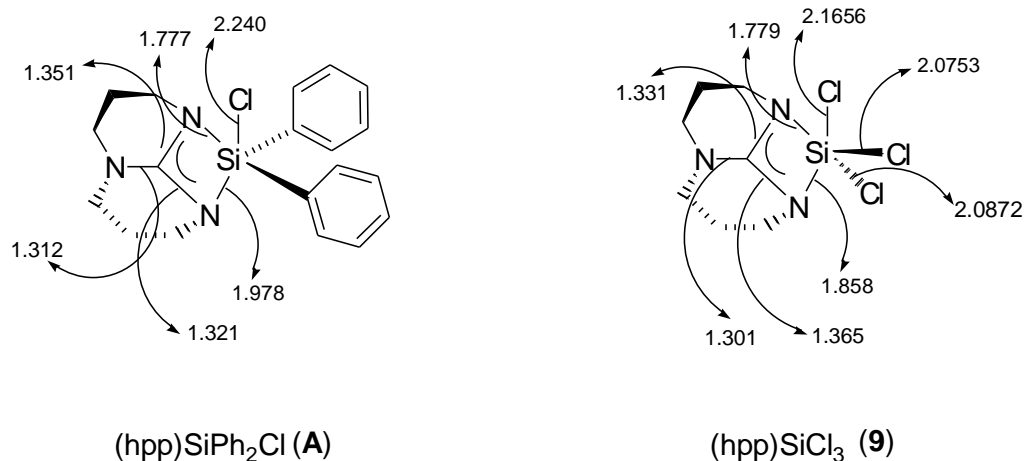


**Figure 3:** Selected bond lengths (Å) of (hpp)SiCl<sub>3</sub> (**9**) and pentacoordinated silicon (hpp)SiPh<sub>2</sub>Cl (**A**)

The first attempt at derivitizing (**9**) was the substitution of a chloride using (LiOAr) where Ar = 2,6-<sup>t</sup>Bu<sub>2</sub>C<sub>6</sub>H<sub>3</sub>. Unfortunately this attempt did not lead to the expected result; no pure compound was isolated.

### 5.3. Synthesis of (hpp)SiPh<sub>3</sub> (**10**) and (hpp)SiMeCl<sub>2</sub> (**11**)

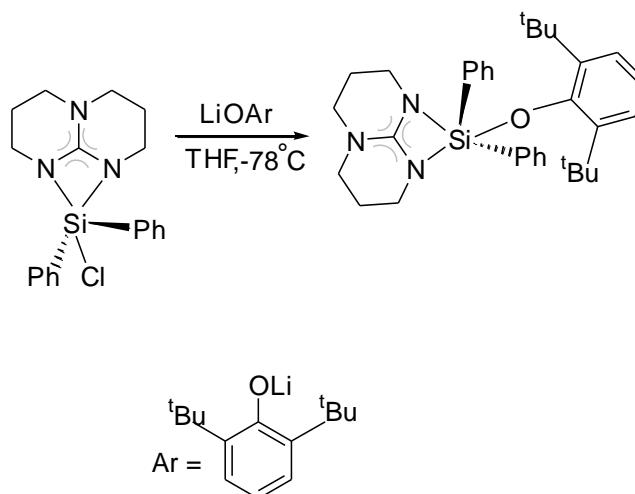
We have prepared (hpp)SiPh<sub>3</sub> (**10**) and (hpp)SiMeCl<sub>2</sub> (**11**) using the same protocol as that used for the preparation of (**9**) (see section 5.2.1). During the reactions the colour changed from colourless to light yellow. The LiCl side product was filtered off and washed with Et<sub>2</sub>O. The solvent was removed and dried under vacuum to afford a white solid (Scheme 4). Analytically pure samples of (hpp)SiPh<sub>3</sub> and (hpp)SiMeCl<sub>2</sub> were isolated as white powders from toluene at -30°C and were sensitive towards H<sub>2</sub>O. A singlet was observed by <sup>29</sup>Si NMR



for (hpp)SiPh<sub>3</sub> and (hpp)SiMeCl<sub>2</sub> at  $\delta$  -18.2 and -73.2, respectively, reflecting the reduced number of chloride ligands. <sup>1</sup>H NMR spectroscopy showed three resonances for the annular methylene protons which again indicate a symmetrically bound guanidinate. Elemental analysis revealed a ratio of C, H and N consistent with both (10) and (11). Furthermore mass spectrometry [EI]<sup>+</sup> analysis showed a fragment at 396 (m/z) and 251 (m/z) for (10) and (11) respectively, corresponding to the molecular ion, [M]<sup>+</sup>.

### 5.6. Synthesis of (hpp)Si(OAr)Ph<sub>2</sub> (Ar=2,6-<sup>t</sup>Bu<sub>2</sub>C<sub>6</sub>H<sub>3</sub>) (12)

Reaction between (hpp)SiPh<sub>2</sub>Cl (A) and LiOAr (Ar= 2,6-<sup>t</sup>Bu<sub>2</sub>C<sub>6</sub>H<sub>3</sub>) afforded a white powder upon work up (Scheme 5).



**Scheme 5:** The preparation of (hpp)Si(OAr)Ph<sub>2</sub> (12)

The analytically pure product was obtained by recrystallisation from refluxing toluene and gradually cooling to -78°C, giving white, needle-like crystals.  $^1\text{H}$  NMR spectroscopy data showed three resonances for the annular methylene of hpp-ligand which reflect the symmetry of the compound, the aromatic group in the range of 7-8 ppm. A singlet in the  $^{29}\text{Si}$  NMR spectrum was observed at  $\delta$  -72.7. The analytical data were in excellent agreement with the calculated values for C, H and N consistent with  $(\text{hpp})\text{Si}(\text{OAr})\text{Ph}_2$ . Furthermore mass spectrometry  $[\text{EI}]^+$  analysis showed a fragment at 602  $[\text{m/z}]$  for  $[(\text{hpp})\text{Si}(\text{OAr})\text{Ph}_2]^+$ .

### 5.6.1. Crystallographic details and crystal structure of $(\text{hpp})\text{Si}(\text{OAr})\text{Ph}_2$ (**12**)

The crystal structure of the compound  $(\text{hpp})\text{Si}(\text{OAr})\text{Ph}_2$  (**12**) is shown in Figure 4. Selected bond lengths and angles are listed in Table 2.

**Table 2:-** Bond lengths [ $\text{\AA}$ ] and angles [ $^\circ$ ] for  $(\text{hpp})\text{Si}(\text{OAr})\text{Ph}_2$  (**12**)

Si-O	1.6919(16)	N(2)-C(1)	1.349(3)
Si-N(2)	1.8194(19)	N(3)-C(1)	1.336(3)
Si-C(22)	1.896(2)	N(1)-C(1)	1.318(3)
Si-C(28)	1.915(2)	O-C(8)	1.378(3)
Si-N(1)	2.039(2)		
N(2)-Si-C(28)	97.22(10)	O-Si-N(2)	125.69(9)
C(22)-Si-C(28)	97.25(10)	O-Si-C(22)	120.23(9)

O-Si-N(1)	90.40(8)	N(2)-Si-C(22)	110.33(10)
N(2)-Si-N(1)	67.90(9)	O-Si-C(28)	95.01(9)
C(22)-Si-N(1)	92.61(9)	C(28)-Si-C(1)	131.55(10)
C(28)-Si-N(1)	164.39(9)	C(8)-O-Si	133.68(14)
N(1)-C(1)-N(2)	108.3(2)	C(1)-N(1)-Si	87.43(14)
C(7)-N(2)-Si	142.44(17)	C(2)-N(1)-Si	150.86(17)
		C(1)-N(2)-Si	96.10(15)

As in (**9**) the geometry about silicon in (**12**) is trigonal bipyramidal, with nitrogen (N1) and carbon (C28) atoms in axial positions, N1-Si-C28 angle is 164.4 (9)° and (C22) and oxygen (O) and nitrogen (N2) atoms in the equatorial plane (Figure 4). The silicon atom is located 0.20 Å outside of this plane displaced towards the side of C28. The length of N1-C1 bond is 1.318(3) Å, N2-C1 is 1.349(3) Å and N3-C1 is 1.336(3) Å, indicating more symmetrical delocalization of  $\pi$ -electron density.

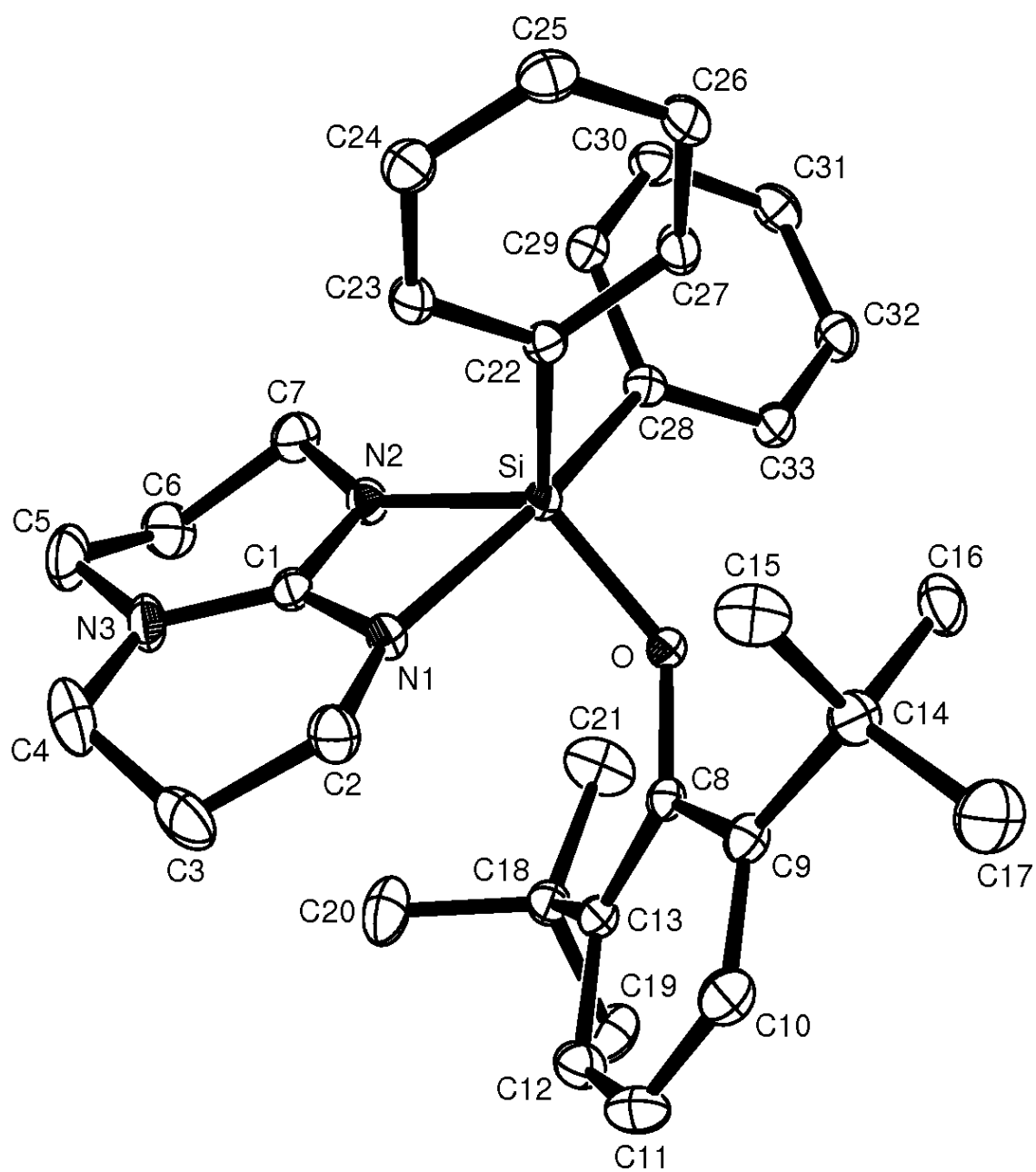


**Figure 4:** ORTEP representation of the structure of (hpp)Si(OAr)Ph<sub>2</sub> (**12**) with thermal ellipsoids drawn at the 30% level.

### 5.3. NMR Spectroscopic analysis of compounds 9-12.

The  $^1\text{H}$  and  $^{13}\text{C}$  NMR data of compounds **9-12** showed that the  $[\text{hpp}]^-$  units were always symmetric, contrasting with the solid-state data for **9** and **12**. There must therefore be a fluxional process occurring in solution, likely involving exchange of the  $\text{N}_{\text{axial}}$  and  $\text{N}_{\text{equatorial}}$  positions. Cooling a solution of **9** to  $-70\text{ }^\circ\text{C}$  in toluene solvent showed only a broadening of the hpp-resonances, indicating a rapid process on the NMR timescale. However,  $(\text{hpp})\text{Si}(\text{OAr})\text{Ph}_2$ , containing bulkier ligands, allowed the fluxionality to be probed in more detail. As the solution cooled to  $-80\text{ }^\circ\text{C}$ , a gradual de-coalescence of the three multiplets of the hpp-group is observed (Figure 5) until at  $-60\text{ }^\circ\text{C}$  two of the  $\text{CH}_2$  groups have resolved (a and c). Using equation 1 and data from NMR for the methylene group an approximate  $\Delta G^\ddagger$  of  $44.2\text{ kJ mol}^{-1}$  was calculated.

$$\Delta G^\ddagger = RT_c[22.96 + \ln(T_c/\Delta\nu)] \quad (\text{equation 1})$$

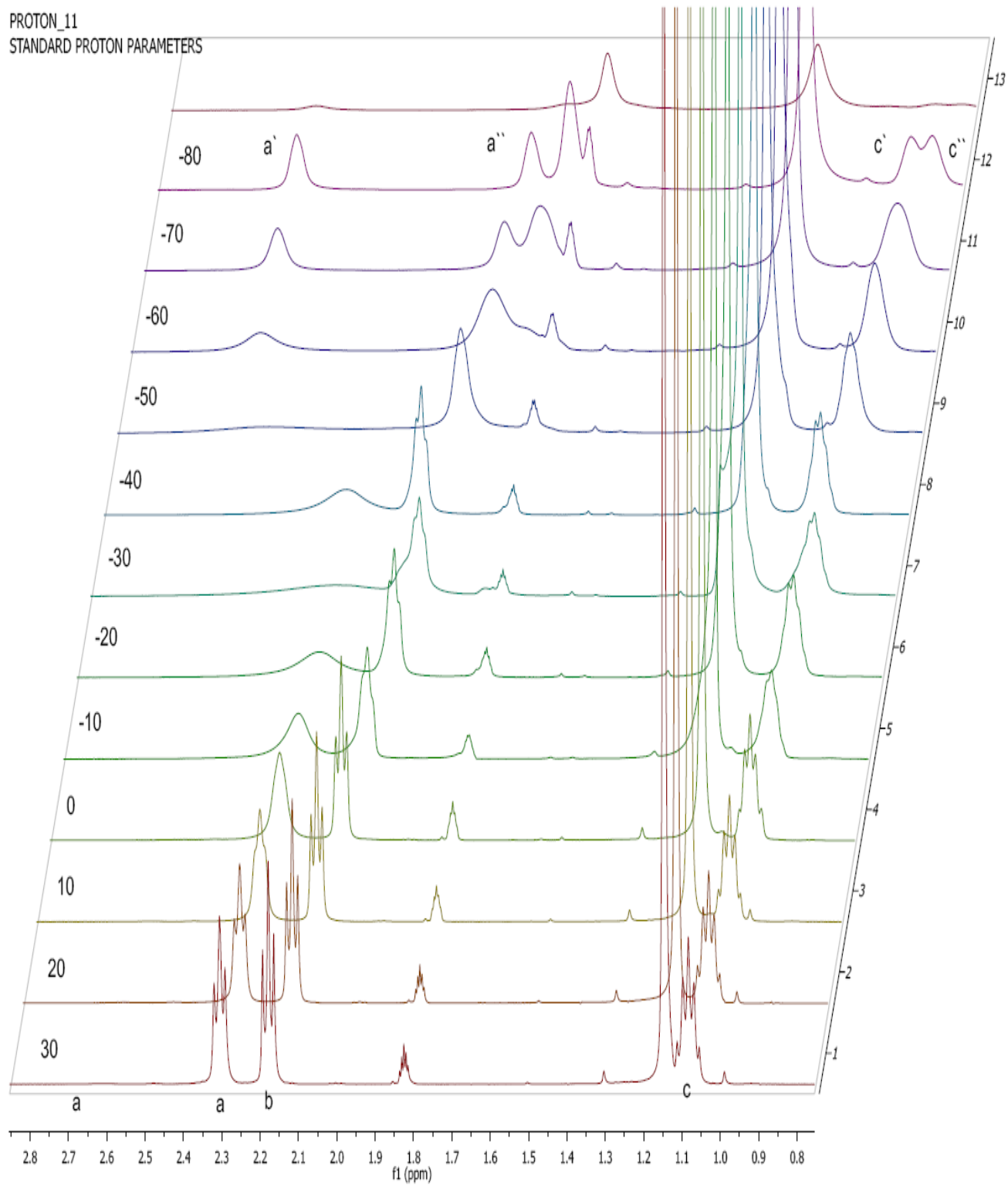


**Figure 5:** Variable temperature  $^1\text{H}$  NMR spectra (hpp-region) of  $(\text{hpp})\text{Si}(\text{OAr})\text{Ph}_2$  in toluene

## 5.7. Summary.

Drawing on the data included in the previous pages, the following points should be mentioned: The length of the Si-N bond is very sensitive to inductive effects, which was noted for all the reactions reported. The Si-N bond has been observed to vary by 0.26 Å between (hpp)SiCl<sub>3</sub> and (hpp)Si(OAr)Ph<sub>2</sub>, where the bond shortens with an increasing number of electron-withdrawing groups on silicon. Moreover, it has been found that the Si-N bond length is longer when the electron-withdrawing group bonded to silicon occupies an axial position than when it occupies an equatorial site. The same trends are observed for the remaining studied compounds and are in accordance with experimental observations for several pentacoordinated compounds. A second point is that the exchange of axial and equatorial positions is rapid on the NMR timescale for compounds with a small substituent at silicon. However, using a bulky ayloshide ligand enabled the process to be slowed sufficiently so that it could be monitored by V. T NMR spectroscopy.

## 5.8. References.

1. D. Kummer, A. Kuhs, G. Mattern, S. Halim, *J. Organomet. Chem.*, 1993, **51**, 446.
2. S. Oakley, PhD thesis 2004, University of Sussex.
3. S. Oakley, M. Coles and P. Hitchcock, *Dalton Trans.*, 2004, 1113–1114.
4. J. Andell, T. Vanne, I. Mutikainen, 2006, **691**, 240-246.

## Chapter 6: Experimental section



## 6.1: General experimental procedures.

All the experiments were carried out under the atmosphere of dry nitrogen using standard Schlenk and cannula techniques or in a conventional nitrogen-filled glovebox unless otherwise stated. All reagents were obtained from the Aldrich, Lancaster, or Acros chemical companies and used as received. All moisture sensitive reactions were carried out in dried glassware under either a nitrogen or argon atmosphere. NMR spectra were recorded on either a Bruker 300 DRX spectrometer or an AV400 spectrometer operating at 300 or 400 MHz, respectively for  $^1\text{H}$  and  $^{13}\text{C}$ . IR spectra were recorded using a Bio-Rad FTS 165 spectrometer. Elemental analyses to determine arsenic content were conducted by S. Boyer at the London Metropolitan University. Low resolution  $[\text{EI}]^+$  mass spectrometry was carried out on VG Autospec Fisons instruments by Dr Ali Abdul-Sadu. Single crystal X-ray crystallography was carried out by Dr Peter Hitchcock and Dr M. P. Coles on a Bruker-Nonius Kappa CCD diffract meter and structures were refined using SHELXL-97. Safety spectacles, gloves and a laboratory coat were worn at the times and all solvents were disposed of in the appropriate metal or organic waste solvent receptacle.

Solvents were distilled under nitrogen from sodium (petroleum ether 40-60%, heptanes and toluene), from potassium (THF), from sodium/potassium alloy ( $\text{Et}_2\text{O}$ , pentane and hexane) or calcium hydride (MeCN and DCM), degassed and stored over a potassium mirror or molecular sieves prior to use. NMR solvents were dried over potassium ( $\text{d}_6$ -benzene and  $\text{d}_8$ -toluene) or calcium hydride ( $\text{d}_1$ -chloroform,  $\text{d}_3$ -acetonitrile) and stored in a nitrogen filled glove box.

## 6. 2: General reagents and starting materials.

In this section we prepared some previously reported reagents and starting materials. NMR data were recorded to provide the purity of the compound.

### 6. 2. 1: [a] Htbo [ $C_5H_9N_3$ ]

Under  $N_2$ , carbon disulfide (7.60 g, 100 mmol) was added to a solution of diethylenetriamine (10.3 g, 100 mmol) in 160  $cm^3$  of *p*-xylene under  $N_2$ . A white precipitate formed immediately. The mixture was heated to boiling until the solid had dissolved. The solution was refluxed until evolution of  $H_2S$  ceased (ca. 10 days), and then the solvent was removed under vacuum, leaving a yellow-white solid. This solid was purified by sublimation, above 158 °C resulting in colourless crystals. Yield 6.87 g (62%).  $^1H$  NMR ( $CDCl_3$ ):  $\delta$  4.51 (s, 1H (NH)), 3.68 (m,  $^3J_{HH} = 8$  Hz, 4H,  $CH_2$ -tbo), 2.95 (m,  $^3J_{HH} = 6$  Hz, 4H,  $CH_2$ -tbo), EI  $[M]^+ = 112$ , melting point (158-159 °C).

### 6. 2. 2: [b] hppH [ $C_7H_{13}N_3$ ] .

hppH was sublimed. NMR analysis in a variety of solvents was performed in order to provide comparative data for the hpp-containing species formed during the course of the work.

$^1H$  NMR  $C_6D_6$ :  $\delta$  1.57 (m, 4H, hpp- $CH_2$ ), 2.61 (t, 4H, hpp- $CH_2$ ), 3.21 (t, 4H, hpp- $CH_2$ ), 7.61 (s, 1H, NH).

$^{13}C$  NMR:  $d_1$  chloroform:  $\delta$  23.8 (hpp- $CH_2$ ), 42.1 (hpp- $CH_2$ ), 48.2 (hpp- $CH_2$ ), 151.6 (hpp- $CN_3$ )

### 6. 2. 3:[c] $PdCl_2(COD)$ .

Original synthesis reported by Retting *et al.* PdCl<sub>2</sub> (2.06 g, 1.16 mmol) was dissolved in concentrated HCl (5 mL) with warming to give a dark brown solution. Upon cooling, it was diluted with absolute ethanol (50-80 mL) and filtered. 1.5 equivalents of COD (2.2 mL, 1.74 mmol) were added to the stirred filtrate resulting in the formation of a thick yellow precipitate. This was collected by filtration, washed with Et<sub>2</sub>O and dried in vacuo.

Yield 3.11 g

## 6. 3: Experimental data for Chapter 2.

### 6. 3. 1 Synthesis of [H<sub>2</sub>tbo][Cl] (1)

[H<sub>2</sub>tbo][Cl] was made according to the procedure outlined for [hppH<sub>2</sub>][Cl] , using 0.10 g Htbo (0.90 mmol) and 0.12 g [HNEt<sub>3</sub>][Cl]. Removal of the volatiles afforded a white solid that was washed with hexane, giving pure [H<sub>2</sub>tbo][Cl]. Yield 0.12 g (91%). Crystals suitable for analysis by X-ray were grown by the slow cooling of a MeCN solution. <sup>1</sup>H NMR (400 MHz, CD<sub>3</sub>CN): δ 3.97 (m, 4H, tbo-CH<sub>2</sub>), 3.95 (s br, 2H, NH), 3.42 (m, 4H, tbo-CH<sub>2</sub>). <sup>13</sup>C{<sup>1</sup>H} NMR (100 MHz, CD<sub>3</sub>CN): δ 166.8 (CN<sub>3</sub>), 50.7, 47.6 (tbo-CH<sub>2</sub>). IR (nujol mull): 3453 (m), 3392 (m), 3361 (m), 1682 (s, sh), 1584 (m), 1310 (w), 1276 (m), 1220 (w), 1111 (m), 1038 (m), 992 (m), 945 (m), 812 (w), 667 (m).

## 6. 4 Experimental data for Chapter 3

#### 6.4.1 Isolation of Lithium Guanidinate Complex $[\text{Li}_2(\text{tbo})(\text{A})(\text{Htbo})]$ (2)

A sample of the neutral contaminated guanidine, Htbo, was dissolved in THF and cooled to  $-78\text{ }^{\circ}\text{C}$ .  $^n\text{BuLi}$  (1.0 equivalents of a 1.6 M solution in hexanes) was added *via* syringe and the reaction allowed to warm to room temperature. The solution was filtered to remove particulate material and heating ( $\sim 70\text{ }^{\circ}\text{C}$ ) and filtering gave a clear solution that was allowed to cool slowly to room temperature. Isolation of  $[\text{Li}_2(\text{tbo})(\text{A})(\text{Htbo})]$  (2). A small quantity of crystals suitable for X-ray analysis were isolated from a reaction between  $^n\text{BuLi}$  and Htbo contaminated with the monocyclic compound, 1-(2-aminoethyl)-2-imidazolidinethione. No further analysis was obtained on this product.

#### 6.4.2 Synthesis of $\text{Li}_6(\text{tbo})_6(\text{Htbo})_3$ (3)

A Schlenk was charged with 0.25 g Htbo (2.25 mmol) dissolved in  $\text{Et}_2\text{O}$  and cooled to  $-78\text{ }^{\circ}\text{C}$ . 1.4 mL  $^n\text{BuLi}$  (1.6 M solution in hexanes, 2.25 mmol) was added by syringe and the mixture was allowed to warm to room temperature and stirred for 15 h. The resultant cloudy solution was filtered and stored at room temperature, affording colourless crystals suitable for X-ray diffraction. Yield 0.12 g, 46% (based on Htbo). Anal. calc. for  $\text{C}_{45}\text{H}_{75}\text{Li}_6\text{N}_{27}$  (1036): C 52.17, H 7.30, N 36.51%. Found: C 52.09, H 7.28, N 36.41%.  $^1\text{H}$  NMR (400 MHz, 303 K,  $\text{C}_6\text{D}_6$ ):  $\delta$  4.31 (s, 1H, NH), 3.78 (pseudo t, 4H,  $\text{CH}_2\text{-tbo}$ ), 3.06 (pseudo t, 4H,  $\text{CH}_2\text{-tbo}$ ).  $^{13}\text{C}$  NMR (100 MHz, 303 K,  $\text{C}_6\text{D}_6$ ):  $\delta$  154.2 ( $\text{CN}_3$ ), 54.6 ( $\text{CH}_2\text{-tbo}$ ), 50.4 ( $\text{CH}_2\text{-tbo}$ ). Mass spec ( $\text{EI}^+$ ,  $m/z$ ):  $[\text{M}]^+ = 111$ .

#### 6.4.3 Synthesis of $[\text{Al}(\text{tbo})\text{Me}_2]$ (4)

1.12 mL of a hexane solution of  $\text{AlMe}_3$  (2.0 M, 2.25 mmol) was added dropwise to a slurry of Htbo (0.25 g, 2.25 mmol) in  $\text{Et}_2\text{O}$  at  $-78\text{ }^\circ\text{C}$ . The mixture was allowed to warm to room temperature and was stirred under ambient conditions for 15 h. The solution was filtered and maintained at room temperature, affording small colourless crystals of **4**. Yield 0.26 g, 68%. Anal. calc. for  $\text{C}_7\text{H}_{14}\text{AlN}_3$  (334.38): C 50.29, H 8.44, N 25.13%. Found: C 50.18, H 8.58, N 24.98%.  $^1\text{H}$  NMR (300 MHz, 303 K,  $\text{C}_6\text{D}_6$ ):  $\delta$  3.58 (pseudo t, 4H, tbo- $\text{CH}_2$ ), 2.28 (pseudo t, 4H, tbo- $\text{CH}_2$ ),  $-0.26$  (s, 6H,  $\text{AlMe}_2$ ).  $^{13}\text{C}$  NMR (100 MHz, 303 K,  $\text{C}_6\text{D}_6$ ):  $\delta$  176.1 ( $\text{CN}_3$ ), 54.6, 47.8 (tbo- $\text{CH}_2$ ),  $-8.1$  ( $\text{AlMe}_2$ ). Mass Spec ( $\text{EI}^+$ ,  $m/z$ ) 319 [ $(\text{C}_7\text{H}_{14}\text{AlN}_3)_2 - \text{Me}$ ] $^+$ .

#### 6.4.4 Synthesis of $\text{Zn}_3(\text{tbo})_4\text{Me}_2$ (**5**)

1.80 mL of a toluene solution of  $\text{ZnMe}_2$  (2.0 M, 3.60 mmol) was added dropwise to a solution of Htbo (0.40 g, 3.60 mmol) in toluene at  $-78\text{ }^\circ\text{C}$ . The mixture was allowed to warm to room temperature and was stirred under ambient conditions for 18 h, affording a cloudy solution. Heating ( $\sim 80\text{ }^\circ\text{C}$ ) and filtering gave a clear solution that was allowed to cool slowly to room temperature, affording colourless crystals suitable for X-ray analysis. Yield 0.39 g, 65% (based on Htbo). Anal. calc. for  $\text{C}_{22}\text{H}_{38}\text{N}_{12}\text{Zn}_3$  (766.4): C 39.63, H 5.74, N 25.21%. Found: C 39.72, H 5.79, N 25.19%.  $^1\text{H}$  NMR (400 MHz, 303 K,  $\text{C}_6\text{D}_6$ ):  $\delta$  3.82 (m, 4H, tbo- $\text{CH}_2$ ), 3.73 (m, 12H, tbo- $\text{CH}_2$ ), 2.71 (m, 16H, tbo- $\text{CH}_2$ ),  $-0.39$  (s, 6H,  $\text{ZnMe}_2$ ).  $^{13}\text{C}$  NMR (100 MHz, 303 K,  $\text{C}_6\text{D}_6$ ):  $\delta$  182.2 (br,  $\text{CN}_3$ ), 178.5 ( $\text{CN}_3$ ), 55.8, 55.7, 50.8, 48.8 (tbo- $\text{CH}_2$ ), 1.5 ( $\text{ZnMe}_2$ ).

## 6.5: Experimental data for Chapter 4.

### 6.5.1: Synthesis of $\text{H}_2\text{C}\{\text{tbo}\}_2$ (6)

A mixture of Htbo (1.00 g, 9.0 mmol), NaH (0.216 g, 9.0 mmol) and dichloromethane (0.28 mL, 4.5 mmol, 0.5 equiv) in THF (20 mL) was stirred at room temperature for 2 days with venting to an external mercury trap for the first 3 h. A white precipitate formed and the reaction was filtered and the volatiles were removed *in vacuo* to afford a white powder. Washing with hexanes afforded analytically pure  $\text{H}_2\text{C}\{\text{tbo}\}_2$ . Yield 0.75 g (71% based on Htbo). Crystals suitable for an X-ray study were isolated by crystallization from  $\text{Et}_2\text{O}$  at  $-30^\circ\text{C}$ . Analysis: Calc'd for  $\text{C}_{11}\text{H}_{18}\text{N}_6$  (234.31): C 56.39, H 7.74, N 35.87%. Found C 56.43, H 7.81, N 35.73%.  $^1\text{H}$  NMR ( $\text{C}_6\text{D}_6$ , 400 MHz, 303 K):  $\delta$  4.76 (s, 2H,  $\text{H}_2\text{C}\{\text{tbo}\}_2$ ), 3.93, 3.52, 2.59, 2.38 (m, 4H, tbo- $\text{CH}_2$ ).  $^{13}\text{C}$  NMR ( $\text{C}_6\text{D}_6$ , 100 MHz, 303 K):  $\delta$  169.2 ( $\text{CN}_3$ ), 59.3 ( $\text{H}_2\text{C}\{\text{tbo}\}_2$ ), 56.7, 51.6, 51.5, 46.4 (tbo- $\text{CH}_2$ ).

### 6.5.2: Generation of $\text{H}_2\text{C}\{\text{tbo}\}_2\cdot\text{H}_2\text{O}$ (6')

A Schlenk was charged with 250 mg (2.25mmol) of Htbo with NaH which was dissolved in toluene. 1.25 cm<sup>3</sup> of CH<sub>2</sub>Cl<sub>2</sub> was added to the solution and stirred overnight. Cloudy solution was formed, heated and filtered. The solvent was removed and dissolved in Et<sub>2</sub>O for recrystallization in warm water overnight. Colourless crystal formed which was sufficient for X-ray diffraction, crystal system was Monoclinic, yield 75%. Mass spectrum (EI) show [MH]<sup>+</sup> = 235 amu. <sup>1</sup>H NMR (C<sub>6</sub>D<sub>6</sub>): δ 4.76 (s, 2H, H<sub>2</sub>C{tbo}<sub>2</sub>), 3.93 (t, <sup>3</sup>J<sub>HH</sub> = 8 Hz, 4H, CH<sub>2</sub>-tbo), 3.52 (t, <sup>3</sup>J<sub>HH</sub> = 6 Hz, 4H, CH<sub>2</sub>-tbo), 2.59 (t, <sup>3</sup>J<sub>HH</sub> = 6 Hz, 4H, CH<sub>2</sub>-tbo), 2.38 (t, <sup>3</sup>J<sub>HH</sub> = 6 Hz, 4H, CH<sub>2</sub>-tbo). <sup>13</sup>C NMR (C<sub>6</sub>D<sub>6</sub>): δ 169.2 (CN<sub>3</sub>), 59.3 (CH<sub>2</sub>-tbo), 56.7 (H<sub>2</sub>C{tbo}<sub>2</sub>), 51.6 (CH<sub>2</sub>-tbo), 51.5 (CH<sub>2</sub>-tbo), 46.4 (CH<sub>2</sub>-tbo) .

### 6.5.3: Synthesis of [Pd (H<sub>2</sub>C{tbo}<sub>2</sub>)<sub>2</sub>] [Cl]<sub>2</sub> (7)

A solution of PdCl<sub>2</sub>(COD) in CH<sub>2</sub>Cl<sub>2</sub> (0.10 g, 0.53 mmol) was added drop wise to a solution of H<sub>2</sub>C{tbo}<sub>2</sub> in CH<sub>2</sub>Cl<sub>2</sub> (0.25 g, 1.05 mmol). The mixture was stirred for 24 h at room temperature, during which time the colour changed from red to brown. The reaction was filtered and the volatiles removed *in vacuo* to afford a red powder. Crystals suitable for an X-ray diffraction study were obtained by layering a dichloromethane solution with Et<sub>2</sub>O at room temperature. Yield 0.16 g, 47%. Analysis: Calc'd for C<sub>22</sub>H<sub>36</sub>N<sub>12</sub>Cl<sub>2</sub>Pd (645.93): C 40.91, H 5.62, N 26.02%. Found C 40.81, H 5.56, N 25.93%. <sup>1</sup>H NMR (D<sub>2</sub>O, 400 MHz, 303 K): δ 7.06 (d, <sup>2</sup>J<sub>HH</sub> = 16.0 Hz, 1H, H<sub>2</sub>C{tbo}<sub>2</sub>), 4.73 (d, <sup>2</sup>J<sub>HH</sub> = 16.0 Hz, 1H, H<sub>2</sub>C{tbo}<sub>2</sub>), 4.17, 3.97, 3.63, 3.39 (m, 2H, tbo-CH<sub>2</sub>-). <sup>13</sup>C NMR (D<sub>2</sub>O, 100 MHz, 303 K): δ 168.3 (CN<sub>3</sub>), 57.3 (H<sub>2</sub>C{tbo}<sub>2</sub>), 54.1, 53.7, 48.5, 46.1 (tbo-CH<sub>2</sub>).

#### 6.5.4: Synthesis of (Me<sub>3</sub>Si)HC{hpp}<sub>2</sub> (8)

A Schlenk was charged with (0.20 g 0.688 mmol) of H<sub>2</sub>C{hpp}<sub>2</sub> dissolved in THF. One equivalent of <sup>t</sup>BuLi in hexane (0.37 mL 0.688 mmol) was added drop wise at -78°C and the mixture stirred 1 hour affording a red solution. One equivalent of SiMe<sub>3</sub>Cl (0.087 mL, 0.688 mmol) was added drop wise at -78°C during stirred, solution has changed to colourless the mixture stirred overnight. Heating and filtering gave a clear solution that was allowed to cool slowly to room temperature affording colourless crystals suitable for X-ray diffraction. Yield 0.142 g, 57%. Mass spectrum (EI) Show [M]<sup>+</sup> = 362. <sup>1</sup>H NMR *d*<sub>6</sub>-benzene: δ= 5.63(s,1H, HC{hpp}<sub>2</sub>), 3.61(t, hpp-CH<sub>2</sub>), 3.49(t, hpp-CH<sub>2</sub>), 2.71(t, hpp-CH<sub>2</sub>), 2.55(t, hpp-CH<sub>2</sub>), 1.63(quin, hpp-CH<sub>2</sub>), 1.51(quin, hpp-CH<sub>2</sub>), 0.25(s,9H, CH<sub>3</sub>-Si). <sup>13</sup>C NMR (C<sub>6</sub>D<sub>6</sub>): δ 152 (CN<sub>3</sub>), 63.8 (CH<sub>2</sub>-hpp), 49.4 H<sub>2</sub>C(hpp), 44.5 (CH<sub>2</sub>-hpp), 44.2 (CH<sub>2</sub>-hpp), 24.5 (CH<sub>2</sub>-hpp), 24.3 (CH<sub>2</sub>-hpp), 5.0(CH<sub>3</sub>-Si).

### 6.6. Experimental data for Chapter 5.

#### 6.6.1 Synthesis of (hpp)SiCl<sub>3</sub> (9)

A Schlenk was charged with (0.45 g, 3.2 mmol) of hppH dissolved in 50 mL of THF. One equivalent of <sup>n</sup>BuLi 1.3 mL (3.2 mmol) was added drop wise at -78°C and the mixture stirred 1 hour. Affording a yellow solution. One equivalent of SiCl<sub>4</sub> 0.37 mL (3.2 mmol) was added drop wise at -78°C during stirred time the colour has changed from yellow to colourless. The mixture stirred overnight and it was slightly cloudy, and then filtered recrystallise using



toluene. Yield 0.805 g (91%). Anal. Calc. For  $C_7H_{12}N_3SiCl_3$  (272.64): C, 30.75; H, 4.33; N, 15.48%; requires C, 30.84; H, 4.44; N, 15.41 %. Mass spectrum (EI) Show  $[M]^+ = 272$ .  $^1H$  NMR ( $C_6D_6$ ):  $\delta$  2.94 (m, 4H,  $CH_2$ -hpp), 2.14 (m, 4H,  $CH_2$ -hpp), 1.18 (m, 4H,  $CH_2$ -hpp).  $^{13}C$  NMR ( $C_6D_6$ ):  $\delta$  169.2 (hpp-CN<sub>3</sub>), 48.2 ( $CH_2$ -hpp), 42.1 ( $CH_2$ -hpp), 23.8 ( $CH_2$ -hpp).  $^{29}Si$  NMR ( $C_6D_6$ ):  $\delta$  -103.74

### 6.6.2 Synthesis of (hpp)SiPh<sub>3</sub> (10)

A Schlenk was charged with (0.4 g, 2.9 mmol) of hppH dissolved in 50 mL of THF. One equivalent of  $nBuLi$  1.15 mL (2.9 mmol) was added drop wise at  $-78^\circ C$  and the mixture stirred 3 hour. Affording a yellow solution. One equivalent of  $Ph_3SiCl$  (0.848 g 2.9 mmol) in THF was added drop wise at  $-78^\circ C$  and stirred for 24h the colure has changed from yellow to colourless. The mixture stirred overnight and it was slightly cloudy, and then filtered recrystalise using toluene. Yield 0.77 g (67%). Anal. Calc. For  $C_{25}H_{27}N_3Si$  (398.49): C 75.61; H 6.98; N 10.42% requires C 75.52; H 6.98; N 10.57%, Mass spectrum (EI) Show  $[M]^+ = 396$ .  $^1H$  NMR ( $C_6D_6$ ):  $\delta$  7.88 (Ar, 6H), 7.32 (Ar, 9H), 2.96 (m, 4H,  $CH_2$ -hpp), 2.55 (m, 4H,  $CH_2$ -hpp), 1.30 (m, 4H,  $CH_2$ -hpp).  $^{13}C$  NMR ( $C_7H_8$ ):  $\delta$  155.8(CN<sub>3</sub>), 141.2 (CH), 134.7(CH), 132.7 (CH), 129.7 (CH), 52.8 ( $CH_2$ ), 47.1 ( $CH_2$ ), 28.3 ( $CH_2$ ).  $^{29}Si$  NMR ( $C_7H_8$ ),  $\delta$  -18.2.

### 6.6.3 Synthesis of (hpp)SiMeCl<sub>2</sub> (11)

A Schlenk was charged with (0.4 g, 2.9 mmol) of hppH dissolved in THF. One equivalent of  $nBuLi$  1.15 mL (2.9 mmol) was added drop wise at  $-78^\circ C$  and the mixture stirred 3 hour. Affording a yellow solution. One equivalent of  $MeSiCl_3$  (0.35 mL, 2.9 mmol) was added drop wise at  $-78^\circ C$  and stirred for 24h the colure has changed from yellow to light yellow.

The mixture stirred overnight and it was slightly cloudy, and then filtered recrystallise using toluene. Yield 0.44 g (60%). Anal. Calc. For  $C_8H_{15}N_3SiCl_2$  (398.49): C 38.09; H 6.04; N 16.74% requires C 38.1; H 6.0; N 16.7%, Mass spectrum (EI) Show  $[M]^+ = 251$ .

$^1H$  NMR ( $C_6D_6$ ):  $\delta$  3.12 (m, 4H,  $CH_2$ -hpp), 4.09 (m, 4H,  $CH_2$ -hpp), 4.80 (m, 4H,  $CH_2$ -hpp), 2.89 (s,  $CH_3$ -Si).  $^{13}C$  NMR ( $C_6D_6$ ):  $\delta$  155.44 (hpp-CN<sub>3</sub>), 45.02 ( $CH_2$ -hpp), 38.43 ( $CH_2$ -hpp), 23.64 ( $CH_2$ -hpp), 12.86 ( $CH_3$ ).  $^{29}Si$  NMR ( $C_7H_8$ ),  $\delta$  -73.2.

### 6.6.3 Synthesis of (hpp)SiClPh<sub>2</sub> (A)

(0.4 g, 2.9mmol) of hppH dissolved in THF. One equivalent of  $nBuLi$  1.15 mL (2.9 mmol) was added drop wise at -78°C and the mixture stirred 3h. affording a yellow solution. One equivalent of  $Ph_2SiCl_2$  (0.6 mL, 2.9 mmol) was added drop wise at -78°C the mixture stirred overnight and it was slightly cloudy, and then filtered add recrystallized using toluene. Yield 0.795g (77%). Anal. Calc. For  $C_{19}H_{22}N_3SiCl$  (356.49): C 64.32; H 6.19; N 11.52% requires C 64.11; H 6.23; N 11.81%, Mass spectrum (EI) Show  $[M]^+ = 354$ .  $^1H$  NMR ( $C_6D_6$ ):  $\delta$  7.88 (dd, 4H, CH), 7.32 (d, 2H, CH), 7.24 (d, 4H, CH), 1.38 (m, 4H,  $CH_2$ -hpp), 2.55 (m, 4H,  $CH_2$ -hpp), 2.96 (m, 4H,  $CH_2$ -hpp).  $^{13}C$  NMR ( $C_6D_6$ ):  $\delta$  154.8(CN<sub>3</sub>), 142.2 (Cq), 134.0(CH), 128.5 (CH), 127.5 (CH), 44.9 (CH<sub>2</sub>), 39.3 (CH<sub>2</sub>), 23.2 (CH<sub>2</sub>).  $^{29}Si$  NMR ( $C_6D_6$ ,  $\delta$ ): -71.2.

### 6.6.5 Synthesis of (hpp)Si(OAr)Ph<sub>2</sub> (Ar=2,6 $tBu_2C_6H_3$ ) (12)

A Schlenk was charged with (0.35 g, 0.70 mmol) of (hpp)SiClPh<sub>2</sub> dissolved in THF. One equivalent of LiOAr (0.15 g, 0.70 mmol) in THF mL was added drop wise at -78°C. The mixture was allowed to warm to room temperature and was stirred under ambient conditions for 24 h, affording a cloudy solution; LiCl was filtered off and washed with Et<sub>2</sub>O. Heating

(~80 °C) and filtering gave a clear solution that was allowed to cool slowly to room temperature, affording colourless crystals suitable for X-ray analysis. Yield 0.205 g, 56%. Anal. calc. for  $C_{33}H_{43}N_3OSi$  (617.9): C 75.84, H 8.35, N 7.73%. requires: C 75.35, H 8.24, N 7.99%, Mass spectrum (EI) Show  $[M]^+ = 602$   $^1H$  NMR ( $C_6D_6$ ,  $\delta$ ): 7.86 (Ar, 5H), 7.26 (Ar, 8H, CH), 2.60 (m, 4H,  $CH_2$ ), 2.38 (m, 4H,  $CH_2$ ), 1.48 (s, 18H,  $C(CH_3)_3$ ), 1.30 (quin, 4H,  $CH_2$ -hpp). NMR ( $C_6D_6$ ):  $\delta$  155.72 (hpp- $CN_3$ ), 153.41 ( $C_q$ ), 144.64 (CH), 141.66 (CH), 137.83 (CH), 128.11 (CH), 126.99 (CH), 126.46 (CH), 119.82 ( $C_q$ ), 45.88 ( $(CH_3)_3$ ), 40.53 ( $CH_2$ -hpp), 36.28 ( $CH_2$ -hpp), 33.3 (C- (based on Htbo).  $(CH_3)_3$ ), 23.3 ( $CH_2$ -hpp)  $^{29}Si$  NMR ( $C_6D_6$ ,  $\delta$ ): -72.7.

# Appendix

## Publications

- Majid S. Khalaf, Martyn P. Coles and Peter B. Hitchcock, A structural, theoretical and coordinative evaluation of the bicyclic guanidinate derived from 1,4,6-triazabicyclo[3.3.0]oct-4-ene, *Dalton Trans.*, 2008,**10**, 4288-4295.
- Majid S. Khalaf, Sarah H. Oakley, Martyn P. Coles and Peter B. Hitchcock, A strategy for the propagation of hydrogen-bonding in bicyclic guanidinium salts†, *Cryst. Eng. Comm*, 2008,**10**, 1653-1661.
- Majid S. Khalaf, Sarah H. Oakley, Martyn P. Coles and Peter B. Hitchcock, Coordination of neutral, methylene bridged bis-guanidyls at palladium, *Dalton Trans.*, 2010, **39**, 1635-164
- Martyn P. Coles, Majid S. Khalaf, Rosa M. Claramunt, M. Angeles García, Ibon Alkorta and José Elguero, Double proton transfer in crystals of 1,3,4,6,7,8-hexahydro-2*H*-pyrimido[1,2-*a*] pyrimidine (hppH):<sup>13</sup>C and <sup>15</sup>N CPMAS NMR study of (hppH)<sub>2</sub>, *J. Phys.Org. Chem.* 2010, **23**, 526–535.